UNIVERSITY OF BIRMINGHAM

The Characterisation and Assessment of Curvature in Asymmetric Carbon Fibre Composite Laminates

By:
Amelia Davis

A Thesis Submitted to The Faculty of Engineering,
The University of Birmingham
for the Degree of

MASTER OF PHILOSOPHY
(MPhil)

Department of Metallurgy and Materials
The University of Birmingham
Birmingham B15 2TT
May 2012

Abstract

The process-induced distortions of asymmetric composite laminates have been the focus of many studies to date, given their 'unpredictable' nature on reaching room temperature, generating either a 'saddle' or cylinder shape and reaching varied degrees of curvature.

Models have been devised and developed using classical laminate theory extensions to predict the room temperature shapes and curvatures with greater accuracy. However, because these shape deviations and curvature are shown to be dependent on many factors, (including laminate size, stacking arrangement, thickness, thermal history and constituent properties) a vast range of studies prove incomparable to one another, and exclude noted ageing and environmental effects.

The aim of this study was to identify the factors controlling curvature generation in asymmetric carbon fibre laminates in order to quantitatively describe their behaviour.

The curvature generation of several cross-ply asymmetric epoxy/carbon fibre composite laminates has been studied by way of composite manufacture (using manual lay-up and vacuum bagging technique) in order to identify the dominant factors controlling curvature, including shrinkage during curing, CTE mismatch and geometry.

Measured curvatures were compared to developed theoretical models under a series of interfacial conditions; taking into account the slippage between plies during laminate cure, unaccounted for in previous work.

The causes of any deviation between theoretical and experimentally achieved curvatures have been determined and attributed to a number of microstructural defects such as delamination, voiding and, in addition, the degree of cure achieved.

This work reveals a linear dependence of radius of curvature values on thickness and establishes that curvature is dominated by CTE mismatch on cooling. This behaviour highly dependent on the quality of the interfacial bond between plies, the extent of which has been validated by image analysis. The dependence of cure shrinkage on curvature formation is negligible for the MTM28-1 epoxy system.

The bistability of asymmetric composite panels has been determined and related to composite cure and bonding as well as panel aspect ratio. Stress relief / creep has been identified as causing a decrease in curvature / bi-stability over time.

The radius of curvature has been modelled based on laminate thickness and CTE values assuming complete stress transfer across ply interfaces.

Acknowledgements

I would like to express my sincere gratitude to my supervisor Dr Martin Strangwood for his endless patience, reassurance, faith and commitment to both myself and research. Without his support, guidance and extensive knowledge this work would not have been possible.

I would also like to thank my family, friends and colleagues for their encouragement, moral support and good humour. Their faith in my ability gave me the confidence to continue through to completion, despite my constitution.

Contents

1.	**Literature review……**	**1**
1.1	Unbalanced laminates……..	1
1.2	Measuring curvature experimentally……	4
1.3	Modelling laminates…….....	5
1.4	Residual stress……..	16
1.5	Evaluation of residual stresses in composites……..	26
1.6	Laminate defects……..	29
1.7	Time and Environment…….....	39
1.8	Applications…….....	44
2.	**Summary: Aims and Objectives……..... **	**48**
3.	**Experimental……..... **	**50**
3.1	Laminate Manufacture…….....	50
3.2	Characterisation of laminates…….....	51
3.3	Pre-curing…….....	61
3.4	Stress relaxation / creep……	64
3.5	Snap-through / bistability…….....	65
4.	**Results and Discussion…….. **	**68**
4.1	Geometry……...	68
4.2	Base Behaviour; Strain/Curvature Relationship……	71
4.3	Model Validation……...	78
4.4	Experimental Deviations from model assumptions and model limitations……	79
4.4.1	CTE with Cure……..	80
4.4.2	Laminate Interply Bonding……	80
4.4.3	Curvature with Laminate Length/Width, Aspect Ratio…….	83
4.4.4	Curve Profiles…….....	88
4.4.5	Development of Curvature with Cure……...	90
4.4.6	Pre-Cure…….....	94
4.4.7	Interrupted Cure Cycles (ICC)…….....	102
4.4.8	Modulus Development with Cure, ICC…….....	104
4.4.9	End Constraints…….....	105
4.4.10	External Factors; Deviations from Baseline Curvature…….....	106
4.5	Limitations of linear theory; Model boundary conditions and assumptions……..	116
4.6	Applications…….....	122
5.	**Conclusions and Further Work…… **	**128**
6.	**References……... **	**130**

1. Introduction

1.1. Unbalanced laminates

As a general rule, unbalanced composite laminates are usually avoided commercially as they are considered to be ‘unpredictable’ [2,3], with a need to consider residual stresses (in addition to in-situ external loads) and panel warpage in addition to the general considerations for most standard engineering materials. However, more recent interest in bistable and morphing structures [4,5] means that unbalanced, asymmetric composites are receiving greater interest.

It is possible that this so-called ‘unpredictable’ behaviour is not due to the nature of the composite, but more due to poor characterisation, non-controlled variables and lack of consistency of findings in this area, detailed in the following sections.

In symmetric laminates; the material and orientation of any ply at any distance above the mid-plane is exactly matched at the same distance below the mid-plane, (Figure 1.1). This means that the centre-line of the laminate is a mirror plane with respect to ply material and orientation. Thickness of plies should also remain constant and/or symmetric about the mid-plane. A symmetric laminate is typically indicated by an ‘s’ subscript, e.g. $[0/60/120]_s$.

‘Balanced’ laminates are those for which the number and type of plies with their fibres oriented in the $+\theta$ direction (angle to the main fibre direction) are ‘balanced’ by the same number and type in the $-\theta$ direction.

As asymmetric laminate has no mirror plane along its centreline, whilst an un-balanced laminate is one which contains an unequal number of plies in the + and $-\theta$ directions, e.g. $[0/30/60]_s$ ‘Balance’ refers to plies oriented off the two principal axes and so is not strictly applicable to laminates composed of 0° and 90° plies only.

The effect of asymmetry is more important than imbalance. Eg: A [+45/-45] laminate is balanced but will exhibit similar behaviour to a [0/90] laminate.

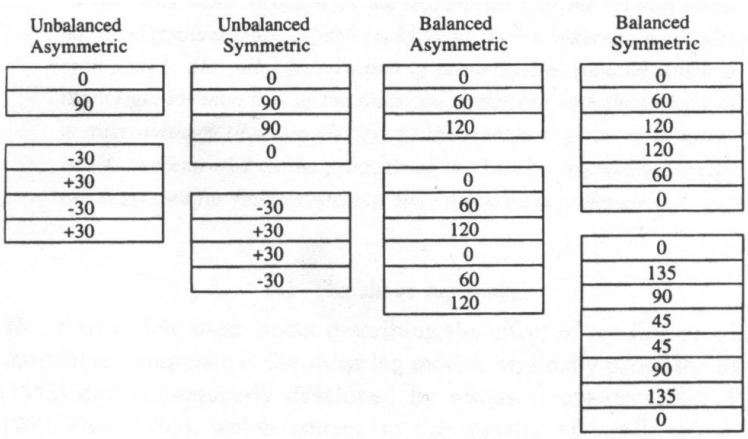

Figure 1.1: Laminate stacking sequence examples and definitions [1]

In UD plies the thermal expansion coefficients and elastic properties vary with direction [6-9]; in balanced, symmetric laminates the variations in these properties from one ply are countered by the balancing ply so that distortion is minimised.

When the laminates are unbalanced and asymmetric this countering effect does not occur, but, instead, coupling of forces and residual stresses occurs in the plane normal to the tensile axis of the laminate. The consequence is a double curvature or 'saddle-shaped' laminate deformation [6,7], Figure 1.2 a.

The laminate will have a tendency to 'bend' or 'warp' towards the ply with the higher coefficient of expansion, likely to be 90º plies and then stabilise in the state of minimum potential energy.

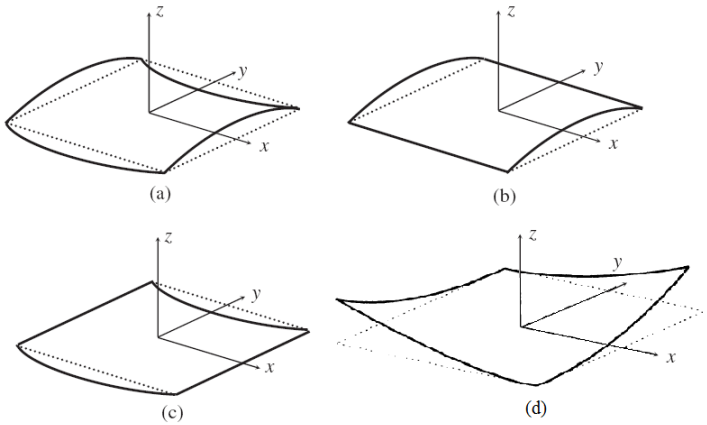

Figure 1.2. Possible curvature shapes of asymmetric cross-ply laminates at room temperature: (a) saddle shape; (b) and (c) reciprocal cylindrical shapes; and (d) twisted laminate (adapted from [8,10-12,13-15].)

In order to make use of asymmetric laminates, it is critical that cured shapes of asymmetric laminates can be well predicted.

Hyer (1982) [13-15] investigated the shapes of several asymmetric laminates and observed that the room temperature shapes do not always conform to the linear predictions of classical laminate theory (CLT).

Instead of being a saddle shape, as predicted by the classical theory (Figure 1.2 a), many asymmetric laminates exhibit a cylindrical shape at room temperature [16,17]. A second cylindrical shape can sometimes be obtained by a simple 'snap-through' action (Figure 1.2 b and c), the point at which this occurs is referred to as the laminates bifurcation point.

Other shapes include unbalanced 'twisted laminates' (Figure 1.2 d) formed through the stacking of angle plies, $(0_2 60_2, 45/-45)$ which changes the principal direction of curvature [11]. The sensitivity of unbalanced room temperature shapes to fibre angle suggests that any deviation from the absolute 0 / 90 fibre configuration in a standard cross ply laminate would cause warpage in directions other than longitudinal and transverse.

It has been shown that room-temperature shapes (saddle-cylinder behaviour) are a strong function of the size, stacking arrangement, fibre angle and thickness of the laminates with an increase in the number of plies decreasing curvature (Figure 1.3) [11], resulting in an increase in radius of curvature. Degree of curvature is not determined solely by thickness, but is reported to be more a function of length-thickness ratio. While a cylindrical shape is observed for large side length-to-thickness ratios, a saddle shape is observed for small side length-to-thickness ratios [8].

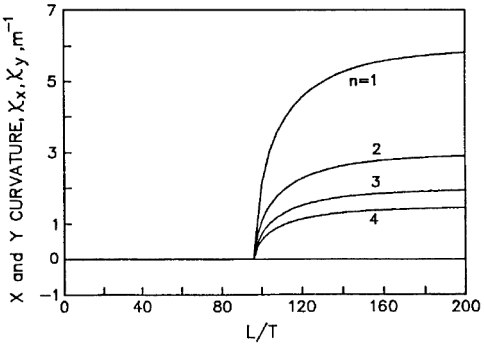

Figure 1.3; Decrease in curvature with an increase in numbers of plies.

L/T is the length to thickness ratio of panel geometry, X and Y are the principal laminate axes [11].

Curvature is also influenced by the magnitude of residual stresses (direct function of microstructural parameters such as v_f and resulting degree of resin shrinkage during the cure cycle and can vary extensively depending on environmental conditions. (covered in Section 1.4). The time at which curvature occurs in the curing cycle has been the focus of many studies [18].

1.2. Measuring curvature experimentally

In experimental studies of asymmetric laminates (used for validation of models), the curvature is normally calculated from measured values of: height (h), out of plane deformation/height (h), side length (L), thickness (t) [8,19], Figure 1.4, Equation 1.1.
In most recent experiments [11], the calculations also include the angle θ for improved accuracy.
Curvature of curved shape calculated using:

$$\begin{cases} h_1 = h - t\cdot\cos\theta \\ R_{\text{out}} = \dfrac{(L'/2)^2}{2h_1} + \dfrac{h_1}{2} \\ \theta = \arcsin\left(\dfrac{L'}{2R_{\text{out}}}\right) \\ L = 2R_{\text{out}}\theta \end{cases}$$

Equation 1.1

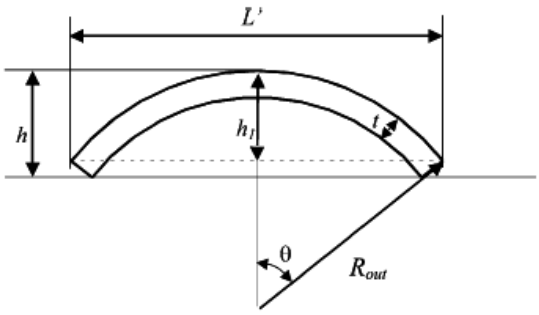

Figure 1.4; Calculation of curvature from experimental results [19].

1.3. Modelling laminates

Many researchers have focussed on the prediction of curvature in unbalanced composite laminates. Whilst one research field focuses on the influence of processing parameters during the cure cycle on residual thermal stresses [20-23]; another field, developed by Hyer, deals with multi-stable shapes [11,13-15] and curvatures [5,10] of asymmetric laminates generated by residual thermal stresses.

1.3.1. Classic Laminate Theory (CLT)

CLT describes the macro-mechanical behaviour of laminates made from orthotropic plies, with the following major assumptions [24,25]:

i) Displacements, *w* are continuous throughout the laminate
ii) Line elements which were originally perpendicular to the middle surface of the plate remain straight and normal to the deformed middle surface and suffer no change in length. This (and assumption i) effectively defines the laminate interface to be perfectly bonded and, with assumption v) to be infinitely thin (as the interface will not be homogeneous with the bulk of the ply)).
iii) The strain-displacement relationships are linear.
iv) Plane stress conditions apply for the laminate plies ($\sigma_z = \sigma_{yz} = \sigma_{zx} = 0$).
v) The laminate is constructed of an anisotropic, homogeneous, linearly-elastic material with properties independent of temperature.

The assumptions above for CLT are somewhat restrictive, but are necessary for ready solution of the tensor relationships for stiffness and compliance in a three dimensional structure.

Tsai and Hahn [3] highlighted the flaws in basic laminate theory, as the rule of mixtures predicts linear behaviour, (linear σ-ε relations) in contrast to the non-linear relationships they determined. For example; stress is not constant in multidirectional laminates as modulus (E) varies from ply to ply. In addition, the out-of-plane displacement *w* of the room temperature shapes of asymmetric laminates can be many times the plate thickness, therefore strain-displacement relations cannot be taken to be linear.

Figure 1.5 illustrates the non-linear behaviour of an unbalanced laminate under tensile loading.

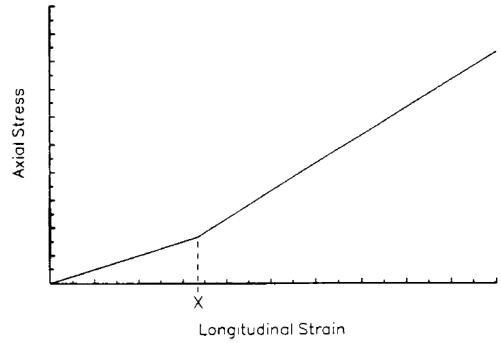

Figure 1.5. Schematic stress-strain curve for an asymmetric laminate [26]

During tensile loading, Figure 1.5, the point at which the laminate becomes straight (X) causes a change in longitudinal modulus to a value comparable with that in a symmetric laminate and a change in the slope of the tensile stress-strain curve [26].

The in-plane, through-thickness and flexural moduli of various unbalanced cross ply laminates (with differing ply groupings) have been calculated using the approach of Tsai and Hahn [3], in respect to ply positioning around the composite mid line, thickness and number of plies. Findings reveal that composite modulus is proportional to the modulus of each ply and its distance from the midline.

When simulating a tensile load on symmetric laminates, the stress distributions are symmetric about the mid-plane. Therefore, only one quarter of the laminate is modelled. However, if the laminate is asymmetric, the entire thickness of the laminate has to be modelled, adding to the complexity of unbalanced, UB models [26].

The need to incorporate non-linear effects into CLT modelling is apparent as an unstable equilibrium saddle shape is always predicted when geometric nonlinearities are ignored, contrary to the two cylinders generated in many experiments.

1.3.2. Models for generation of curvature

1.3.2.1. CLT extensions: displacement functions

In order to extend CLT to include non-linear strain-displacement behaviour observed in UB laminates, Hyer *et al.* [15] developed an earlier approximate theory for predicting the room-temperature shapes of $0_2/90_2$ and $0_4/90_4$ laminates, adding non-linear terms to the strain-displacement relations, (based on the polynomial expansion of displacements) and principle of virtual work/minimum of total potential energy (PMTPE), which includes thermal effects such as coefficient of thermal expansion (CTE). Generalised carbon fibre composite (CFC) properties were used for development of the model, with modulus values (E_1 at 181 GPa and E_2 at 103 GPa).

The approach of Hyer provides a baseline for the majority of current advanced unbalanced laminate models.

As cross ply 0/90 laminates can cure into a number of predefined shapes, Hyer [13-15] used a third order approximation for the out-of-plane displacement *W*, in *x* and *y* directions leading to cylinder / saddle shapes:

$$W(x,y) = \tfrac{1}{2}\,(ax^2 + by^2)$$

Equation 1.2 [13-15]

where *a* and *b* are constants that dictate the shape of the laminate where $a>0$, $b<0$ corresponds to saddle (Figure 1.2 a), $a>0$, $b=0$ corresponds to a cylinder (Figure 1.2 b) and $a=0$, $b<0$ is the secondary cylinder (Figure 1.2 c).

Through coordinate transformation, the displacement field was then approximated using the Rayleigh-Ritz methodology, containing a finite number of independent coefficients. A general form of in-plane displacement was chosen, based on Timoshenko kinematics, Figure 1.6 [27] (strains and curvatures are expressed in terms of displacements using extended Kirchoff hypothesis), working out assumptions in the displacement field and substituting in the strain-displacement relations to give the laminate strain field:

$$\epsilon_x = a_1 - \frac{aby^2}{4} - az \qquad \epsilon_y = b_1 - \frac{abx^2}{4} - bz \qquad \epsilon_{xy} = 0$$

Assumptions:

$u^o(0,y) = 0$; $v^o(x,0) = 0$

$\varepsilon^o x$ independent of x ; $\varepsilon^o y$ independent of y, $\varepsilon^o xy = 0$

Equation 1.3

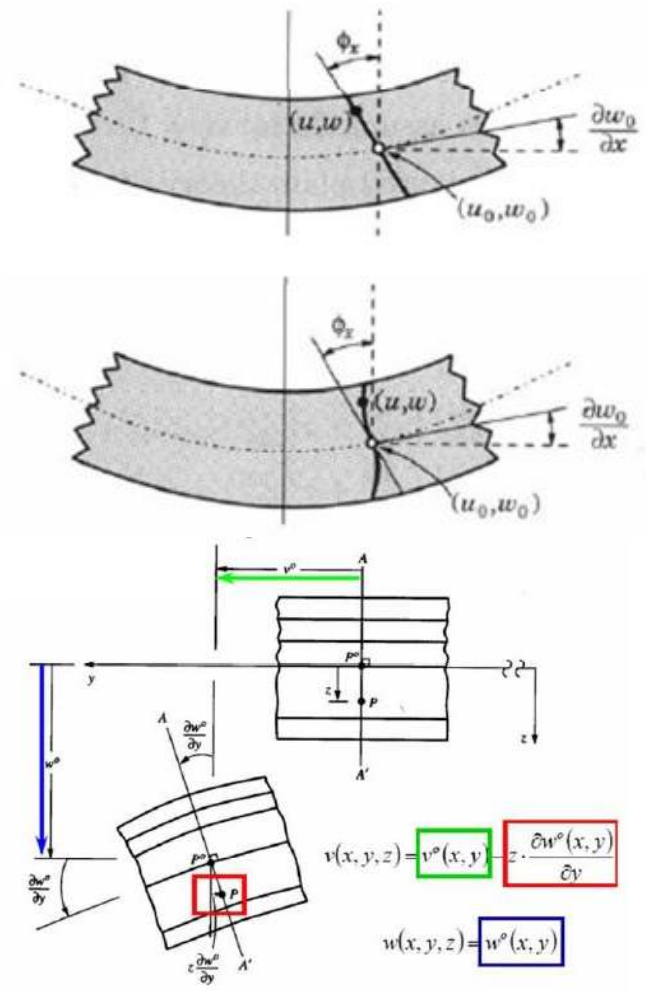

Figure 1.6; (a) First order Timoshenko kinetics, 1964 [27] (b) Higher order plate/beam kinematics allow for warping in the ply (c) Resulting displacement in *y, x* plane

The strain field equations (determined using strain-displacement relations) were then substituted into the developed version of the 'total potential energy', where 'total potential energy' is minimised, giving 4 unknown Rayleigh-Ritz coefficients.

The 4 unknown Rayleigh-Ritz coefficients can be determined analytically or numerically to calculate the dimension-curvature relationship, giving a prediction of room temperature shape and influence of side length on curvature/saddle-cylinder bifurcation point of a typical square cross ply, Figure 1.7.

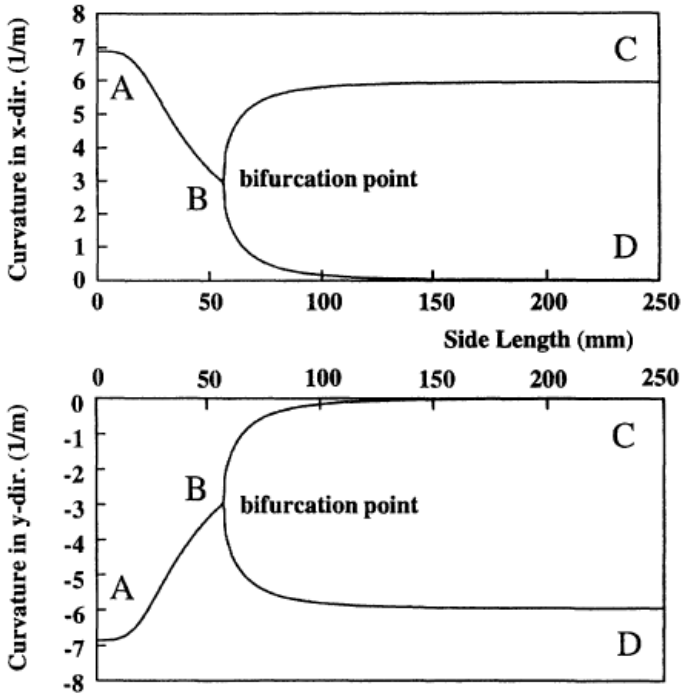

Figure.1.7 Typical cross-ply dimension-curvature relationship [13-15, 28]

Jun and Hong [11] modified Hyers [13-15, 28] original approximate displacement field by considering all spatial variation of strains and displacement functions (Equation 1.3); adding more terms in the polynomials to account for the presence of thermal residual in-plane shear strain (significant at corners) due to free-edge effects caused by deviation from a perfect cylinder.

It must be noted that shear strains are previously assumed negligible for the cross-ply case in CLT [13-15] and that free-edge effects cannot occur because constants (curvature) are deemed independent of *x* and *y*.

$$u^0(x,y) = x\left(a_1 - \frac{a^2}{6}x^2 + a_3y^2\right) \quad v^0(x,y) = y\left(b_1 - \frac{b^2}{6}y^2 + b_3x^2\right)$$

$$w(x,y) = \frac{1}{2}(ax^2 + by^2)$$

Equation 1.4 [11]

Comparison of dimension-curvature relations for the methods of Hyer, Jun and Hong predicts similar results for large area 2 ply cross ply laminate panels, Figure 1.8 indicating shear strain should be negligible for square laminates with a very large or

very small length-to-thickness ratio. However, at intermediate length-to-thickness ratios, shear strain is predicted to be important and should not be neglected.

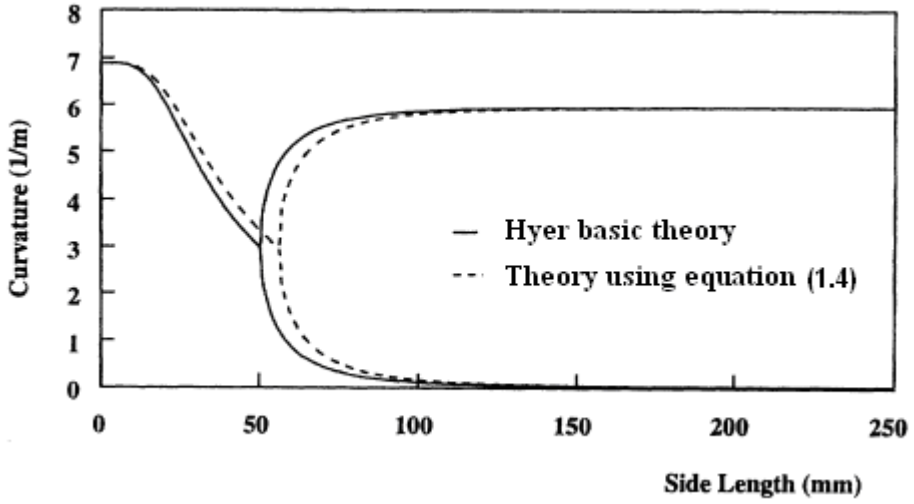

Figure 1.8; Theoretical cross-ply dimension-curvature relationship using equation 1.4.

Later work by Hahn and Hwang [29] succeeded in easing the prediction of curvature x_c for large cylindrical cross-ply laminate, Equation 1.5.

$$x_c = \frac{(A_{11}A_{22} + A_{12}^2)M_x^T - B_{11}(A_{22} - A_{12})N_x^T}{D_{11}(A_{11}A_{22} - A_{12}^2) - B_{11}^2 A_{22}}$$

Equation 1.5 [29]

where N_{Tx} is the thermal force resultant per unit width along the x-direction, M_{Tx} is the thermal moment resultant per unit width along the x-direction and A_{ij}, B_{ij} and D_{ij} are the laminate stiffnesses.

Experimental observations of a cross ply cylindrical laminate cross section revealed edge effects, showing non-zero curvature present at edges classified as ‘straight’ [10,11,17] suggesting poor description of the out-of-plane displacement field $w(x)$ of equations 1.1 - 1.5.

A higher approximation of a circle was thought to improve the accuracy of calculated curvature [30], thus equations 1.6 - 1.7 were developed using complex displacement expressions and trigonomic relations to give out-of-plane displacement field:

$$w(x,y) = \frac{1}{2}ax^2 + \frac{1}{8}a^3x^4 + \frac{1}{2}by^2 + \frac{1}{8}b^3y^4 + O(x^6,y^6)$$

where 0 (x^6,y^6) indicates terms of sixth or higher order in the x or y which are not taken into consideration:

Equation 1.6

In-plane displacement functions,

$$u^0(x,y) = x\left(a_1 - \frac{a^2}{6}x^2 - \frac{a^4}{10}x^4 - \frac{a^6}{56}x^6 + a_3y^2\right)$$

$$v^0(x,y) = y\left(b_1 - \frac{b^2}{6}y^2 - \frac{b^4}{10}y^4 - \frac{b^6}{56}y^6 + b_3x^2\right)$$

assuming $\varepsilon^o x$ independent of x ; $\varepsilon^o y$ independent of y.

Equation 1.7

Despite the increased complexity of models based on equations 1.6 - 1.7, differences in predicted curvatures are negligible when compared to the dimension-curvatures predicted by Hyer, Jun and Hong's methods, equations 1.3 and 1.4, Figure 1.9.

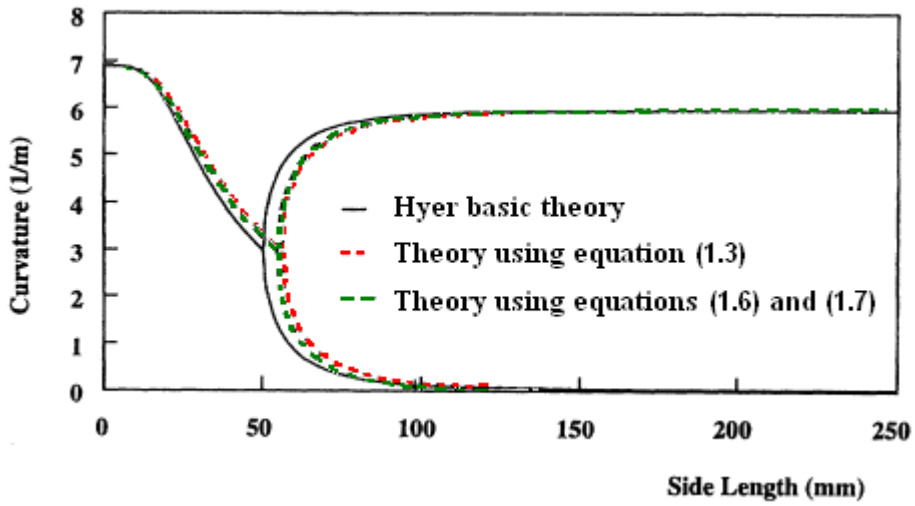

Figure 1.9; Comparison of theoretical cross-ply dimension-curvature relationship using equation 1.3, 1.6 and 1.7. Adapted from Peeters [10].

Peeters *et al.* [10] manufactured several asymmetric glass- fibre reinforced PEI (Polyethermide, Ultem 1000) laminates for comparison of experimental of curvatures with theoretical models (using mechanical and thermal model inputs measured and determined during the study). Experimental curvatures are shown in Figure 1.10 and show good agreement of the laminate bifurcation point (predicted at 57 mm side length)

to model predictions, though experimental curvature results are generally over predicted by 15%.

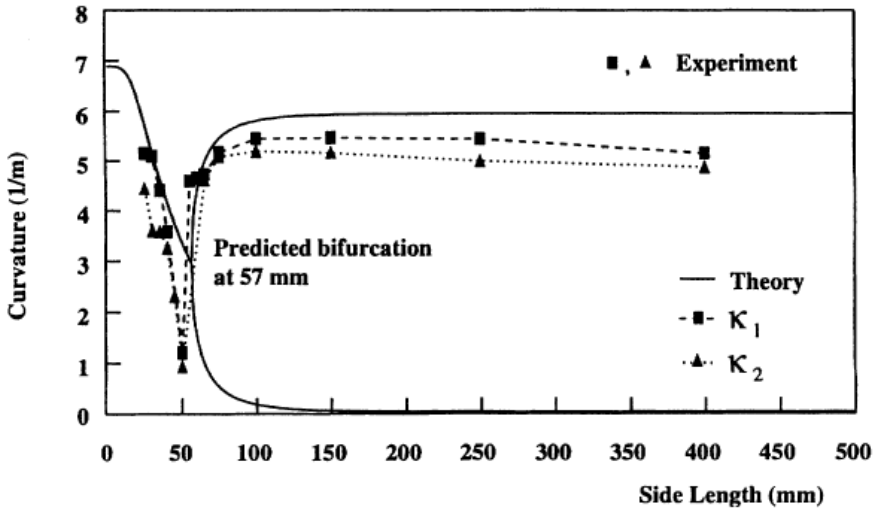

Figure 1.10, Predicted and experimentally measured curvatures for a $0_2 90_2$ glass/PEI laminate, ply thickness 0.18 mm, Peeters [10]

The 'over prediction' of curvature, Figure 1.10, [10] may not be representative of the poor prediction of model data, but more indicative of differences caused by the manufacturing process, in which damage to the materials may have influenced experimental curvatures achieved, detailed below.

Peeters *et al.* [10] chose to use a mould designed to disallow polymer flow, with the intention of ensuring that fibres remained in position during cure. They also trimmed the laminate edges post cure to make 400 x 400 m^2 laminates, cutting smaller laminate geometries from the initial larger laminates, such that central point was the same. In following this process, (trimming laminate edges and cutting smaller laminates in preference to manufacturing them), they may have inadvertently caused damage to the materials and excluded additional factors responsible for generating curvature in the smaller laminates upon curing, leading to this lack of curvature generation. They also acknowledged the presence of edge effects in 200 x 200 mm 0/90 laminate, resulting in non-perfect cylinders, which would also be responsible for the deviation from model predictions.

In addition, Peeters *et al* also raised uncertainties regarding the accuracy of their thermal and material input values used in model predictions, due to inhomogeneities in materials (ie: the non-uniform fibre distribution between layers) which would further influence experimental curvatures and the fitting of experimental results to model predictions.

Hyers simple displacement functions are shown to be sufficient for finding the majority of saddle-cylinder solutions (within experimental error), providing the foundation for many model predictions. However, in general, extended CLT models are normally confined to square or rectangular cross ply/angle ply plates, unlike more recent additions to Hyer's theories by FEA modelling [8] allowing custom solutions to the same problem, inclusive of geometric imperfections.

FEA models are commonly validated by comparing predictions with the published out-of-plane deformation of well documented asymmetric cured panels [13-15].

Peeters *et al.* [10] drew comparisons between FEA, advanced laminate theory and experimental data, developing a theory for square angle-ply laminates based on the work of Jun and Hong [11] by modelling a laminate quarter, further modifying their displacement functions. The value of the laminate principal curvature direction was fixed at 45^{o} relative to the laminate edges, based on advanced linear theory which predicts angle ply laminates exhibit equal curvatures in x and y directions using a more complete set of third-order polynomials to compute the total potential energy.

Curvatures predicted using a finite element method (obtained through similar application of the principle of minimum potential energy used by Jun and Hong [11]), gave similar results when compared with preliminary values calculated using Hyer's simple displacement functions, Equation 1.3, Figure 1.11.

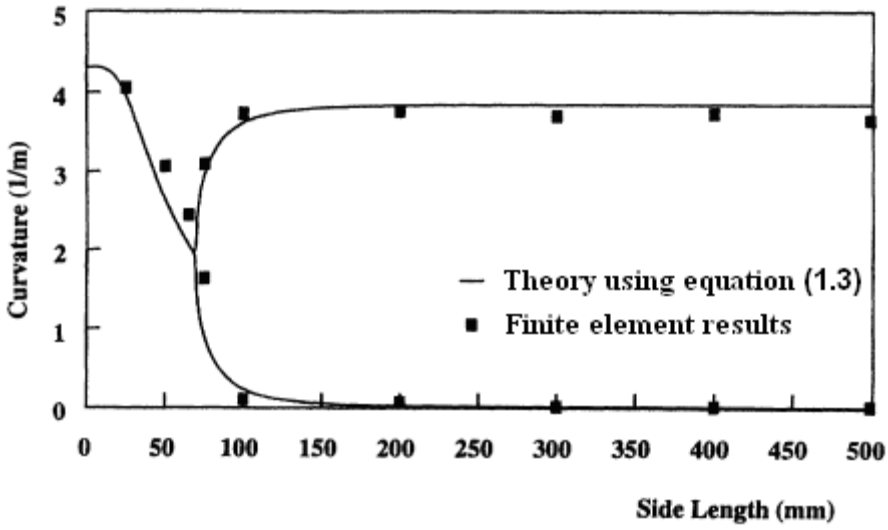

Figure 1.11; Theoretical cross-ply dimension-curvature relationship using equation 1.3 [13-15] when compared to FE results [10].

Dano and Hyer (1998) [31] challenged the priori assumptions made by Peeters [10] about orientation of principal curvature coordinate systems and used polynomial expressions for the strain. Experimental principal curvatures and principal curvature directions were then compared with predictions, obtaining good agreement.

Schlecht [17] also studied the stability of room temperature shapes of unbalanced laminates through comparison of finite element analysis, CLT and experimental methods. He found correct laminate shapes were observed, but models underestimated the radius of curvature of laminates (2.7% lower than experimental data) and failed to account for edge effects, when compared to measurement of experimental curvatures. This underestimation of panel curvature was due to side length effects [17,32].

A more recent study by Pirerra (2009) [32] used FEA paired with advanced laminate theory to predict the bistability and curvatures of unbalanced laminates cured on a semi-circular mould.

Results show good correlation between experimental and predicted trends for the general curve shape, though their models were still unable to accommodate for edge effects (out by 4 mm), resulting from imperfect cylindrical shapes, Figure 1.12.

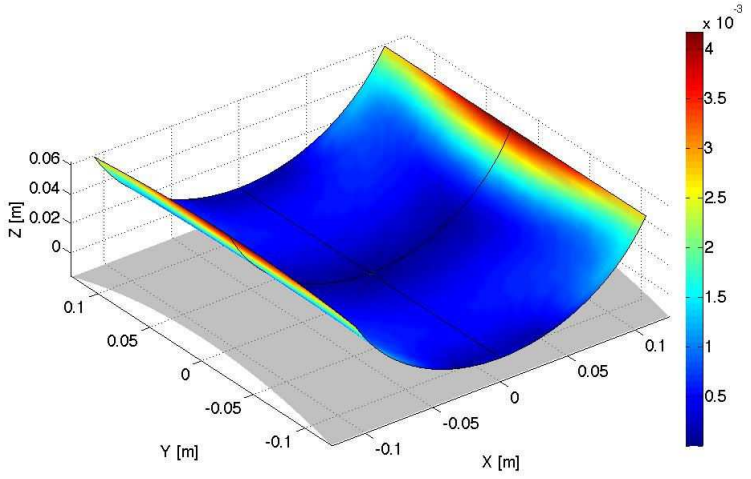

Figure 1.12; Difference between finite element analysis and experimental data
The colour bar refers to the error (*x*,*y*) from model predictions to experimental findings.
The grey area indicates the initial mould shape (dimensions in m) [32]

More recently, Vargas *et al* (2009) [33] developed a new approach for determining thermo-mechanical stresses in both un-symmetric cross-ply [$0_n/90_n$] and bi-modulus curved laminated strips subjected to thermal and mechanical loading, accurately predicting the in-plane and out-of-plane stresses. They found in-plane and out-of-plane

stresses to be dependent on geometric conditions as thickness ratio, material relations as modulus ratio and other variables related to loading parameters as span length.

The finite element approach to UB laminates proves a popular modern tool as the approach can easily be applied to general problems and issues can be studied in more detail. However, FE approaches can lead to difficulties finding multiple solutions and dealing with metastable equilibrium conditions. Applying constraints to a model may force a single solution, when experimentally there may be multiple solutions as a result of many factors, such as material or process variations or inhomogeneities.

It must be noted that the materials used by these authors are varied widely in both model development and experimental validation of models, although the in cases the same baseline datasets were used. This may be why a large discrepancy is seen between predicted and real values in some studies and not in others, 15% overprediction [10], 2.7% [17].

Peeters et al [10] used a glass fibre / PEI (with laminate properties of E_1 43.1 GPa and E_2 14.3 GPa) in comparison to the majority of studies making use of carbon fibre/epoxy systems, meaning comparison between thermoplastic (PEI) and thermoset (epoxy) behaviour. In general, thermoplastic matrices would be of lower strength and more prone to stress relief / creep so that the time elapsed from manufactured would need to be well characterised. The possibility of slippage at matrix / fibre interfaces is greater for a thermoplastic matrix so that the assumptions inherent in the models may not be equally applicable to both types of experimental data.

1.3.2.2. Conclusion of modelling UB laminates using extended CLT

In general, it is acknowledged that simple modelling based on extended CLT provides a good approximation of the cured shapes of asymmetric cross-ply and angle-ply laminates when input parameters, such as mechanical and thermal properties (difference between T_{SF} and RT) are known [11] and exact (especially $\alpha 2$) [10].

However, the absence of extensive verification of curvature models and lack of consideration of many factors affecting material input properties during the manufacturing process means that CLT predictions should only be used as ‘guidelines’ for design and used for the ‘best case’ composite material. More experimental is data

needed to provide more appropriate fitting parameters from the idealised (CLT) case to the ‘real’ situation.

1.3.2.3. Deviations from model curvature predictions

Deviations from CLT-based model predictions (saddle/cylinder behaviours) [10,17] are suggested to be due to lack of consideration of the relative effects of the following factors, usually neglected in modelling, including:

- Volume fraction (v_f)
    - Matrix / fibre and ply interactions
- Thermal Expansion Coefficient (CTE) of constituents
    - Lay up angle
- Cure history
    - Resin shrinkage
    - Residual Stress
- Defects
- Ply thickness
- Moisture, temperature, hygrothermal gradients
- Part / tool interactions

[18,26, 34-37]

The mechanisms that contribute to causing stresses can be further divided into:

1. Thermal stresses and strains arising from the mismatch in the thermal properties of the plies within the laminate;
2. Stresses and strains arising from chemical shrinkage of the resin;
3. Stresses and strains caused by interaction with the tool; and
4. Stresses and strains arising from non-uniform degree of cure, temperature or fibre volume fraction through the thickness [19].

These factors and their effect on curvature will be detailed in the following sections.

1.4. Residual stress

The majority of current models are not fully capable of predicting laminate properties effectively, as ‘by-products’ of the curing cycle (such as residual stresses / strains and

chemical shrinkage) that are not accounted for, giving a false interpretation of true physical behaviour of the composite system [25,38].

In support of these theories, the symmetric nature of most commercial laminates result in the majority of these strains produced during curing being offset by the opposing plies about the mid-plane, and therefore can be considered negligible in balanced laminate modelling. However, these residual strains in unbalanced, curved or cylindrical laminates are not offset [38,39] and can pre-stress the laminate, affecting the stress-strain behaviour, inducing warpage, reducing the predicted overall strength, leading to poor surface finish [39] and even initiating matrix cracks and delamination [9,18,40,41].

The magnitude of these residual stresses in a multilayer composite is dependent on the curing process, history of environmental exposure, as well as the constituent properties and micro-structural parameters such as v_f, with the ratio of 0º to 90º plies proven to be the dominant source of residual stress [42].

The distribution of residual stresses has been shown to be a function of stacking sequence and processing temperature [42], which is in contrast to classical laminate theory (CLT) predictions.

Figure 1.13 shows the predicted distribution of residual stresses in both balanced and unbalanced laminates. The presence of tensile stresses in the 90° ply in Figure 1.13 (b) suggests that this was restrained externally to remain flat. The low modulus of this orientation means that the strain can be resisted with a low stress, whereas the smaller strain in the 0° ply gives a much higher residual stress due to its higher modulus.

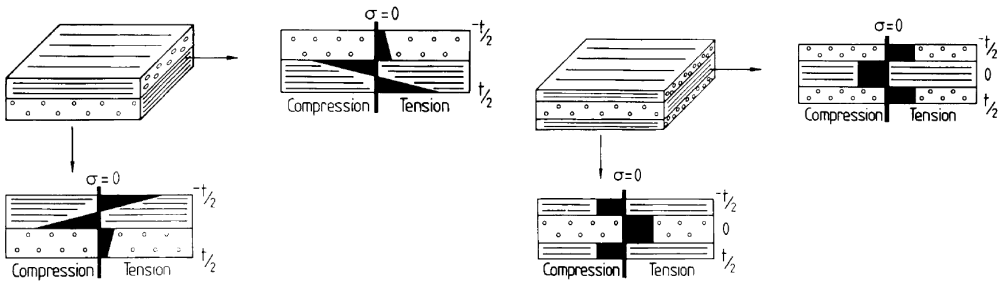

(a) Balanced **(b) Unbalanced**

Figure 1.13; Residual stress distributions calculated for (a) $90_2/0_4/90_2$ and (b) $0_4/90_4$ laminates [21].

Resulting residual stresses can generally be divided into micro-mechanical and macro-mechanical effects, Table 1.1

Table 1.1 Summary of micro- and macro-mechanical residual stress effects in composites.

The micro-mechanical scale	*The macro-mechanical scale*
The residual stress acting between matrix and fibres are as result of the 'mismatch' between matrix volume change (chemical shrinkage due to polymerisation) and the stable volume of the fibre at curing temperature. These stresses are tensile in the resin matrix and compressive in fibres.	The anisotropic nature of carbon fibre composites causes non-uniform shrinkages of different ply layers. This is due to a significant dissimilarity in thermal expansions of both constituents on cooling from curing temperature to ambient temperature. For non-unidirectional composites the effects of this 'mismatch' are increased.

1.4.1. Evolution of residual stresses during cure.

The mechanical properties of the fibre phase are assumed to be independent of cure. In contrast, the mechanical properties of the thermosetting resin matrix are largely dependent on the cure history; transitioning from a low modulus, low viscosity substance (in its partially cured state), into a highly cross-linked viscoelastic / elastic solid (in its fully cured state).

This transition causes a volume change due to both the thermal expansion and chemical shrinkage, (4 - >7 % for typical epoxy resin systems at full degree of cure) [18,39-41]. Identifying a need for separating chemical shrinkage from thermal expansion/contraction effects [9,18].

This volume change on curing is the focus of much literature and has been characterised for a number of systems in terms of both chemical and physical effects. However, the majority of studies do not consider composites as an entirety and focus on unconstrained resin systems. Clearly the constraint of fibres would reduce the resin's ability to crosslink causing less cure shrinkage and a reduced volume change between 1 and 2 % [6].

Baseline texts by Hull *et al*. [7] state that most resin shrinkage occurs whilst the resin is still liquid so that stresses do not develop.

In contrast, Wisnom *et al.* [18] investigated the mechanisms generating stresses and distortions in AS4/8552 asymmetric laminates by interrupting the curing cycle at varied intervals (ICC) and found nearly all the chemical reaction and cure-related chemical shrinkage to occur at the later stage of cure [41] leading to significant residual stresses which cannot be relieved. Laminate curvature was shown to develop linearly with decreasing temperature due to the development of thermal stresses during cooldown after vitrification (from 180 - 20 ºC) [18].

Figure 1.14 shows the volumetric change of epoxy resins during the cure cycle, and the stages at which it occurred.

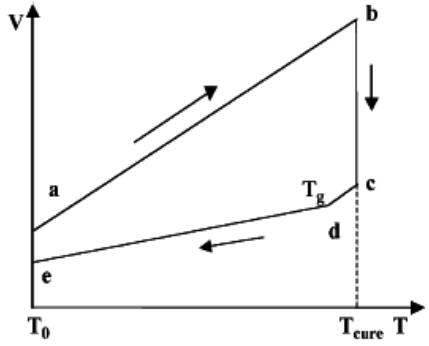

Figure 1.14; Schematic of volume change of epoxy resins during cure [18]

Stage a–b: the volume of the resin increases when it is instantaneously heated up from reference temperature, T_0, to a curing temperature, Tc, due to thermal expansion before any chemical shrinkage occurs;

Stage b–c: the volume decreases due to chemical shrinkage at a constant curing temperature, as weaker bonds are broken and covalent bonds are formed causing atoms to move closer together.

Stage c–e: The volume decreases due to thermal contraction when it cools down to room temperature.

Point d corresponds to the volume at the glass transition temperature T_g, at which the thermal expansion coefficient of the resin changes dramatically.

The glass transition temperature T_g, is largely dependent on the degree of cure of the resin, as well as the chemical composition of the resin and hardener and is an important factor for residual stress development. If cured at temperatures > T_g, polymerisation

shrinkage and residual stresses are small; at temperatures $<T_g$ polymerisation shrinkage and residual stresses are significant [41,43].

Both Wisnom *et al* [18] and Giggliotti *et al* [19] showed chemical shrinkage of the curing resin to be a linear function of the degree of cure, with curvature increasing with increasing cure but attaining a constant value after the vitrification point. They speculated that the certain percentage of non-thermoelastic stress captured during the cycle, Figure 1.15 was a result of resin chemical shrinkage, contributing about 5 % to the curvature, despite several other possible sources of non thermoelastic strain being identified, namely:

1. Stress relaxation at high temperature, acting over long times, which tends to reduce the final curvature.
2. Tool interaction due to shear stresses arising at the part-tool interface as a result of differences in thermal expansion.

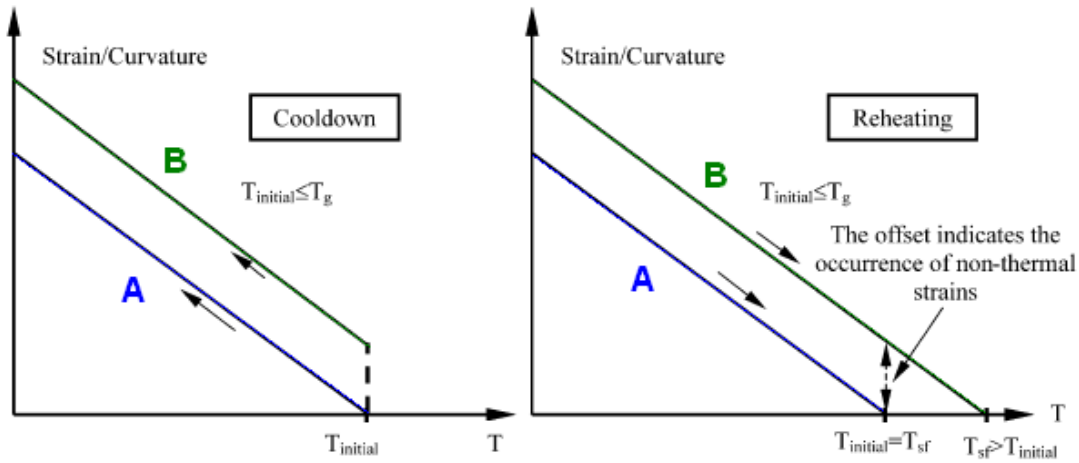

Figure 1.15; (a) Cooldown and (b) reheating of a composite system from a cure temperature below T_g, where A: only thermoelastic strains are in the structure, B: non thermo-elastic strains are in the structure.

The numerous contradictions in shrinkage values and stages of occurrence (Hull and Wisnom in complete contrast) are likely to be due to variations in experimental procedure, materials, stacking sequence and thickness [39], and methodology for differentiating between CTE and shrinkage effects.

1.4.2. Chemical shrinkage and modulus interactions

Interactions between chemical shrinkage and resin modulus development during curing (as a result of polymerisation, Figure 1.16 b) are shown to significantly influence the process-induced stress distributions in thick thermosetting laminates [42] and is proven a critical factor in the 'storage/setting' of residual stresses within unbalanced laminate structures, when the matrix has sufficient stiffness to 'hold' the residual stresses generated [21,33,43].

This relationship between modulus and chemical shrinkage is indicated by ~75% of residual stress level in laminates building up between the glass transition temperature, T_g and room temperature [21]. This relationship is challenged by the experimental work of Peeters and co-workers [10], who concluded that curvatures are not very sensitive in changes in Young's modulus.

In terms of measurement of modulus during the period of curing of the resin, a number of techniques have been studied,

Capehart *et al.* [44] simulated the time evolution of the modulus of individual plies using a one-dimensional finite element model (FEM). The measured temperature profiles of the composite layers during curing were semi-quantitatively reproduced by the model indicating the degree of cure for each composite layer.

Figure 1.16 shows the change in modulus and specific volume of a standard epoxy resin during curing. Region II, indicates that a significant increase in modulus (through chemical hardening) and a reduction in specific volume (chemical shrinkage) occur simultaneously.

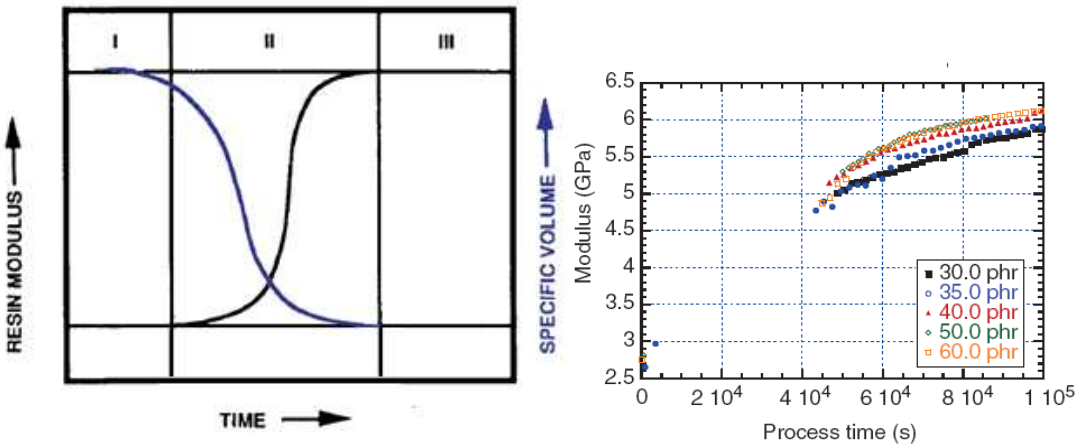

Figure 1.16; (a) Resin modulus development and chemical shrinkage during the curing cycle (adapted from Bogetti and Gillespie [42]). Region I denotes a fully un-cured resin,

Region II during curing, Region III end of curing process. (b) Modulus variation in resin samples with different amounts of hardener (Epon 828/Epicure 3046) [39]

It is clear that increased availability, accuracy and inclusion of the history of modulus development with cure would significantly enhance the accuracy of future models for residual stress and deformation [39].

1.4.3. Coefficient of thermal expansion, CTE

In addition to the cure-induced volume change from chemical shrinkage, geometric variations resulting from large dissimilarity in thermal expansions between consituents (non 'isotropic') and between the fibre direction and the fibre transverse direction in plies (α2) [45], Figure 1.17, on cooling from curing temperature to ambient temperature is shown to induce curvature in 0/90 cross ply laminates, (section 1.1). This curvature is largely driven by the transverse coefficient of thermal expansion, α2 [19].

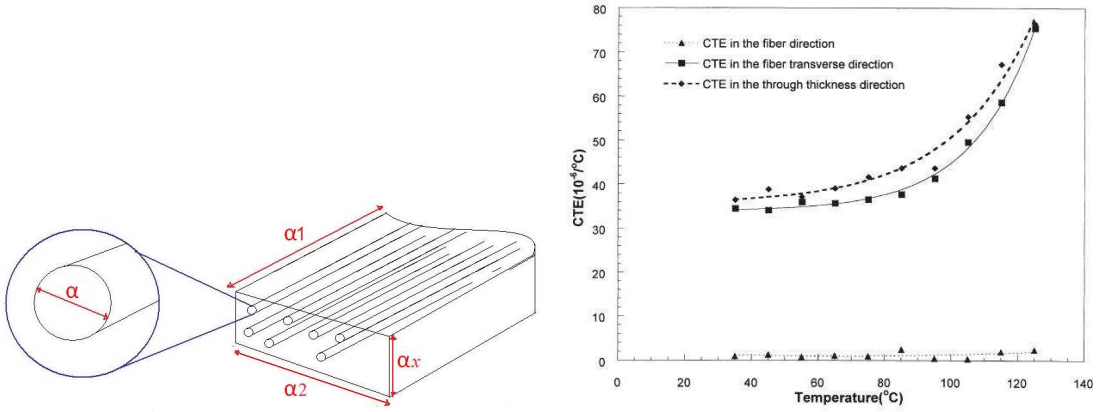

Figure 1.17; (a) Principal directions of CTE in composite, (b) measured CTEs in the material principal directions of 20x50 [0_8] AS4/PEEK thermoplastic composite laminates on heating from RT to 130 ºC [9].

Figure 1.17 (b) shows CTE in the transverse direction is slightly lower than the CTE in the through thickness direction. Theoretically, this should not be the case. Yoon and Kim [9] attributed the difference to variations of microstructural fibre alignment in the through thickness direction and transverse direction, reinforcing the sensitivity of factors to manufacturing techniques.

Stacking and bonding plies to form a laminate, the individual plies are constrained from undergoing 'free thermal contraction', causing the formation of internal stresses later 'fixed' into the matrix post cure [21,43] causing curvature, Figure 1.18. Laminate strain is influenced by the elastic moduli and CTEs of individual plies, with each lamina influencing the expansion or contraction of the other.

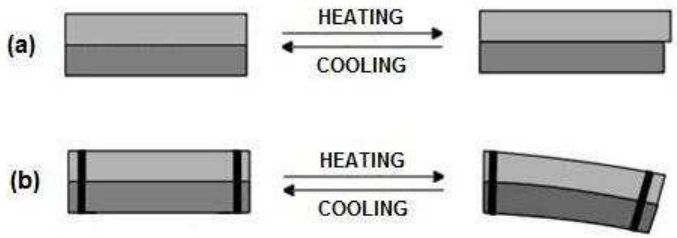

Figure 1.18. Effect of interfacial constraint on expansivity

Variation in CTE with temperature is only a smooth function if the material is undergoing no phase transitions, such as re-arrangements at the glass transition temperature, T_g that lead to discontinuities of CTE as the thermoset transitions from a glassy viscous fluid to a rubbery solid.

Zarelli *et al* [41] carried out a series of measurements using a combination of standard [9] and novel thermo-analytical techniques. They found CTE in the glassy state to be low, whereas there is a marked increase in CTE above the glass transition temperature, T_g in rubbery state, increasing to 3 or 4 times the value determined below T_g due to increased degrees of molecular segmental motion, Table 1.2, Figures 1.19 and 1.20.

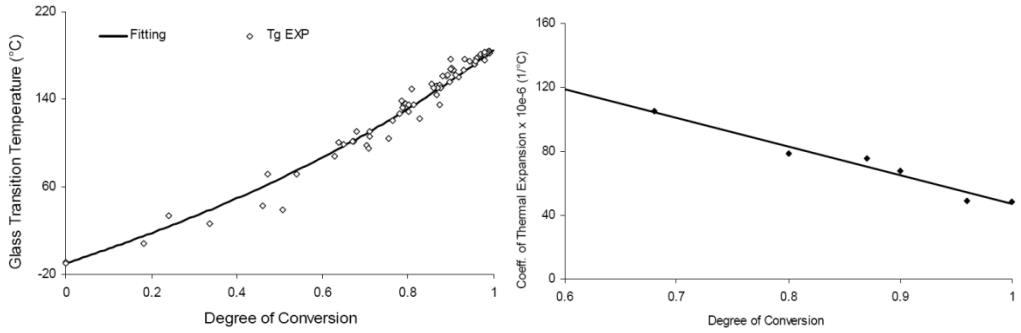

(a) (b)

Figure 1.19; (a) Glass transition temperature versus conversion for experimental data (EXP) and model fit, and (b) coefficient of thermal expansion versus conversion in the glassy state. [41]

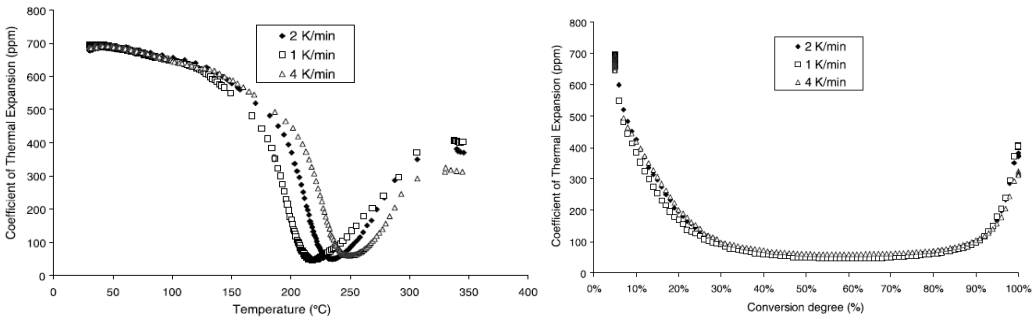

(a) (b)

Figure 1.20; Calculated evolution of CTE (a) as a function of temperature and (b) as a function of conversion degree [46].

Table 1.2. Variations in measured CTE for a filled epoxy, above and below T_g.

Coefficient of thermal expansion ($\alpha 10^{-6}$ K^{-1})	
Below T_g	Above T_g
30 - 60	60 - 240

The measured variations in CTE with temperature/degree of conversion detailed above, means that using generic CTE input values for modelling of curvature does not enable true prediction, failing to account for experimental deviations.

Peeters *et al* [10] showed the significance of variation in model input expansion values in transverse orientation (α2) to have a significant effect on the predicted curvature using CLT extensions, Figure 1.21.

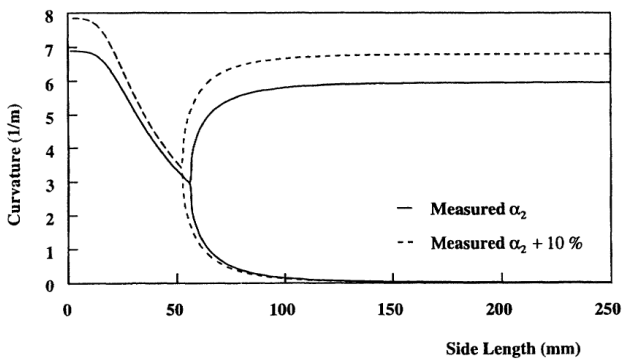

Figure 1.21, The effect of a 10% change in α_2 on the predicted curvatures of a $0_2/90_2$ of a glass/PEI laminate [10].

1.4.4. Stress-free temperature

The temperature at which a laminate bears no residual stress is referred to as its 'stress-free temperature'. This temperature can be used to calculate residual stresses and is linked to the matrix crystallisation temperature.
The shape produced at this temperature is shown in Figure 1.22.

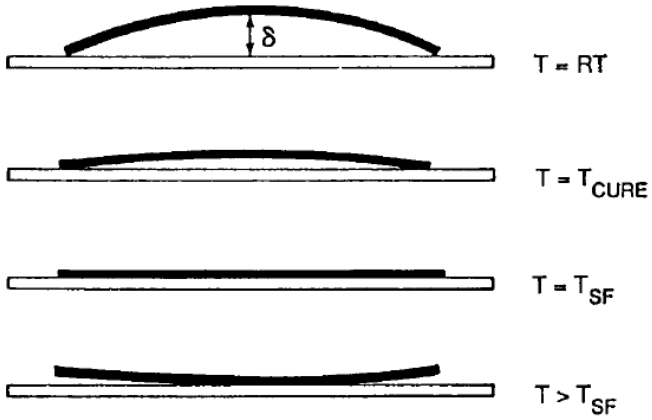

Figure 1.22: The resulting warpage of a $0_4/90_4$ unbalanced laminate at room (T_{RT}), curing temperature (T_{CURE}), stress-free (T_{SF}) and below stress-free ($T>_{SF}$) temperatures [47].

In a thermoset graphite/epoxy composite, Crasto and Kim (1993) [47] showed the stress-free temperature to be 15 ºC higher than the curing temperature, T_{CURE} , with T_{SF} increasing with increasing degree of cure [19].
The stress-free temperature of samples cured beyond vitrification is systematically higher than their cure temperature. This is in contrast to earlier work by Hahn (1976) who identified the stress-free temperature to be lower than the curing temperature. However, this was found to depend on the curing process. Post-cure of laminates that have not been fully cured tends to increase their ''residual'' curvature, but the effect of the post-cure is relatively small for specimens cured beyond the vitrification point [19].

Stress free temperature is commonly used in modelling the residual stresses and curvature of asymmetric laminates.
The effect of changing T_{SF} input in modelling using extended CLT is shown in Figure 1.23.

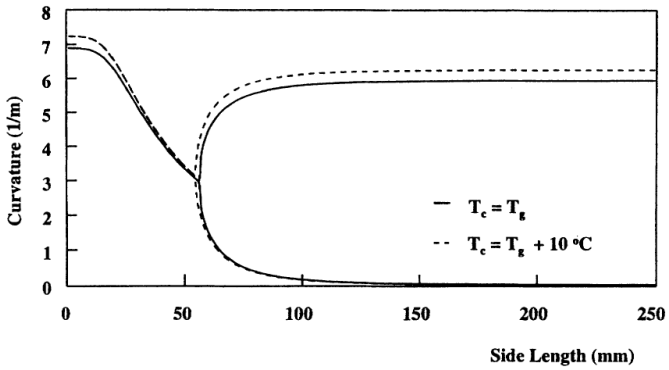

Figure 1.23; The effect of a 100 ºC change in T_{SF} on the predicted curvatures for a $0_2/90_2$ glass/PEI laminate [10].

1.5. Evaluation of Residual Stresses in Composites

1.5.1.Model prediction

Traditional analysis of residual stresses in thermosetting composite laminates is based on thermal expansion mismatch between adjacent plies and a uniform temperature difference between the cure and ambient temperature, assuming no stress is developed prior to completion of the curing process.

These analyses are moderately successful in predicting residual stresses in thin laminates, where the assumed even heat distribution through-thickness is justified. However, in general, the magnitude of the residual stresses calculated theoretically is usually greater than that found using experimental methods, listed in Section 1.5.3.

1.5.2. Predicting residual stresses through laminate 'warpage'

A knowledge of the moduli, E_1 and E_2, the thickness, s, of the unsymmetrical laminate and the radius of curvature, ρ_c, only is required to determine the residual stress at any temperature.

$$\sigma_R = \frac{E_1 E_2 h}{\rho_c (E_1 h + E_2 k)} \left[\frac{b+d}{2} + \frac{E_1 b^3 + E_2 d^3}{6(b+d)} \left(\frac{1}{E_1 b} + \frac{1}{E_2 d} \right) \right]$$

Equation 1.8, [48]

The thicknesses of the longitudinal and transverse plies in the unsymmetrical laminate are denoted by b and d respectively, while *h* and *k* are the corresponding ply thicknesses in the symmetrical lay-up.

1.5.3. Experimental

(a) Destructive methods

Destructive methods require the removal of material from laminate structures, meaning specimens cannot be re-used. They have been widely criticised as the introduction of moisture from cutting/drilling processes can induce swelling and also stress fields, interfering with already sensitive residual stress measurements.

Destructive methods are:

- Hole-drilling method
- Cutting method
- Ply sectioning
- Process simulated laminate (PSL)
- First ply failure

(b) Non-destructive methods

Non-destructive methods allow the measurement of laminate residual strain 'in-situ' with little or no damage.

Non-destructive methods are:

- Warpage
- Embedded strain gauges
- XRD

1.5.4. Estimation of chemical shrinkage

Provided that thermal expansion coefficients of the resin at different points during the curing cycle and the T_g are know, total chemical shrinkage during curing is given by;

$$\left(\frac{\Delta V}{V}\right)_{b-c} = \left(\frac{\Delta V}{V}\right)_{a-e} + 3\,x\,(\alpha_1 - \alpha_2)(T_g - T_o) \qquad \text{Equation.1.9}$$

where, $(\Delta V/V)_{a\text{-}e}$ is the volume difference between the uncured resin and fully cured resin (measured at a reference temperature ~20 C), T_o. α_1 is the linear thermal expansion

coefficient (CTE) of the resin above T_g, (from a-b and c-d). α_2 is the linear CTE below T_g from d-e, Figure 1.14 [18]

However, this method is only an approximation of shrinkage as it does not take into account the degree of cure and its subsequent effect on the CTE of the CFC [41], which is dependent on many factors such as v_f, fibre arrangement, fraction of covalent bonding [49] and E_f/E_m [7].

Wisnom *et al*. [18] found this method to underestimate the chemical shrinkage by 0.8 % in comparison to in-situ cure monitoring. The curvature change of a curved section of laminate (due to chemical shrinkage) can be better predicted by recording the chemical shrinkage strains in the in-plane and through-thickness directions, which occur during a cure process [9].

$$\Delta\theta_{chemical} = \theta_0(\varepsilon_z^{0C} - \varepsilon_x^{0C})$$

Equation. 1.10

where ε_x^{0C} and ε_z^{0C} are the chemical shrinkage strains in the in-plane and in the through thickness direction, respectively, which are occurring during a cure process [9].

1.5.5. Cure monitoring

Given the relationship between degree of cure on mechanical properties of thermosetting resin matrix properties, cure monitoring and control are of paramount importance for quality control in laminate production and is to ensure complete polymerization of the matrix [50].

There are many current methods available for cure monitoring and shrinkage development over the entire curing cycle; most commonly used to verify model results.

1) Differential Scanning Calorimetry, DSC.
2) Dynamic Mechanical Analysis.
3) Infrared spectroscopy.
4) Optical techniques.
5) Dielectometry.
6) Ultrasonic velocity.
7) Nuclear magnetic resonance.
8) Raman spectroscopy.

9) Optical fibre based sensor systems.
10) Dilatometry
11) Novel methods; gravimetric

Not all of these methods can be used in-situ. Whilst DSC and DMA can analyse the cure of a set specimen, cross-linking of the sample may occur on transporting the sample to and from testing locations for analysis, adding a high risk of misinterpreting data

1.6 Laminate Defects

The manufacturing processes of carbon fibre reinforced polymers (CFRPs) can introduce a number of characteristic flaws which can modify composite and laminate mechanical and physical properties [51,52].

The most common defects observed in CFRPs are:

(i) Delamination.
(ii) Voids.
(iii) Inclusions.
(iv) Disbonding
(v) Resin-rich regions; within an individual ply or at a ply interface.
(vi) Matrix cracking.

These defects, their rates of occurrence and the extent of their effects on composite and laminate behaviour are covered in the following sections.
Wang *et al.* [52] examined the risk of defect formation in laminates of varying geometric characteristics. Delamination was found to be the dominant defect type accounting for more than half of the defects observed in that study, independent of laminate shape. Voids/pores were the second most common form of defect, Figure 1.24.

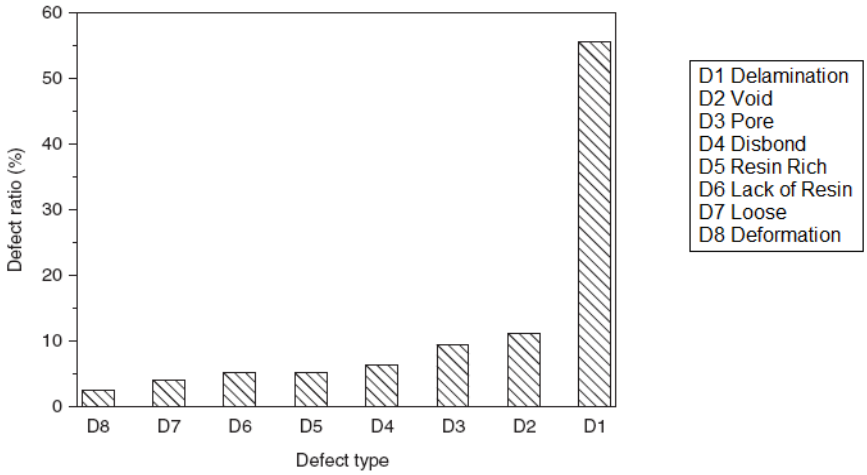

Figure 1.24; Comparison of manufacturing defects in autoclaved laminates, where 'defect ratio' refers to the proportion of affected laminates in a batch [52]. * 'Loose' defect is not defined in literature.

A correlation was found between the radius of curvature of components, and number of manufacturing defects at corners (delaminations/voids) due to the interaction of shear flow and non-uniform pressure in corner sections [52].

The size of delaminations for small curvature radii are much larger than those for a larger curvature radius, Figure 1.25

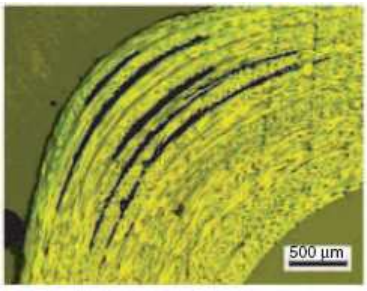

Figure 1.25; Delamination in a corner section for curvature radius of 2 mm. [52]

It can be seen from Figure 1.26 that as the curvature radius of components increases, the defect ratio gradually decreases. This is likely due to a variance in resin shrinkage due to thickness and tensile stresses in the upper plies.

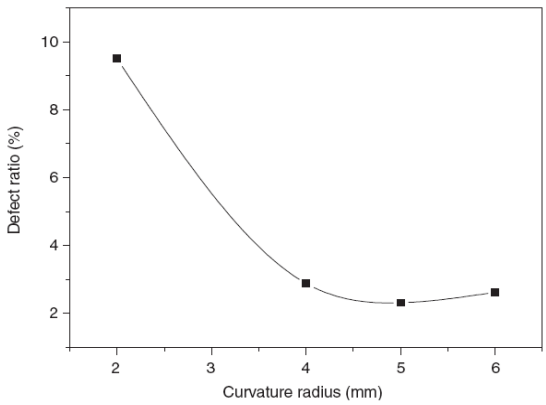

Figure 1.26; Variation in occurrence of manufacturing defects with radius of curvature [52], where 'defect ratio' represents the ratio between the number of defects and the number of total components in view of curvature radius.

CLT is largely applied to 'elastic' properties, but prediction of plastic failure and fracture can be important. These aspects can be more sensitive to defect type and location. For example, if a laminate is subjected to a bending moment; delaminations or voids located in the plies subjected to tension would have a much larger effect on mechanical properties compared to any located in the middle plies (neutral plane) which would have minimal impact. Also, tensile strength of long fibre composites would be very sensitive to fibre damage, in comparison to compressive properties, which are largely influenced by matrix fracture, most particularly de-laminations [53].

The fracture/damage mode depends upon a large number of parameters, such as the properties of the constituents, loading condition, the fibre stacking sequence and environmental conditions.

Figure 1.27 shows the crack propagation in a fibre composite in tensile loading, with subsequent debonding and fibre breakage as a result.

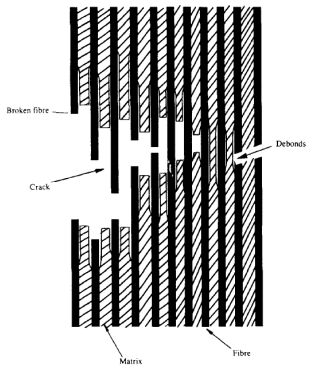

Figure 1.27; Schematic representation of crack propagation in a fibre reinforced composite [53]

The many defect types; their geometry, orientation, location and behaviour under different possible loading conditions of composite materials make it difficult to summarise the subsequent detrimental effects on its properties [51]. However, the determination of the effects of particular defect types in standard test-pieces under controlled conditions does allow criteria to be established, which, when used in finite element analysis (FEA), allows the potential effects of defects on laminate performance to be assessed.

1.6.1. Delamination

Interply delamination, Figure 1.28, is one of the most frequently observed type of defect and discussed mode of failure in composite materials [52,53].

Delaminations most commonly occur where inter-laminar stresses develop due to high resin content between plies, impeding stress transfer between layers; hence their severity in bending (Figure 1.25). Residual stresses (generated by shrinkage during curing or differential thermal expansion and contraction) have also been identified [26] as one of the causes of delamination.

Delaminations located in outer/top plies are generally more severe as they can result in the opening out of the initial delamination causing a marked decrease in laminate properties and inevitable failure.

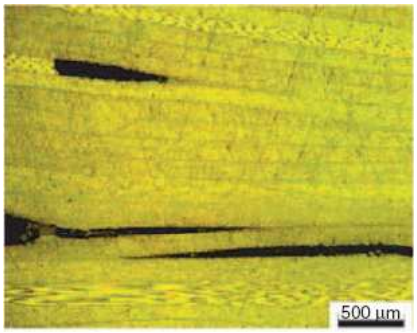

Figure 1.28; Micrograph of delaminations in a laminate. [52]

Determination of the effect of defects, such as delamination, requires that the defect is quantified in some manner, after which the extent of the defects' effects on properties can be determined and the two related. A common measure of the extent of delamination is the length of delaminated interface as a function of total interface. This measure has been used [54] to model the stiffness of a cantilever containing a defect of varying severity (based on earlier work by Shen and Grady [55] from which natural

vibration frequencies in bend could be predicted and verified against experimental frequency measurements for a damped-free cantilever, Figure 1.29. As shown in Figure 1.29, the agreement is good with little effect on frequency being observed or predicted for a normalised delamination length up to 20 %. For greater degrees of delamination the effect on stiffness and decrease in frequency is greater (33 % decrease in frequency for 80 % normalised delamination length) with the prediction accurately accounting for the experimental trend line.

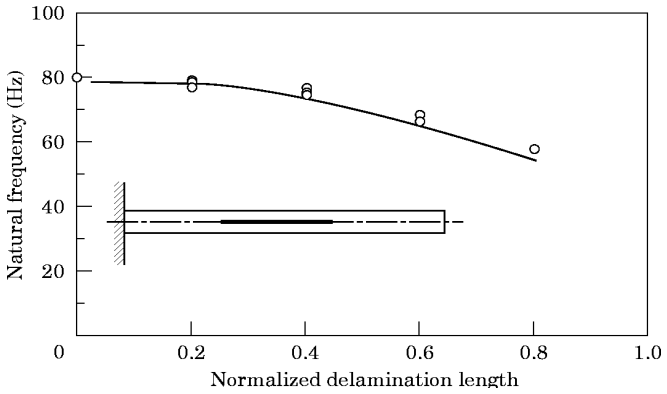

Figure 1.29; The predicted effect of a central delamination on the fundamental natural frequency of a beam, where the solid line is the predicted variation and the open circles are experimental data [54].

The analysis of Saravanos *et al.* [54], whilst giving good agreement for a single delamination in a laminate, does not deal with multiple delaminations, particularly those between different plies in the same laminate. Hence, the full extent of through-thickness delamination has not been quantified and requires further characterisation and study.

As noted above, CLT assumes that the interfacial bond between plies is infinitely thin and gives good load transfer. As shown by the presence of delamination and varied ply thicknesses, this is not always the case.

Pagano [25] proposed that the inter-laminar normal stress is responsible for the dependence of laminate strength on stacking arrangement, Figure 1.30.

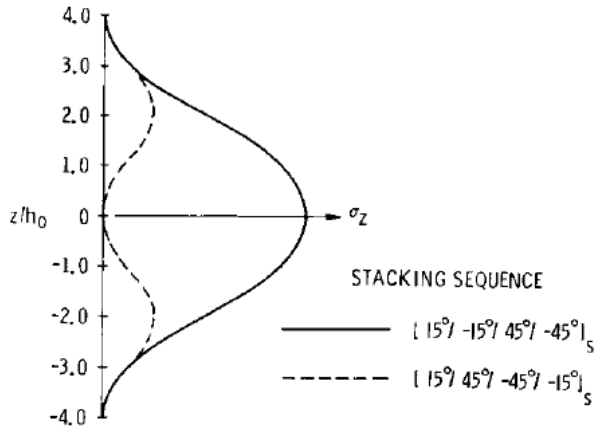

Figure 1.30; Distribution of inter-laminar normal stress in boundary layer region, where Z is the laminate through-thickness [25].

The behaviour shown in Figure 1.30 indicates that layers of specific orientations should be arranged through the thickness to provide optimum protection against delamination through appropriate width-to-thickness ratio enabling good stress transfer between plies. The risk of delamination can also be reduced by improving interfacial adhesion [56,57] through manipulation of pressure and temperature profiles throughout the curing cycle to suit specific material requirements [58].

1.6.2. Voids, pores and inclusions

Voids and pores are common in many composite parts and are usually situated within plies.

The extent of voiding is dependent upon a number of parameters including the water content, applied pressure during the cure cycle and the dwell time during the cure [51,53,58].

Water content can usually be reduced by ensuring the pre-preg is fully defrosted before use and that maximum pressure is maintained throughout the cycle.

These controllable factors are constantly re-analysed to reduce the number of defects introduced as part of the manufacturing stages and consequently optimise properties of the finished laminate [58].

Joseph *et al*. [58] used an autoclave with an ‘on-line’ model feedback to maintain an optimum laminate thickness (specified through input of pre-preg. raw data, such as % weight of resin in pre-preg.) via manipulation of pressure and temperature profiles throughout the curing cycle.

This method was found to significantly reduce void size, as the correct application of pressure causes excess resin to squeezed out of the laminate, allowing optimum laminate properties to be obtained.
It is for this reason that autoclaving is shown to reduce the void content in comparison to vacuum bagging due to increased pressure during the curing cycle [58].

Inclusions are very similar to voids in structure. Both are thought to act as micro-crack initiation sites [38] as stress concentrations are severe around inclusions and pores, especially when in close proximity to each other.
The difference is the cause, as inclusions are caused by solid, foreign material trapped inside/in-between pre-preg. layers during production or laminate manufacture and so can be avoided if precautions are taken to ensure the use of lint/paper-free surfaces and dust-free preparation rooms.
The effect of void/inclusion size has not yet been directly related to laminate properties in current literature, although some characterisation of the effects on composite mechanical properties have been reported.
Cantwell *et a.l* [53] showed that 10% voiding in a composite laminate reduced the compressive strength by 15% and shear modulus/interlaminar shear stress (ILSS) by 30 %. Presumably voiding had a more significant effect on shear stress due to the tensile forces acting on the laminate plies.
Inclusions are equally as detrimental, resulting in a ~20% loss of ILSS. However, their experiments do not report the size or frequency of voids or inclusions in the specimen entirety so it is hard to relate the detrimental effects to the degree of voiding present.

1.6.3. Debonding/disbond

Debonding represents a localised mode of failure that is often very difficult to detect using conventional defect detection techniques, such as ultrasound.
The amount of debonding present within a composite depends upon the level of interfacial adhesion between carbon fibre reinforcement and polymer matrix on a microscopic scale, Figure 1.31.
This area is referred to as "interphase" region, where fibre and matrix phases are chemically or mechanically combined.

The strength of the bonding between constituent components in a composite laminates plays an important role in binding and transferring the forces to the fibre, thus determining the mechanical and chemical properties of the resulting composites.

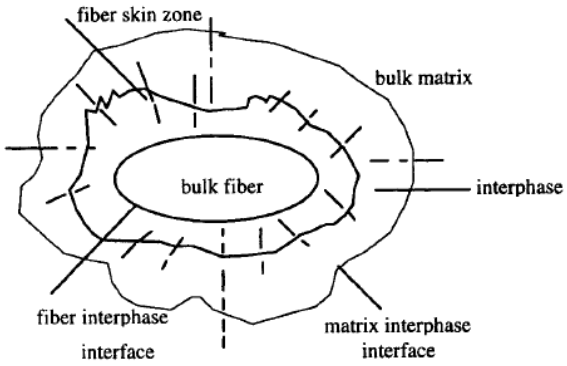

Figure 1.31; Interface and interphase of fibre reinforced composite [59].

Generally, fibres with low levels of surface treatment tend to debond more easily [53]. Therefore the surface morphology of the carbon fibre used and the chemical 'wetting' by the resin of the fibres is crucial to achieve a strong interfacial bond [56].

Internal stresses arising from hygrothermal gradients can result in the expansion of fibres inside the matrix and cause debonding between constituents [26].

Needles *et al.* [57] examined the effect of high temperature curing on the interfacial bonding between unsized or epoxy-sized graphite fibre tow and epoxy-amine resin fibre composite system by scanning electron microscopy of compression and freeze fractured specimens.

Shrinkage of the resin away from the graphite fibres during high temperature cure was observed due to the lack of fibre adhesion. The mechanical properties such as interlaminar shear values for graphite fibre-resin composites are low attributed to poor fiber-matrix adhesion.

1.6.4. Fibre volume fraction (resin-rich regions)

The fibre volume fraction (v_f) refers to the fraction of fibre by volume within the composite microstructure.

Traditionally, composite pre-pregs are manufactured with around 55% v_f. However, v_f has been seen to vary substantially from manufacturers specifications, which can have a

significant effect on laminate mechanical performance, up to 48% variation in composite modulus [60].

Carbon fibre composite are usually associated with linear stress-strain behaviour on loading. Any 'increase' in polymer matrix due to a low v_f could result in non-linear behaviour giving greater strain- and strain rate-dependent mechanical properties. The last points would result in visco-elastic hysteresis energy losses during deformation. The occurrence of inhomogeneities (such as non-uniform distribution of fibres [10]) along with non-linear elastic behaviour invalidate the assumptions of CLT, reducing the accuracy of mechanical property predictions based on this theory, Figure 1.32.

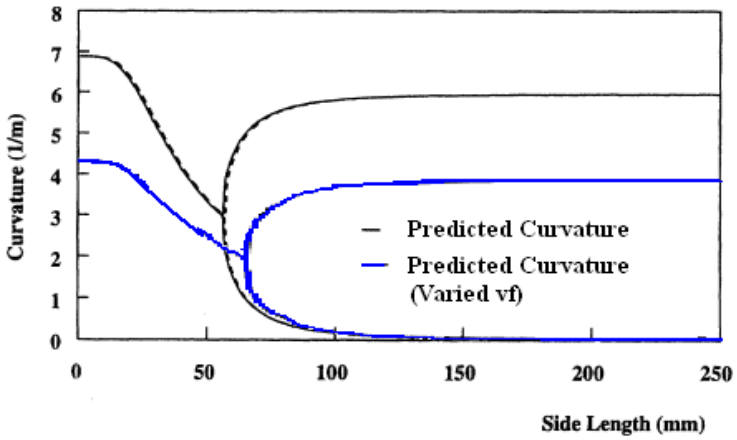

Figure 1.32; Adapted from Peeters [10].

A low v_f can also lead to the formation of resin-rich regions which can act as damage initiation sites for matrix cracking [52,53], low modulus regions leading to non-uniform recoverable deformation [60], Figure 1.33.

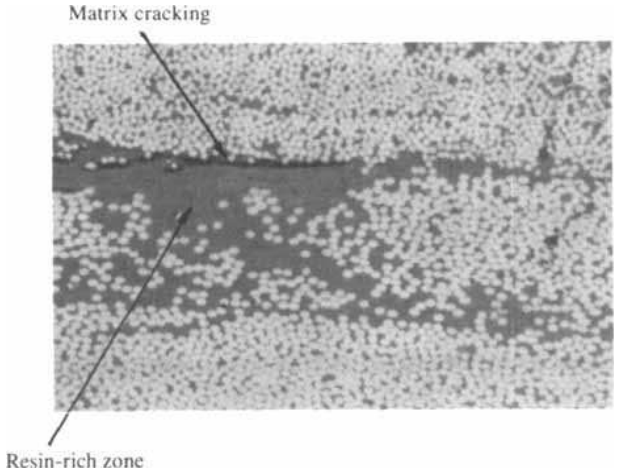

Figure 1.33; Resin-rich region as a result of low fibre v_f and matrix cracking as a consequence [53]

Resin-rich regions and fibre clumping can often be observed in composite materials even though the part has been processed according to the manufacturer's specifications [52,53].

These resin-rich regions usually arise from initial v_f variations in the pre-preg., are very dependent on the geometry and stacking method of the structure being formed [60]; commonly, due to high resin flow, these occur around the ends of plies in laminate sheets.

A low v_f in the pre-preg. can also create a resin-rich region within plies, as non-uniform flow of low viscosity resin fills the area of low v_f during curing.

A higher fibre volume fraction generally results in a stiffer composite and is therefore more desired for sporting applications and for use in rigid structures.

High v_f is normally associated with processing by autoclaving in preference to vacuum bag techniques [58]. This is due to the increase in pressure which compacts the plies to the point in which the fibres are close-packed, resulting in a high v_f and the lowest possible ply thickness [18,58] without the fibres touching (as this would provide a damage path through the composite).

In addition, a larger v_f pre-preg. would require higher pressures during the cure due to the greater constraint provided by the fibres. Therefore the volume fraction can be related to laminate thickness. Any variation in v_f would cause thickness to differ through a standard curing cycle.

1.6.5. Matrix cracking

Localised matrix cracking most commonly results in the matrix region, Figure 1.34, as a result of residual stresses during the cure (due to shrinkage) [7], thermal stresses (due to differences between thermal expansion coefficients of the matrix/fibre) and/or environmental effects (hygrothernal gradients) [7,18,16,53] during the processing cycle.

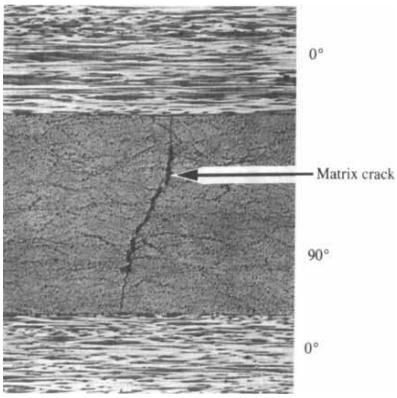

Figure 1.34; A matrix crack in a carbon fibre epoxy composite resulting from excessive thermal stresses [53].

Matrix cracking can be found on the straightening of some unbalanced laminates [26] suggesting matrix cracking may cause premature failure at a lower external stresses than predicted; by acting as delamination initiation sites.

1.6.6. Summary of defect behaviour

The coverage of defects above, has indicated that their presence can modify the mechanical and physical properties of composites. As the formation of many defects can be linked to the manufacturing process and not the structure of plies and their lay-up, then scatter in properties due to defects cannot realistically be predicted using CLT.
The likely variation in composite mechanical and physical properties can be estimated if defects are characterised post-production or parts are monitored parts in-situ during processing and service.

1.7. Time and environment

In addition to the cure-dominated behaviour detailed above, time and environment are also key factors in the long-term behaviour of cured composite parts.

1.7.1.Temperature

Whilst fibres (traditionally used as the reinforcement phase in polymer matrix composites) do not show a large property dependence on temperature, the epoxy matrix is very sensitive to temperature variations causing brittle and elastic behaviour at low temperatures or ductile and viscoelastic behaviour at high temperatures [61-63], specific to the resin used and the composite fibre density. Consequently, the mechanical properties of composite components will vary significantly within their operating

environment; with asymmetric cross ply laminates failing to retain their curvature in a hot/wet environment, but returning on re-exposure to an ambient environment on cooling [26].

This is due to the 'make up' of all polymer based materials which is characterised by a constant molecular motion/re-arrangement in the amorphous state.

Generally, the re-arrangement rate increases with temperature increase. As a result, most polymer matrix composites experience a marked drop in their modulus as the temperature rises, Figure 1.35 and an increase on cooling.

Normal to the fibres, it has been shown that polymeric matrices create compressive stresses in the reinforcement material upon cooling to cryogenic temperatures [61] adding stresses to those already existing from cooling from the cure temperature to room temperature. This is primarily manifested as shear stress at the resin-fibre interface, causing a decline in strength properties sensitive to debonding of the matrix-reinforcement interface, Section 1.6.3 [31].

The changes in material properties, E and respective states upon heating of polymer matrix materials are commonly illustrated using modulus versus temperature curves, Figure 1.35; the shape of which are strongly influenced by the extent of cross-linking*.

1) **Glassy stage:** Fairly stable values of E. Molecular motion is restricted and displays vibrational motion.
2) **Glass transition region (α transition**): modulus of the material drops significantly (generally divided by 10^3). Interpreted as the onset of long-range, coordinated molecular motion.
3) **Rubbery Stage*:** Often shows stable values of E. End of the 'rubbery plateau' is characterised by the presence of a mixed region; with a pronounced modulus drop. Short times are characterised by the inability of entanglements to relax (rubbery behaviour) while long times allow coordinate movements of molecular chains (liquid flow behaviour).

   *For cross-linked materials the plateau (post 'rubbery stage') remains flat due to crystallites acting like physical cross-links tying chains together.

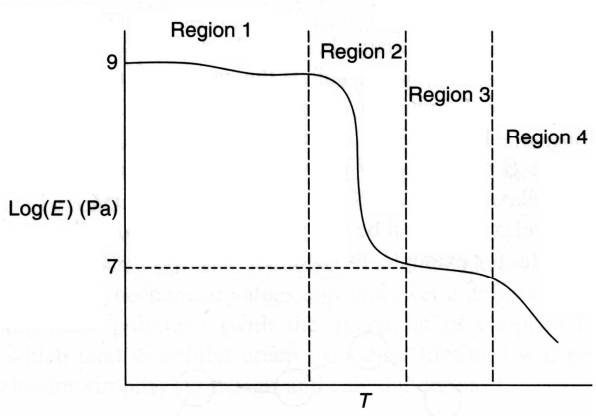

(a)

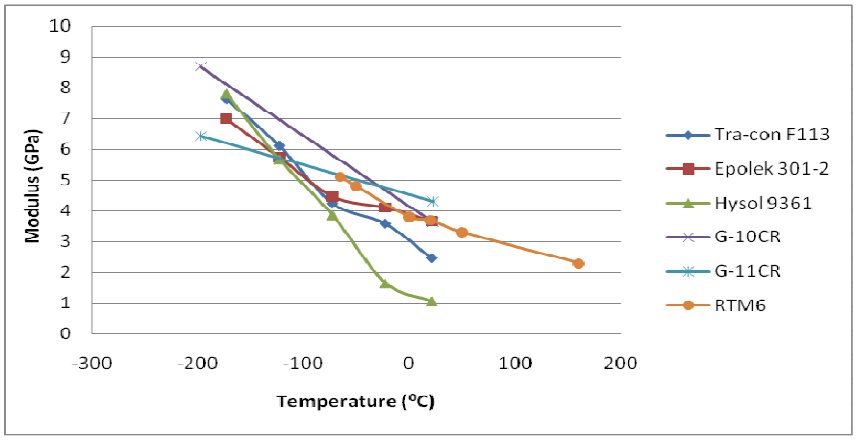

(b)

Figure 1.35, Modulus versus temperature curves for (a) a typical polymer and (b) for select cross-linked epoxy systems, detailed in Table 1.3.

Table 1.3. Summary of source data for resin property – temperature tests.

Author & Year	**Epoxy**	**Geometry**	**Test type**
Cease (2006) [61]	Tra-con F113, Epo-tek 301-2, Hysol 9361	Dogbone machined specimens	Tensile
Ledbetter (1980) [62]	G-10CR, G11CR	5 mm cylindrical specimen	Frequency
Deng (2007) [63]	Hexflow RTM6	Mechanical tests with different loading fixtures	DMA

1.7.2. Time: stress relaxation / creep

In addition to the temperature dependence of the epoxy matrix in CFCs, many composite materials also exhibit highly non linear time-dependent behaviour [64-66], even at room temperature.

Though reinforcements, such as carbon fibres, exhibit negligible viscoelastic behaviour and only very small amounts of creep or stress relaxation occur in the reinforcement direction, plies may still exhibit considerable amounts of creep in transverse and shear directions [65].

Consequently, when these plies are combined to form a laminate and an instantaneous load is applied, the structure will experience instantaneous deformation, followed by a time-dependent deformation or 'creep' and may stress rupture, yield, craze, or simply deform excessively over their service life. The creep properties are highly dependent on the resin system and its properties, fibre types, stress, time, strain rate and environmental conditions such as temperature and humidity. At elevated temperatures this time dependence is even more significant [66].

A perfectly elastic material stores all of the energy created by deformation forces so that on removal of the forces (whenever this occurs) it can return to its original dimensions without loss of energy. In contrast, the viscoelastic nature of the epoxy matrix (displaying properties of both elastic solids and viscous fluids depending on the temperature or timescale of the experiment) causes the covalent bonds to extend and the chains to straighten and slip relative to one another on loading

At a given temperature, a maximum level of stress can be applied without any risk of long-term irreversible damage. Past this point, the material will enter into a second creep mode where rapid damage on the polymer can occur if the combination of stress and temperature is excessive [64-66].

During unloading, whilst the chains slip both the covalent bond extension will be relaxed and the chains will start to curl up. The chain curling is not complete by the time that the load is reduced to zero. Chain curling persists for some time after the applied load has returned to zero and is largely responsible for the viscoelastic behaviour of polymers.

Allowance for creep must be made during design. Traditionally, data available to designers have neglected vicoelasticity which is unacceptable given the highly nonlinear

viscoelastic time-dependent behaviour of polymer-based materials (with respect to the applied loading), identified as a reason for a shift in their ductile-brittle transition. More accurate models for description of viscoelastic materials will include high order stress terms and will therefore be more complex than linear theory. The unloading behaviour is underpredicted by traditional linear models [64].

The time and temperature-dependent creep modulus, E_c, as a function of constant stress, and time and temperature-dependent strain, (t,T), can be used in design calculations for constant stress or strain–stress relaxation applications. Since the process of individual testing for long periods of time is not feasible and the stress and environmental conditions are difficult to predict over the long term, methods for interpolating and extrapolating short term information are necessary in order to predict the long-term behaviour of composite parts through linear or nonlinear viscoelastic theory, Figure 1.36.

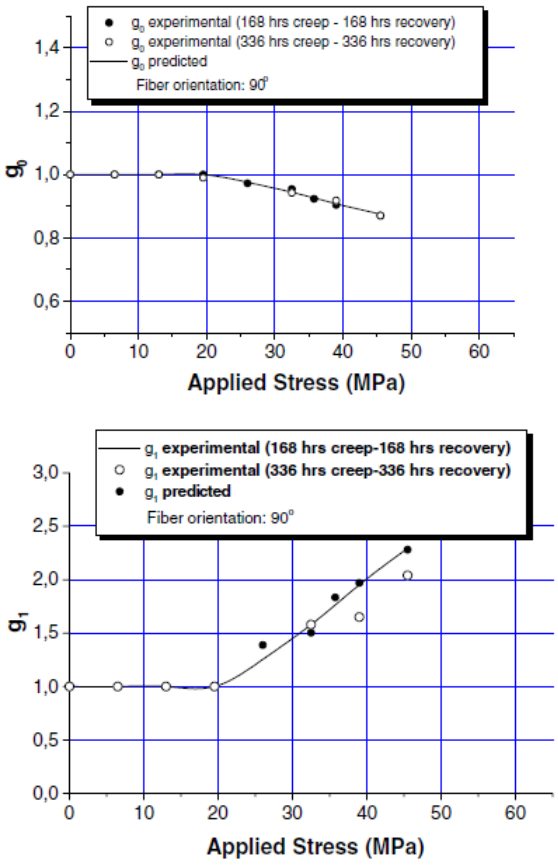

(a)

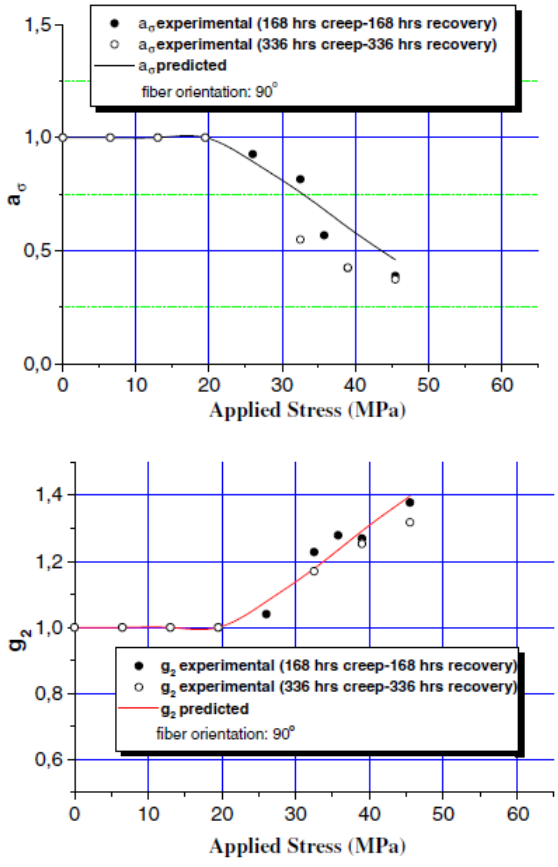

(b)

Figure 1.36 Comparison between the experimental values and the proposed model predictions of the nonlinear factors (a) g_0 and g_1 (b) and a_o and g_2 as a function of stress for the 90º fibre angle specimens [64]

O'brien *et al* [66] recognised the significance of degree of cure on the relaxation rate of the polmer matrix and devised a model capable of determining the cure dependence on shear relaxation modulus, G(t), demonstrated using parallel plate rheometry and 3-point bend creep, Figure. 1.37. They found excellent correlation between model and experimental data.

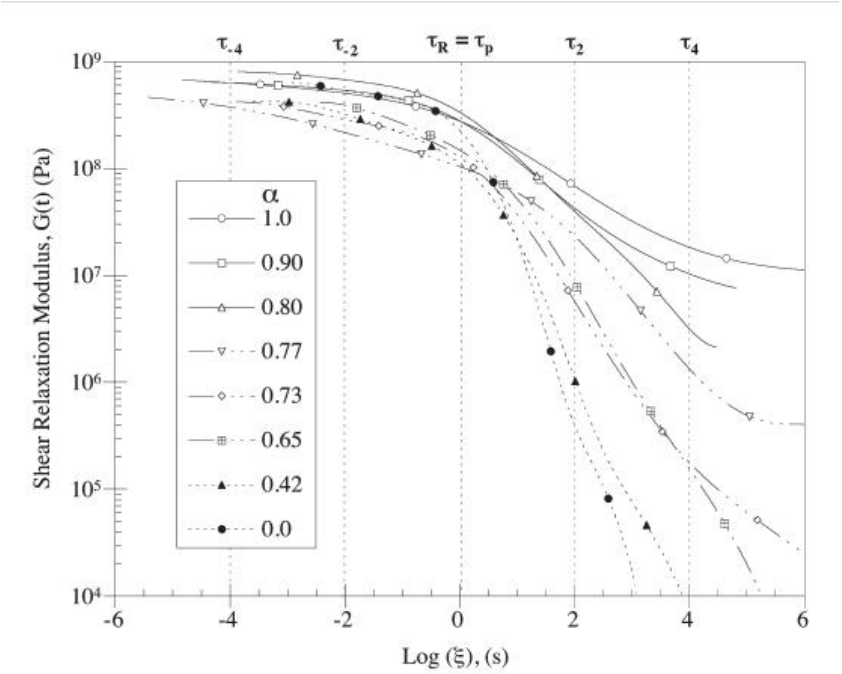

Figure. 1.37, Shear relaxation modulus of EPON 863/W over the entire range of cure after shifting the reference Log (time) axis time

1.8. Applications

1.8.1. Critical aspect ratio for snap-through / bifurcation point

The curing of unbalanced laminates is most likely to result in a cylindrical shape at room temperature, in preference to saddle-shaped deformation predicted by CLT.

Most cylindrical shapes are capable of changing from one stable shape to another, exhibiting a 'bi-stability'. This phenomenon is also referred to as 'snap-through', Figure 1.38, bifurcation point.

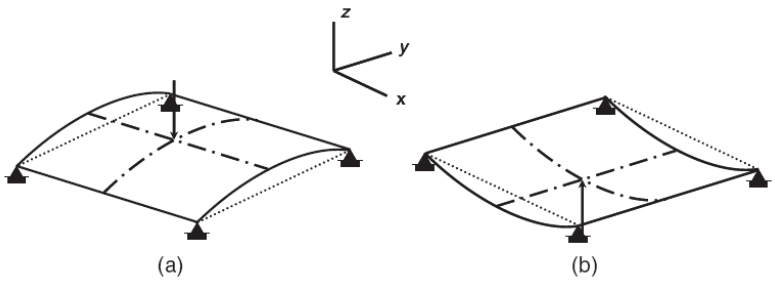

Figure 1.38; Schematic diagram of snap-through for bi-stable unbalanced laminates (Tawfik, 2006) [8].

The 'stablility' of unbalanced laminates has been investigated widely in recent years [8,10,11,13-15].

Hyer et al. [13-15] experimented with differing laminate geometries and studied the resulting cylindrical/saddle-shaped deformations and predicted the critical aspect ratio (AR) for snap-through. Results were not always accurate, although conclusions were drawn that a cylindrical shape is always observed for large side length-to-thickness ratios while a saddle shape is observed for small side length-to-thickness ratios.

Pirrera [32] also investigated the bi-stability of unsymmetrical laminates and found that for a change in temperature close to zero, the only solution is a saddle. At a critical temperature, the saddle becomes unstable and two other stable cylindrical solutions appear.

The majority of snap-through studies are limited to the warping analysis of cross-ply laminates only. Jun *et al.* [11] used multiple angle-ply stacking sequences of T300/5208 graphite/epoxy to investigate the principal direction of curvature according to the length-to-thickness ratios, number of layers and lay-up angles. They found snap-through was always possible in a 45/-45 laminate at a length to thickness ratio of 96, regardless of the number of layers. However, this snap-through ratio is very sensitive to the angle of plies.

Tawfik *et al.* [8] modelled the stability and snap-through ability of 4 ply $(0_2/90_2)_T$ cross-ply laminates (manufactured from Hexcel IM7/8551-7 graphite/epoxy pre-preg) using an extension of CLT in FE ABAQUS^{TM} software [67], in parallel to experimental studies. Specimen aspect ratios (AR) were varied from 1 to 8, with the length constant at 152.4 mm.

They found that a cylindrical shape is observed for large side length-to-thickness ratios while a saddle shape is observed for small side length-to-thickness ratios. In agreement

with Hyer [13-15]. This is a further step to establishing what determines snap through. ARs of 1.0, 1.2, 1.5, 2.0, 3.0 and 6.0 were all shown to snap-through. Figure 1.39, 8.0 did not snap through as predicted analytically.

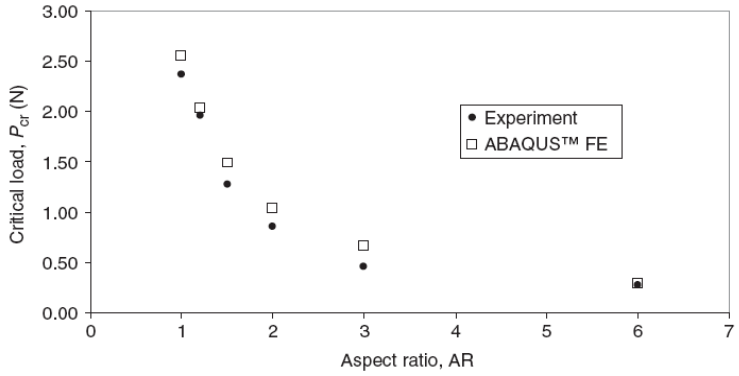

Figure 1.39; Snap-through load as a function of aspect ratio for an asymmetric cross ply laminate ($0_2/90_2$) [8].

Tawfik *et al* [8] found FE modelling an efficient methodology in order to predict the anticlastic behaviour in composites using a commercial finite element code as they generally showed good agreement with experimental data.

Minor discrepancies in snap-through values are thought to be due to differences in loading / boundary conditions effects in experimental versus ABAQUS^{TM} [67]. In the experiment, almost the whole side is sliding against the table in comparison to FE predictions in which corner nodes of the laminate are restricted from moving in the z-direction. This would result in changing frictional effects, changing force and moment resultant distributions within the laminate from those predicted.

Dano and Hyer (1998), [31] developed a static approximate theory for the prediction of snap-through based on assumed forms for the in-plane strain and out-of-plane displacement fields, using the Rayleigh-Ritz technique and virtual work. They showed the snapping force for the graphite-epoxy laminate families of interest ($90_4/0_4$, $-60_4/30_4$, θ-$90_4/\theta_4$, $90-\theta_4/\theta_4$, $-\theta_4/\theta_4$), to depend on the angle between two fibre directions.

Jun and Hong [11] added that in-plane shear strain has a significant influence on the position of the bifurcation point.

These studies indicate the sensitivity of snap-through and bi-stability in unbalanced laminates and demonstrate varied theories to quantify this behaviour.

Clearly many factors have a crucial role affecting the bi-stability of laminated composite structures; from the proposed length-thickness ratios previously suggested to the constraint of aspect ratio [8].

A square laminate (i.e., aspect ratio 1:1) will always snap-through to its reciprocal stable cylindrical shape. In contrast, a thin strip (i.e., a high aspect ratio) will curve into a cylindrical shape in the longer side under thermal curing load but cannot snap-through to its reciprocal cylindrical shape in the shorter side.

The highly anisotropic nature of unbalanced (UB) laminates; the differing resin systems; stacking sequences; thickness; and geometries mean that the idealised snap-through aspect ratio found for one laminate configuration may not be suitable to predict the behaviour of another, making the comparison and prediction of unbalanced laminate properties complex.

2. Summary

This review of the open literature has shown that the room temperature shapes, stability and curvatures of laminates are dependent on many factors, including cure history, constituent properties, ply groupings and position around the laminate midline (stacking sequence), but are dominated by the length to thickness *(l-t)* ratio, mismatch between thermal expansivity (CTE) values of individual plies and quality of interfacial bond between plies.

When large *l-t* ratio laminates are manufactured a cylinder is generated. In comparison, a small *l-t* ratio laminate (L/t <96 [11]) results in a saddle shape, which is in line with classical laminate theory (CLT) predictions. The bifurcation/snap through ability of laminates is dependent on the aspect ratio and *l-t* ratio.

Model extensions of CLT provide a good approximation of 'as cured' curved shapes, providing input parameters (in particular CTE perpendicular to fibre axis, $\alpha 2$) are accurate.

However, as CTE input values are highly dependent on constituent properties, degree of cure, temperature range and fibre alignment, the cure history and effects of variation in CTE input values may need to be considered in further development of models.

In addition, deviations from CLT predicted room temperature shapes and curvatures have been attributed to material inhomogeneities and poor interfacial bonding between plies causing delamination, and/or slippage between plies during curing. This reduces the load transfer between plies during cooling, ultimately affecting the extent of curvature.

Despite the absence of any extensive verification of curvature models between comparable materials and lack of incorporation of many factors affecting input properties (including ageing, time and environment) means that CLT-based model predictions represent largely 'best case' manufacturing, when geometric non-linearities are excluded.

More experimental data are needed to provide appropriate fitting parameters from idealised CLT case to realistic manufacturing situation in order to ascertain the impact of these non-linearities on curvature when compared to linear models.

2.1 Aim

The aim of this project was to identify the factors controlling curvature generation in asymmetric carbon fibre laminates in order to quantitatively describe their behaviour.

2.2 Objectives

Manufacture a range of asymmetric composite laminates in order to quantify the effect of the following variables on curvature and bistability and relate these to a CLT-based model for curvature:

As cured:

- Geometry for UD plies in 0 / 90° stacking;
    - *Thickness*
    - *Aspect Ratio*
- CTE mismatch and shrinkage
    - *Extent of cure*
    - *Laminate constraints*
- Microstructure / Defects
    - *Variations in volume fraction*
    - *Interfacial Adhesion*
    - *Delamination & Voiding*
    - *End constraints*
- Model interfacial conditions
    - *Taking into account slippage between plies, unaccounted for in previous work.*
    - *Strain/Curvature relationship*

Post cure:

- Time, load and environment
    - *Temperature*
    - *Stress Relaxation/Creep under varied loading conditions*

3. Experimental

3.1 Laminate Manufacture

3.1.1 Materials

Composite panels were manufactured from unidirectional (UD) pre-preg. with T800 Toray fibres, (17-19 µm diameter) in a VTM264 or MTM28-1 epoxy matrix [68], Table 3.1.

Table. 3.1, UD Pre-preg information

Roll number	**Pre-preg Material Description**	**Features [68]**	**Tensile Modulus*** (ASTM D3039 Test method) [68]		**Date of prepreg. manufacture (D.O.M)**
			0°	**90°**	
1	VTM 264 / T800	Variable temperature, vacuum processable epoxy system. Typical cure between 65°C/149°F and 120°C/248°F.	131 GPa	9.1 GPa	2005 / 2006
2	MTM 28-1 / T800H	Medium temperature, toughened epoxy system. Typical cure between 85°C/185°F and 160°C/320°F. Recommended cure 120°C/248°F for 1 hour.	127 GPa	8.4 GPa	31/03/2007 (12 month shelf life; 3/2008)
3	MTM 28-1 / T800H				11/03/ 2009

*Modulus data normalised to 55% and 60% vf for VTM and MTM respectively – T700 fibres.

Laminates were fabricated using the vacuum bagging process, Figure. 3.1.

Loctite, Frekote semi-permanent wipe-on-leave-on (WOLO) [69] was used as a release agent for the majority, with release film used for initial panels A1-4, B1-4, C1-4 only.

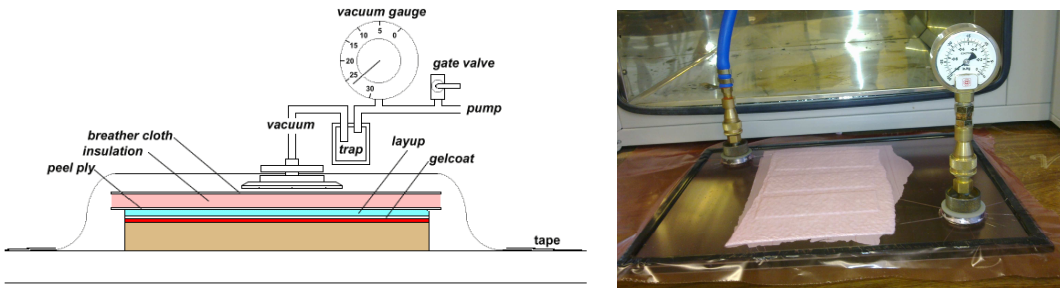

Figure 3.1: Vacuum bagging set-up (adapted from [70]) and image of actual set-up.

Panels of differing aspect ratios and ply stacking sequences were hand laid-up from pre-preg sheets as shown in Appendix I (where 0° is parallel to the panel long axis) and, after evacuation using a rotary pump to a pressure of 88000 - 91000 Pa were cured using the following thermal cycle, Figure 3.2:

1. Heat at 0.5 °C/min. to 125 °C;
2. Hold at 125 °C for 60 min.; and
3. Cool to room temperature at a rate of 3 °C/min..

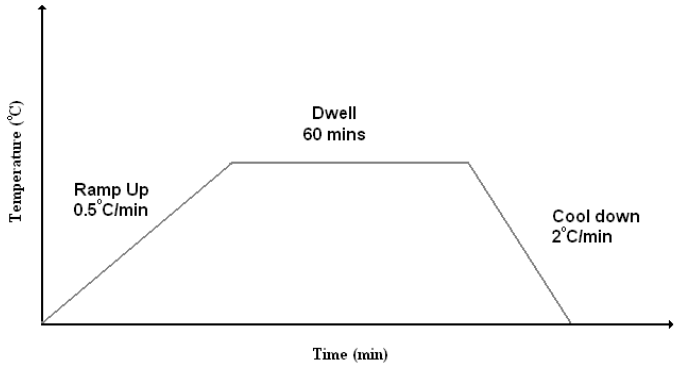

Figure 3.2. Standard curing cycle for MTM28-1,T800H (Advanced composites group).

3.2 Characterisation of laminates

3.2.1 Specimen geometry

Thickness measurements were determined using a combination of both digital callipers (Mitutoyo Series 500; accuracy ±0.02 mm) and micrometer at 8-12 locations around the laminate (3 top, 3 right, 3 left, 3 bottom, Figure 3.3). An average of these measurements was then calculated for use in future equations.

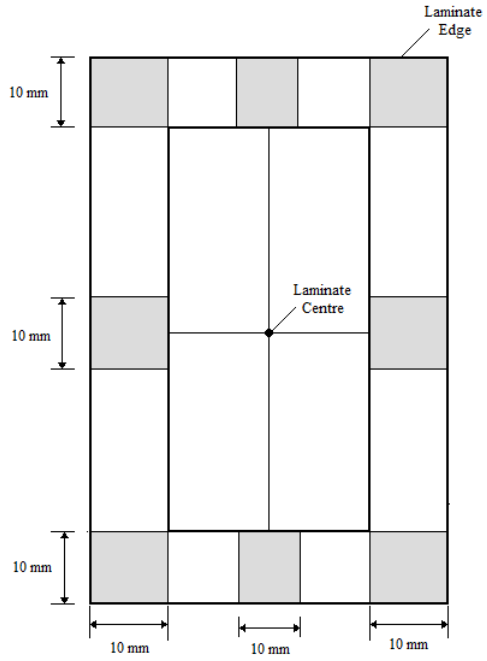

Figure 3.3. Locations of points of thickness measurements for all panels

Length and width dimensions were also assessed using digital callipers (3 length measurements, 3 width measurements) for panels < 145 mm or rulers for panels longer than 145 mm. An average was then determined.

Tables of panel geometries and configurations are given in Appendix I.

3.2.2 Specimen mass and density

Panel masses were measured using digital scales (Electronic Densometer ED-120T) and for density study. For the majority of samples, density was calculated using specimen mass and dimensional data.

3.2.3 Panel curvature

a) Manually

Panel curvature of unbalanced laminates was calculated using Eucludian geometry of a continuous circular arc based on [19], Equation 3.1. Where *h* and *L2*, Figure 3.4, were measured using digital callipers (Mitutoyo Series 500; accuracy ±0.02 mm) or rulers (for panels longer than 145 mm).

Equation 3.1

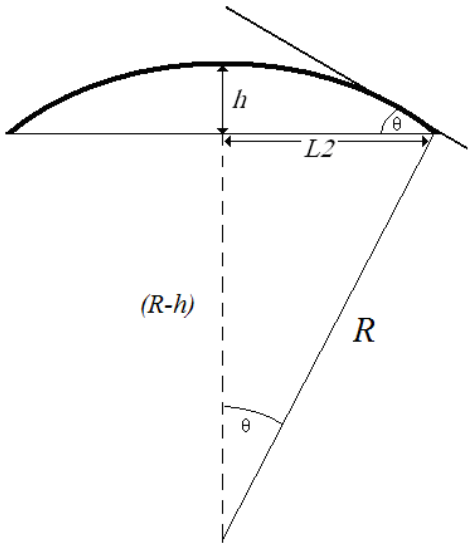

$$\theta \approx \frac{L2}{(R-h)}$$

$$\therefore \quad R = \frac{L2^2}{2h} + \frac{h}{2}$$

Figure 3.4. Schematic diagram of curvature determination (Assuming the specimen is symmetrical, has a large radius, *r*, and *h* << *r*).

b) Laser-based measurement

A non-contact laser scanner (Konica Minolta, at ~0.008 mm accuracy) was used to scan the curve profile over its whole length and radius of all laminates (Figure 3.5) directly comparable to height, length and radius values by manual methods.

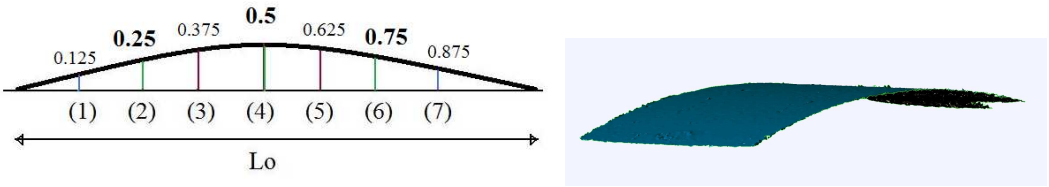

Figure 3.5. (a) Schematic diagram of curve height measurement locations, where '4' is the central point of the laminate (b) laser generated image of curvature.

For 145 x 145 mm square panels, curve profiles were taken in both primary and secondary shapes to compare extent of curvature in both states (Figure.3.6).

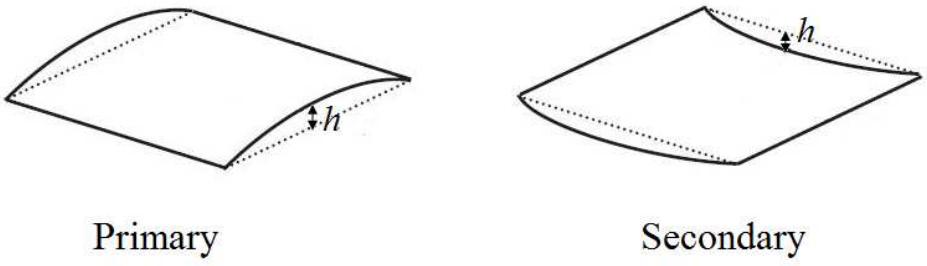

Figure.3.6; Curve profile measurement locations for primary and secondary shapes

3.2.4 Image Analysis

Specimens of fully cured carbon fibre/epoxy composite were sectioned in the transverse plane (Figure 3.7) using a diamond cutting wheel, to produce specimens of 15 x 20 mm approx and mounted in Epofix cold mounting resin (Struers).

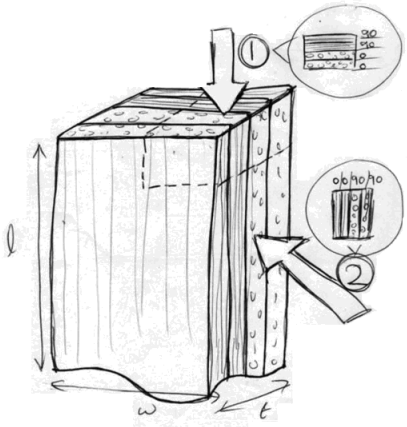

Figure 3.7. Sectioning of laminates in the transverse plane (1).

Specimens were ground briefly using 200, 400, 1200 grade SiC papers and subsequently polished to 6 µm, 3 µm and 1 µm diamond paste finishes.

Specimens were examined using a Leica Axioskop-2 optical microscope with KS400 image capture and analysis software. The structures were quantified in terms of ply thicknesses (at <1 mm intervals) and fibre volume fraction/geometry of the innermost 0 º ply were measured at various intervals along the 15 mm specimen length, at 10x and 100x magnification respectively using methods i and ii (Figure 3.8).

Method i) Fibre v_f variation through laminate thickness, including ply interfaces.
Method ii) Fibre v_f variation within a ply

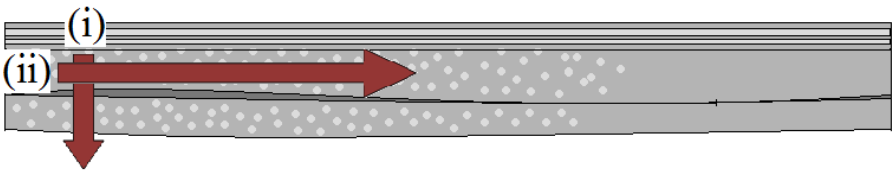

Figure 3.8, Direction of v_f measurement for methods i and ii in a laminate cross-section.

Fibre selection was achieved by enhancing images using contrast/threshold regime and automatic measurement (Figure 3.9). The errors involved as a result of fibre selection miscalculations in the threshold stage due to features such as surface dust particles are as little as ±1.5%. The number, length and location of any voids were also determined where possible.

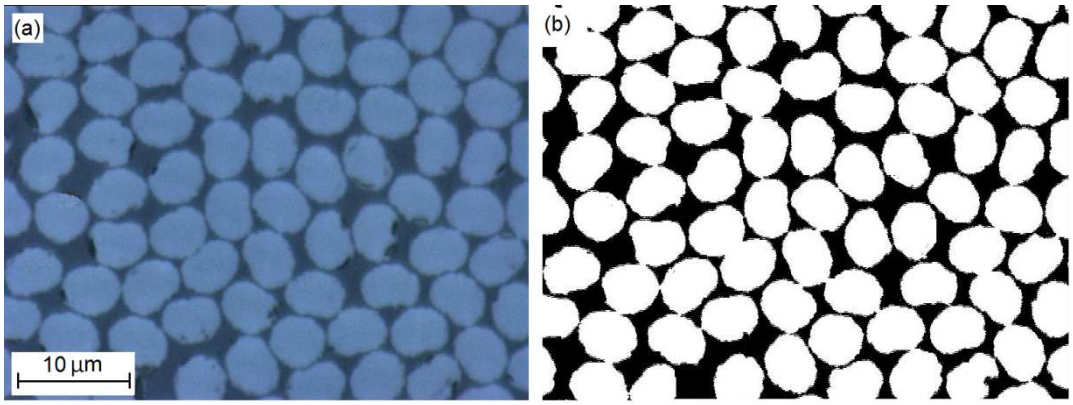

Figure 3.9, Raw image of laminate B6 (a) and subsequent fibre selection (b) at ~60% v_f.

3.2.5. Coefficient of thermal expansion, CTE.

3.2.5.1. UD Laminates, Single plies (Including ICC plies)

Biaxial strain gauges (Kyowa) were bonded to the centre of all single UD ply laminates using strain gauge cement (Kyowa CC-33A), enabling measurement of strain parallel and perpendicular to the fibre axis (Figure 3.10) in either a 0 or 90 degree ply.

Samples were then heated to ~130 ºC at the maximum oven heating rate (~12 ºC/min. for 60 min. pre-cure sample).

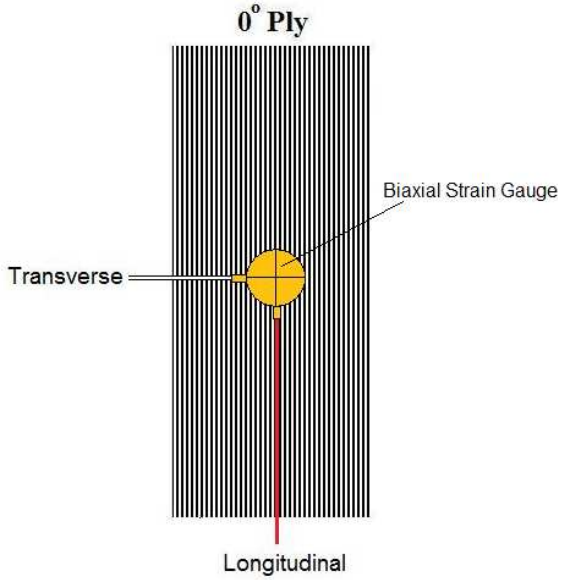

Figure. 3.10; Strain gauge location in relation to fibre axis on 0º unidirectional ply (not to scale).

The CTE of the composite was then calculated using:

Equation 3.2

$$CTE = \frac{\Delta\varepsilon}{\Delta T}$$

over the linear portion of the strain experienced on heating and at 10 º C intervals.
The measured strain was offset to 0 before testing to discount any additional strain added by bonding the strain gauge to the sample.

The CTE of aluminium and steel sheets were also measured for calibration purposes.

3.2.5.2. Unbalanced laminates

For unbalanced laminates, the experimental procedure is identical. The only deviation is the location of the biaxial strain gauge, which is bonded on the 90 degree surface, meaning geometric variations as a result of heating are also measured.

3.2.5.3. Stress free temperature, T_{SF}

In this study, the stress free temperature, T_{SF} of unbalanced laminates is defined by the region where the laminate loses curvature and flattens out on heating to 130 ºC from room temperature. In some cases the T_{SF} is also confirmed visually by filming the heating and cooling of the laminate, matching the strain values.

3.2.6. Differential scanning calorimetry (DSC).

3.2.6.1. Pre-preg. samples

A section of pre-preg. was taken from both an aged*, (Roll 2) and non-aged, (Roll 3) rolls of MTM28-1, punched into 5 mm diameter discs and stacked into masses suitable for power compensation DSC (between 21-25mg), Table 3.2.

* where 'aged' refers to pre-preg. in use for a considerable period of time (up to 12 months of use).

A DSC run (Perkin-Elmer) was then carried out at a rate of 10 º C/min. up to 200 º C, and a re-test was conducted on the aged resin to confirm a full degree of cure.

Table 3.2: DSC Pre-preg sample masses

Pre-Preg		**Mass (mg)**
Aged	MTM28-1/T800H (Roll 2)	21.84
Non-aged	MTM28-1/T800H (Roll 3)	22.57

3.2.6.2. Curing kinetics, degree of cure

The relative degree of cure, α,at time *t* can be calculated according to the cure curve from fractions of the entire exothermic energy (where total energy area, E_{tot} is assumed as 100% cure), as follows:

$$\textit{Percentage Cure, } \alpha = E_t / E_{tot}$$

where, E_t is the energy at time *t*; E_{tot} is the total energy for full cure, assumed at t = 60 minutes.

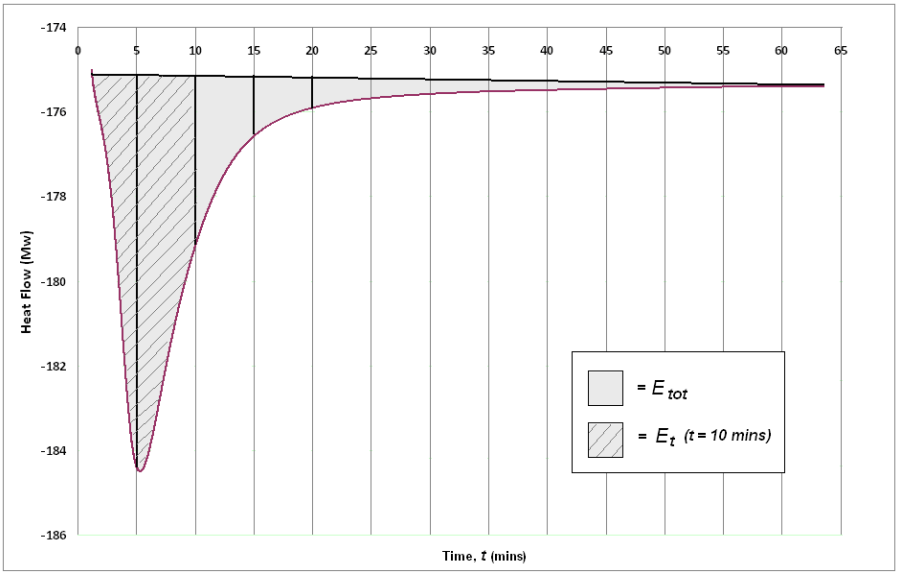

Figure 3.11; Schematic diagram indicating how DSC energy values were used to determine the degree of cure using 10 minutes isothermal hold as an example.

3.2.7. Fourier Transform Infrared Spectroscopy, FTIR

FTIR spectra were determined for pre-cured, ICC and fully cured plies using FT/IR-6300typeA, in order to identify if pre-curing had any effect on material composition/structure.

Tests were conducted using settings detailed in Table 3.3.

Table 3.3. FTIR acquisition details.

	Setting
Light Source	Standard
Detector	Standard
Scanning Speed	2 mm/sec
Resolution	8 cm^{-1}
Data interval	1.92847 cm^{-1}
Gain	16
Accumulation	128
Filter	10000 Hz
Aperture	7.1 mm
Apodization	Cosine

The captured raw data were smoothed and corrected to enable comparison between samples and reduce 'noise'.

3.2.8 Modulus

a) Three point bend testing,simply supported

The static stiffness values for all panels were obtained by a simply supported 3 point bend test, in both concave and convex testing arrangements (Figure 3.12).

Three point bend testing was chosen in preference to four point bend because of the geometrical constraints of the manufactured laminate range.

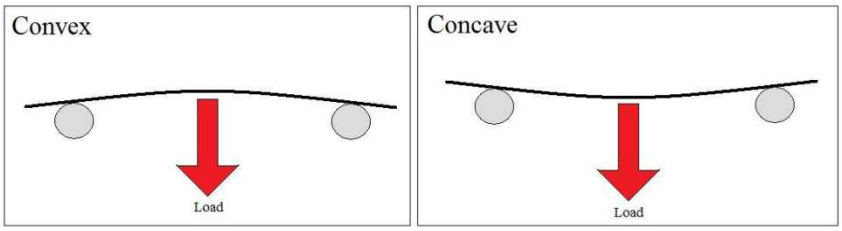

Figure 3.12. Static 3 point bend test in convex and concave orientations

All panels were loaded centrally by up to a maximum of 550 g for > 4 ply laminates and up to 40 g for 2 ply panels in 5 g increments.
The displacement of the loading point was measured using a Solatron C55 displacement transducer.

Stiffness values were then calculated from the slopes of the load - deflection traces.
Modulus values were calculated subsequently using equations appropriate for the experimental set-up [2] Figure 3.13, Equation 3.3.

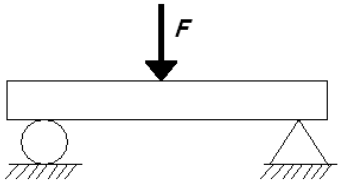

Figure 3.13. Elastic bending of beam

$$E = \frac{F l^3}{48 \delta I}$$

Equation 3.3: [2]

where F = force, l = length of specimen, δ = deflection and I = second moment of area.

b) Three point bend testing, clamped-clamped
Laminate static stiffness values for ICC laminates were obtained by a clamped-clamped 3 point bend test, in the concave testing arrangement (90 degree surface), Figure 3.14.

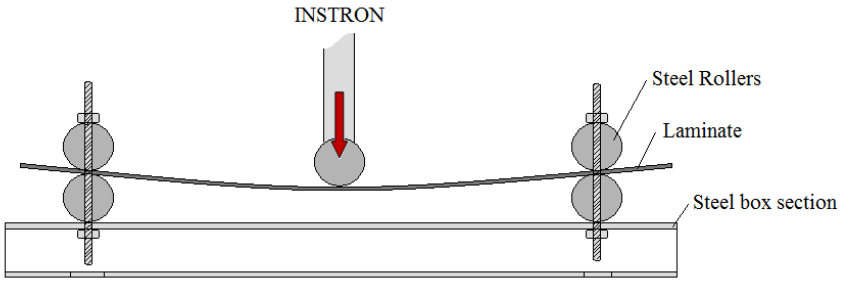

Figure 3.14 Loading condition for unbalanced laminates.

A laminate from each ICC was loaded centrally up to a maximum of 50 N using an Instron 3345 universal tester with a 5 kN load cell.
Stiffness values were then calculated from the slopes of the load - deflection traces.

Modulus values were calculated subsequently using equations appropriate for the experimental set-up [2], Equation 3.4.

$$E = \frac{F l^3}{192 \delta I}$$

Equation 3.4

where F = force, l = length of specimen, δ = deflection and I = second moment of area.

c) Tensile

The stiffness values for 0º single ply ICC samples are obtained by tensile testing 20 x 50 mm UD sections. These sections were taken from 145 x 50 mm ICC single plies, (Figure 3.14 a), with varied cure conditions (detailed in section 3.3.1). Al 'tabs' (15 x 25 mm approx.) are attached to form tensile specimens with 20 mm gauge length, Figure 3.15 b. A similar aluminium sample was also manufactured for data validation.

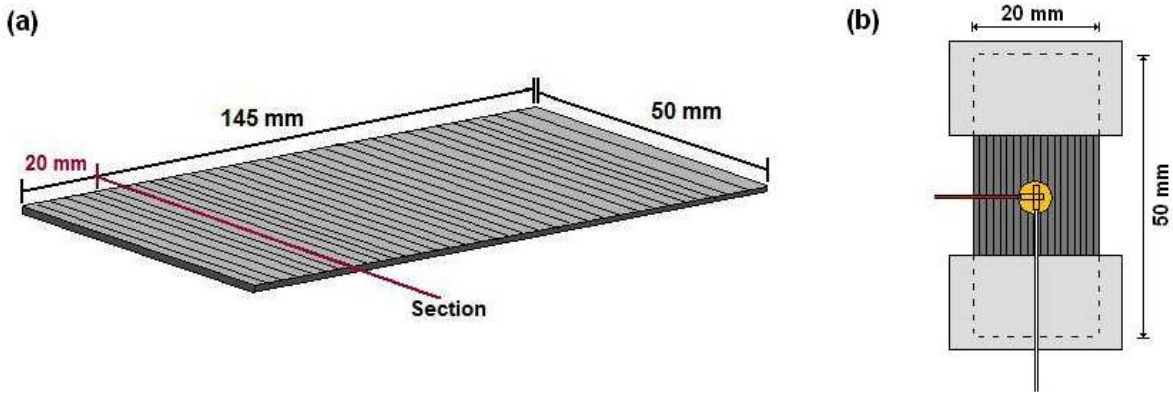

Figure. 3.15, ICC sample section location (a) and tensile (b).

Stiffness values were then calculated from the slopes of the load - deflection traces, obtained using the Instron 3345 universal tester and longitudinal strain values, Poissons ratio values were also calculated using transverse/longitudinal strain relationship.
Longitudinal modulus, E_1 values were calculated using $E_1 = \delta_1 / \varepsilon_1$.

3.3. Pre-curing

Individual plies of 145 x 50 mm 4 ply unbalanced laminates were part-cured for varied times before manually stacking to form a laminate, using the experimental procedures detailed in Table 3.4, Figure 3.16.

For each pre-cure condition (V,W,X,Y,Z & 2,4,6,8,10,12,60) an additional single ply was cut and cured alongside laminate component plies for detailed characterisation.

Table. 3.4, Experimental matrix for all pre-cure experiments, detailing steps 1-4.

<table>
<tr><th colspan="2" rowspan="2">PROCESS STEP</th><th>TRIAL I</th><th>TRIAL II</th><th>TRIAL III</th><th rowspan="2">Pre-cure ply samples 2, 4, 6, 8, 10, 12 & 60 min pre-cure</th></tr>
<tr><th>N,O,R,S,T & U</th><th>V, W, X, Y (a) 1-4 min pre-cure</th><th>V, W, X, Y, Z (b) 2-10 min pre-cure</th></tr>
<tr><td>1. Preparation: Pre-preg defrosted for 1 hour, individual plies cut from pre-preg using a rotary cutting tool.</td><td colspan="3">Proposed top and base plies measured using digital callipers (Mitutoyo).</td><td>N/A</td><td>N/A</td></tr>
<tr><td rowspan="3">2. Pre-cure</td><td>Individual plies arranged on an aluminium sheet</td><td>RT Al sheet. Plastic release material*.</td><td colspan="3">Pre-heated Al sheet. Gloss backing paper release material*.</td></tr>
<tr><td>Ply temperature held at ~125 ºC for varied times (pre-cure)</td><td>Temperature based on oven temperature reading</td><td colspan="3">Ply temperature monitored by thermocouple</td></tr>
<tr><td colspan="4">Plies removed and allowed to cool to RT</td></tr>
<tr><td rowspan="2">3. Geometry & Laminate assembly</td><td colspan="3">Proposed top and base plies measured using digital callipers (Mitutoyo).</td><td>N/A</td><td rowspan="4">N/A</td></tr>
<tr><td colspan="4">Individual plies assembled on glass plate to form a laminate</td></tr>
<tr><td rowspan="2">4. Final Cure</td><td colspan="4">Laminates heated under standard curing cycle** under vac pressure (Between 8600 – 101550 Pa).</td></tr>
<tr><td colspan="4">Oven switched off and laminates allowed to cool to RT</td></tr>
</table>

*Backing paper is used to prevent the carbon fibre pre-preg from adhering to the aluminium (Figure 3.16), in preference to the plastic material used in previous trials which had a tendency to affect the ply surface finish.

**Where ‘standard curing cycle’ refers to the normal curing process for MTM28-1,T800H pre-preg, shown in Figure 3.2.

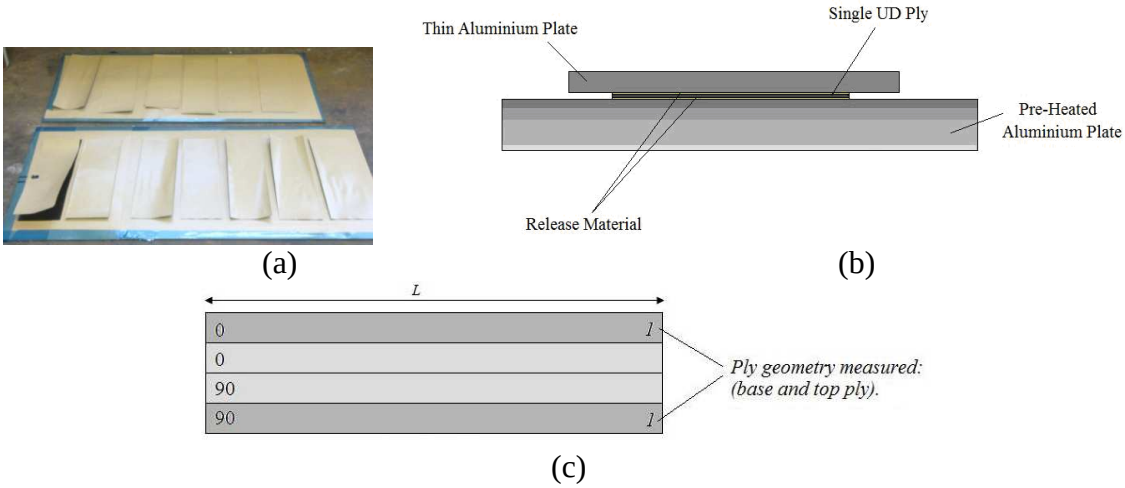

Figure 3.16; (a) Ply arrangement for trials 2 and 3, (b) through-thickness diagram of the experiment set-up and (c) location of base and top plies for measurement (where applicable).

3.3.1. Interrupted cure cycles (ICC)

10 sets of unbalanced 4 ply 145 x 50 mm laminates [0,90] were constructed from MTM28-1,T800 pre-preg using standard cutting, stacking and vacuum bagging techniques.

For each laminate set, the standard curing cycle was interrupted at pre-determined points; A - J , Table 3.5, Figure 3.17 in order to monitor the development of curvature with temperature and cure (Laminate temperature was monitored via thermocouple).

An additional single ply was also cured for future detailed characterisation.

Points at which to interrupt the cure cycle were chosen following examination of DSC traces, which suggested curvature would begin to occur at temperatures ≤100ºC, Tg value (Points D,E,F,G).

At each of these chosen points (A-J), the laminates were removed from the oven and 'quenched' to prevent additional curing that could occur during slow cooling. This was achieved by removing the aluminium plate from the oven and placing it on a thick aluminium block at room temperature covered by a thin layer of water [19]. After the specimen temperature reduced to ~RT, specimens were removed from the vacuum bag ready for subsequent testing.

Table 3.5. Chosen stages to interrupt normal cure cycle.

Laminate Reference	Temperature (ºC)	Time (mins)	Stage	Cooling method
A	70	97	During ramp up to 125 ºC	Quenched
B	80	110		
C	90	137		
D	100	157		
E	110	177		
F	117	192		
G	125	207	End of ramp up, on reaching 125 ºC	
H	125	267	After 60 minute hold at 125 ºC	
I	125	327	After 120 minute hold at 125 ºC extended curing cycle	
J	Room Temperature	.>420	End of standard curing cycle	Standard cooling - no quenching required.

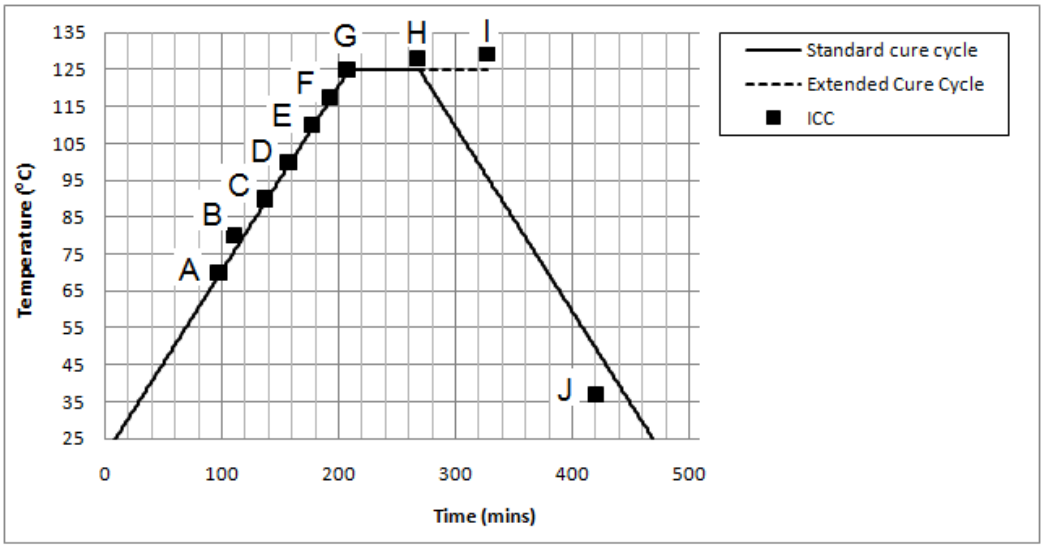

Figure 3.17. Interrupted cure cycles A to J for unbalanced laminates.

3.3.2. Co-curing

A 150 x 50 mm single ply piece was cut from MTM28-1 T800 and exposed to the standard curing cycle (Figure 3.18 a). The fully cured ply was then 'laid up' on lower uncured pre-preg ply, and both plies cut to nominally identical length (145 mm), Figure 3.18 b. The laminate was then subjected to standard curing cycle to create a 2 ply 'co-

cured' laminate, where microscopy of interfacial adhesion/end constraints was carried out, following the image analysis process detailed in section 3.2.4, Figure 3.18 c.

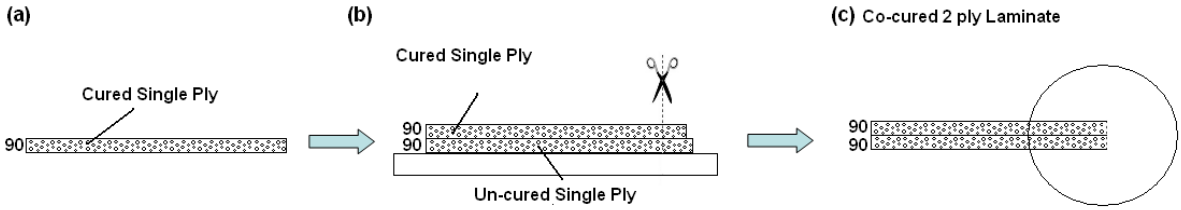

Figure. 3.18, Co-cure laminate methodology, where (c) is the final co-cured laminate.

3.4. Stress relaxation / creep

The curve height of all asymmetric laminates was measured immediately following the standard curing cycle. For selected laminates (N1-3, O1-3, R1, S1, T1, B10, B11, B9, W1, X1, Y1, Z1, Z4 and Y4), the curve height was measured again following a length of time unloaded in ambient temperature environment and then logged. For these laminates, this process was repeated only a couple of times.

For bespoke stress relaxation/creep experiments, the change in central curve height (*h*) of 4 ply 145 x 50 mm laminates as a result of additional loading (laminates 2, 3 & 4: 10, 30 and 49 N, Figure. 3.19) and relaxation of residual stresses (laminate 1: Unloaded) was monitored for >6760 hours / 282 days.

The change in curve height was normalised for comparison between laminates.

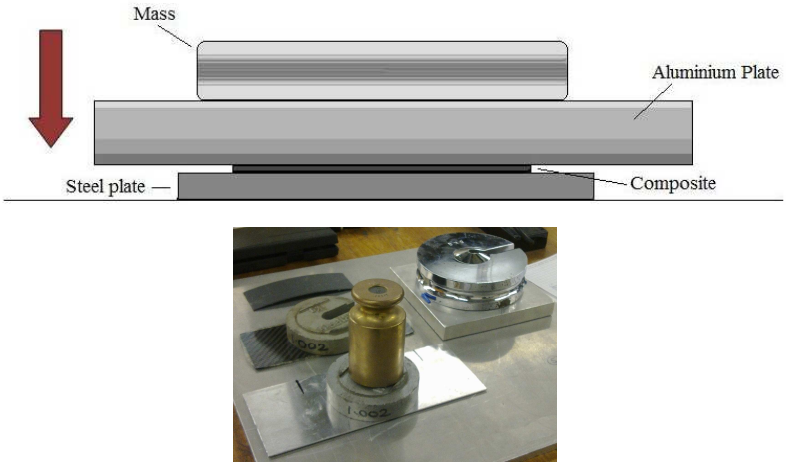

Figure 3.19, loading of composites

3.5 Snap-through / bistability

Specimens exhibiting a ‘bistable’ shape change from primary to secondary positions (snap-through) Figure 3.20, were subjected to point loading at the panel centre to identify the force required for initiation of secondary shape phase.

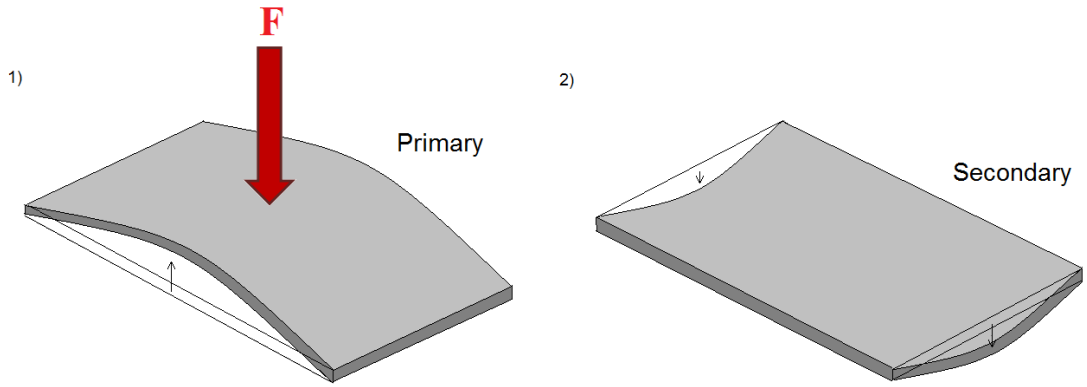

Figure 3.20. Primary and Secondary shapes of bistable laminate. a) Panel sits naturally in primary shape and b) secondary position adopted when loaded centrally

3.5.1. Low temperature testing

A 210 x 170 x 150 mm watertight tank was constructed from 5 mm thick acrylic sheet. Selected laminates (Table 3.6) were simply supported within the tank using a custom made rig, then submerged into an ethanol/liquid nitrogen mix at various concentrations to achieve the desired temperature. Figure. 3.21.

Laminates were loaded at a rate of 5 mm/min. using an Instron 3345 universal tester in 3 point bend set up, Figure 3.21.

Force was applied across the entire width of the laminate centre using a specially made ‘T’ shaped steel loading rig until an adequate load / deflection trace (and ‘snap through’ for unbalanced laminates loaded perpendicular to roller set up, Figure 3.20, 3.23) was achieved.

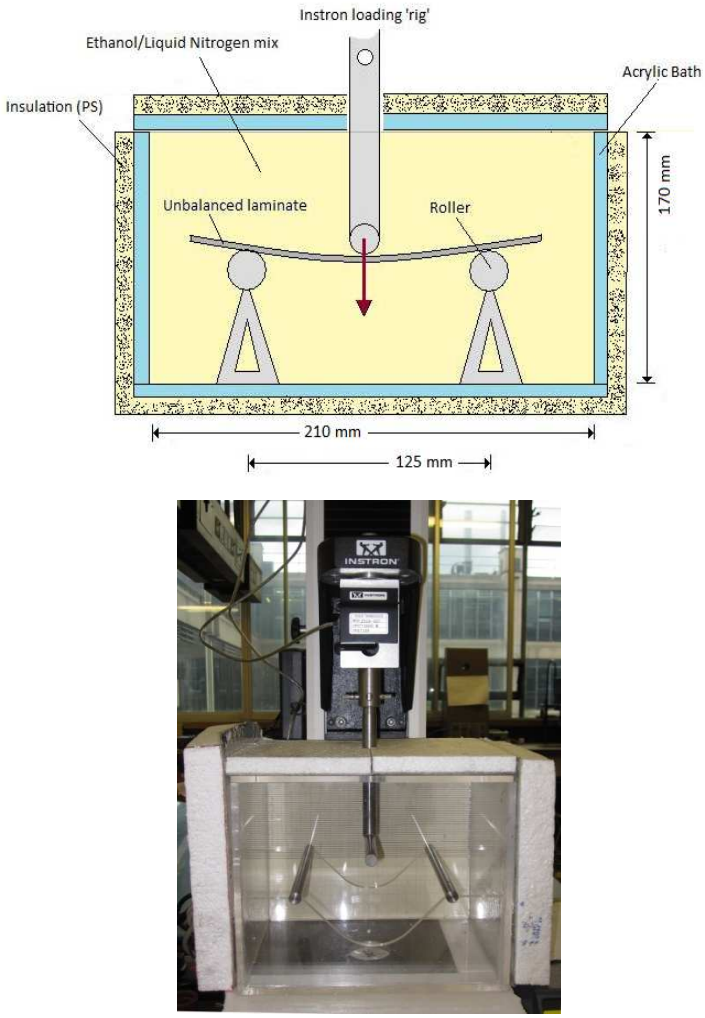

Figure 3.21. Instron test rig and temperature bath set up.

Table 3.6. Testing matrix for temperature experiments.

Laminate Geometry (mm)	**Lay-up**	**Plies**	**Test**	**Test Temperature (□C)**
145 x 50	90° UD	4	Stiffness/Modulus	RT to -30
145 x 50	0° UD	4	Stiffness/Modulus	RT to -30
145 x 145	AR 1: UB, $[90/0]_4$	4	Stiffness/Modulus/ST/Curve height	RT to -30

3.5.2. Modulus

Laminate modulus could then be calculated using Equation 3.3. to give the dependence of modulus [2] on temperature and its subsequent effects on snap through force and curve height for the MTM28-1,T800 carbon/epoxy system.

3.5.3. Snap-through / Curve height

For unbalanced laminates, primary curve height (h) was measured at each temperature via the Instron's deflection (d), using the criterion illustrated below, Figure 3.22.

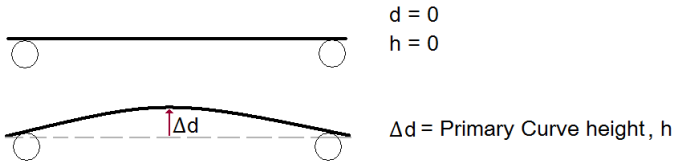

Figure 3.22. Primary curvature height determination.

Initial laminate 'snap through' tests were conducted with the laminates primary curvature parallel to the bend rigs rollers, (case a Figure 3.23), meaning laminates did not experience 'snap through' but instead deflected at the Instrons steady loading rate.

To achieve the 'snap through' phenomenon, laminates were turned through 90° degrees so primary curvature was parallel to the roller set up; Figure 3.21 case b and then loaded until 'snap-through' was achieved.

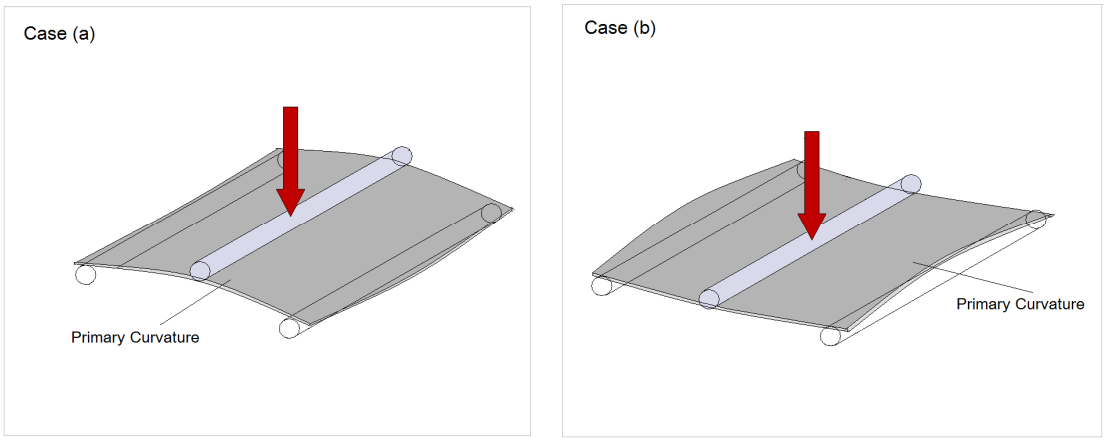

Figure 3.23; Laminate orientation in relation to bend rig roller set-up.

4. Results & Discussion

4.1 Geometry

Actual laminate dimensions are given in Appendix I indicating that length / width values differ slightly from the nominal targets by between 0 and ~1.5 mm.

These length / width variations are due to the method of laminate production, in which individual plies were hand cut from pre-preg sheets. Inevitably there are some geometric variations as a result of blade thickness, ruler positioning and initial marking. However, given the overall size of the laminates, this variation should not have a major affect on measured parameters such as stiffness, contributing a minor 2% length variation for the smallest set of laminates manufactured.

Laminate thickness measurements were found to vary from 0.01 to 0.22 mm around panels, showing a significant through-thickness variation, Figure. 4.1.

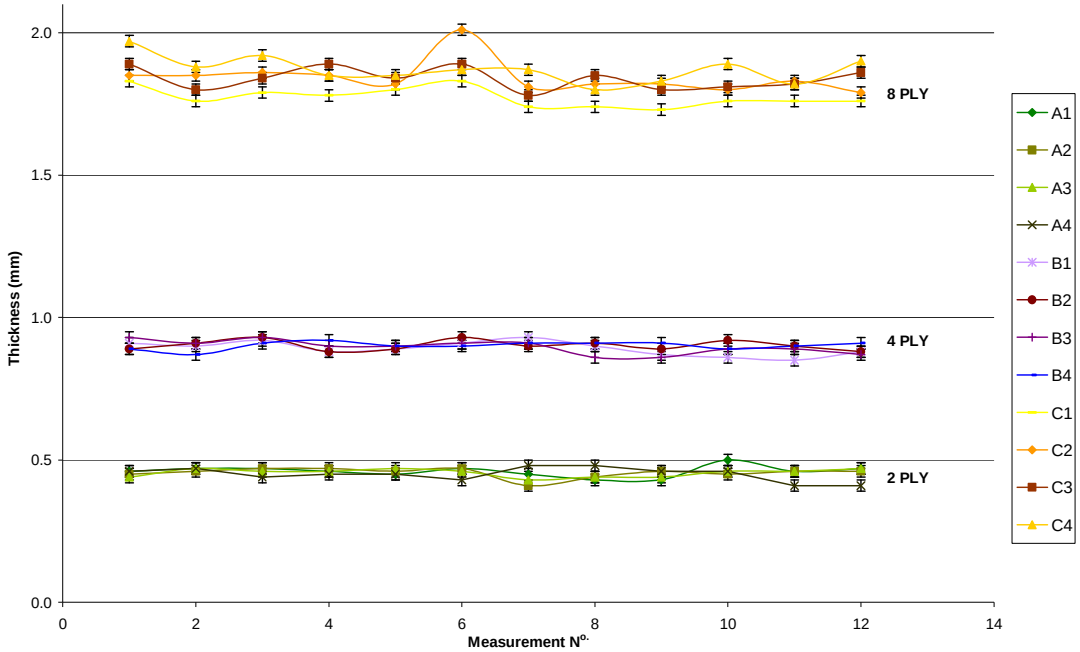

Figure. 4.1, Variation in thickness values for 2, 4 and 8 ply laminates.

This variation is manifested in average thickness values for laminates with the same number of plies. For thicker laminates, this variation is relatively minor, 12% at extreme variation of 0.22 mm. In contrast, thinner laminates would be more severely affected by this variation, with the thickness varying 25%.

These laminate variations represent the baseline scatter for nominally identical materials, vacuum pressure and curing cycle.

The scatter was partly ascribed to variations in achieved vacuum pressure (33850 Pa), which should be small; the release fabric used creating an undulating surface; and variations in initial pre-preg thickness (142-202 µm). As a result, differential flow of the resin during curing gave a varied volume fraction of fibres creating resin-rich regions arranged in a repeated 'pattern' (identified in Figure 4.2 a,b). The irregular fibre distribution from pre-preg manufacture could have contributed to this differential flow. This effect is not seen for all laminates as individual plies were cut from different sections of the pre-preg rolls.

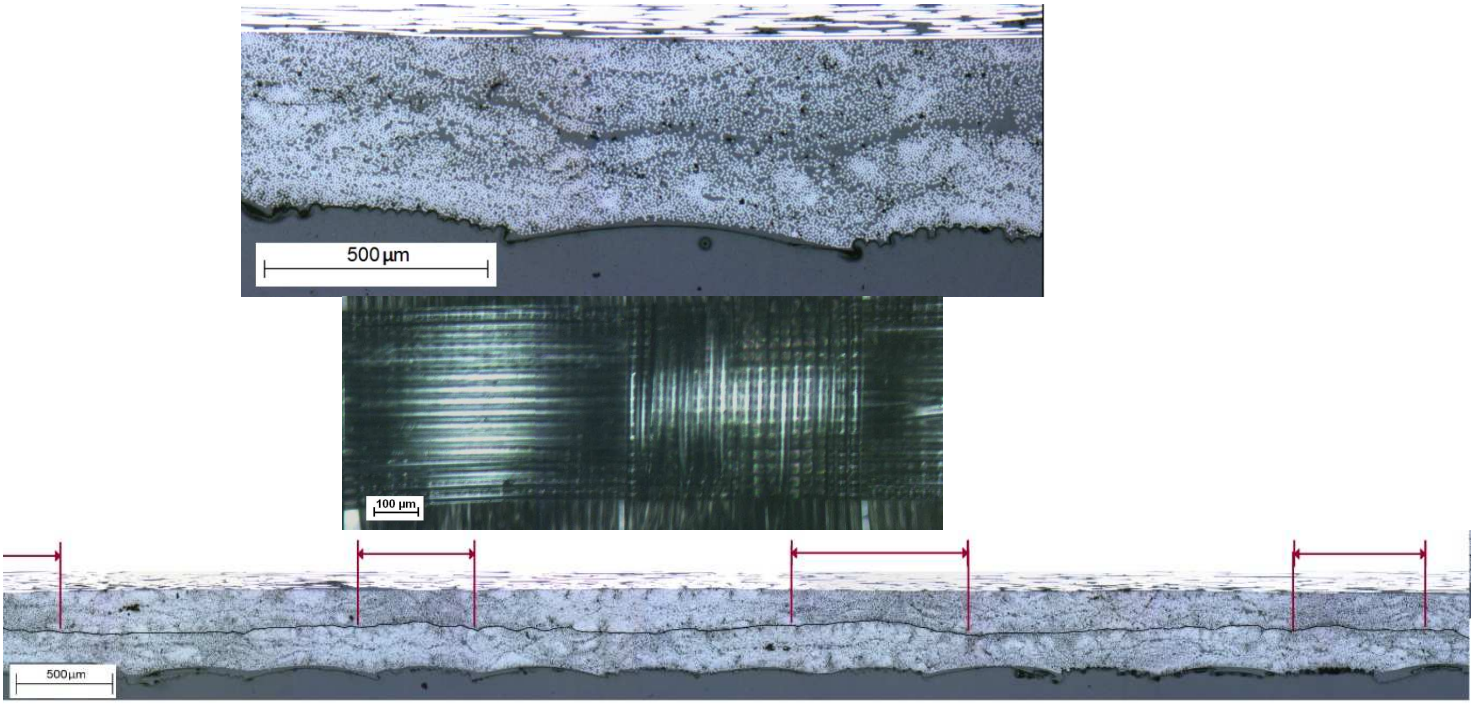

Figure 4.2. Sections of laminate U1 showing (a) detailed undulating surface due to release fabric (b) with (c) regularity of low v_f regions in the central plies, indicated by arrows.

Despite the scale of measured variations in volume fraction, v_f (28 % in resin-rich regions in comparison to fibre-rich areas at 65%), generally, regions with a low v_f are adjacent to areas of high v_f, so that variation in fibre volume fraction should be averaged out on the scale of the property measurements made during this study, giving overall behaviour for a v_f ~50 % for all MTM28-1, T800 pre-preg. laminates.

4.1.1 Initial Curvature

The effect of geometry on panel curvature has been tested using panels of identical stacking sequence but differing in nominal length and width. Grouped nominal laminate geometries are presented in Table. 4.1. Further detailed tables of laminate geometries achieved can be found in Appendix I.

Table 4.1. Range of Asymmetric Laminate Geometries Studied

Length x Width (mm)	**N^{o} of plies**
145 x 50 mm	2, 4, 8
145 x 73	
145 x 97	
145 x 90	
145 x 121	
145 x 145	
185 x 90	
185 x 50	
135.9 x 135.9	
126.88 x 126.88	
108.75 x 108.75	
90.63 x 90.63	
85 x 85	
73.72 x 73.72	4

Radius of curvature values achieved (calculated from experimental measurements, Section 3.2.3) for all unbalanced laminates cured under standard curing conditions (detailed in Section 3.1.21) are discussed in the following sections.

Radius of curvature variation with panel thickness

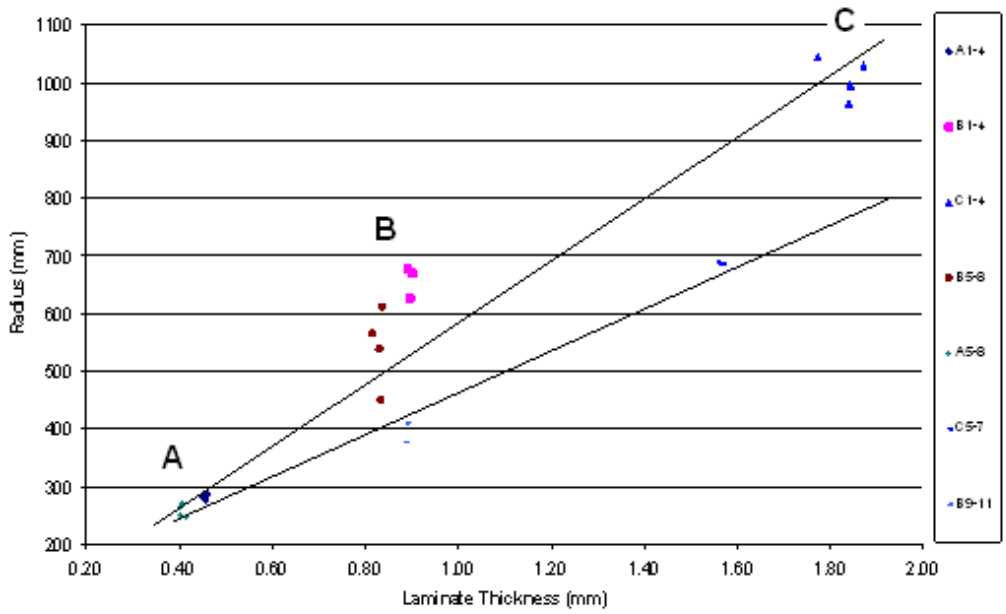

Figure 4.3: (a) Laser curvature results for A, B and C laminates with identical nominal length and width, 145 x 50 mm (±0.02 mm) manufactured by vacuum bagging under standard curing conditions.

In Figure 4.3, laminates A to C have the same nominal length and width values and ratio of 0º and 90º plies. Therefore, the increase in radius of curvature from the A to C series represents an approximately linear dependence of upper surface radius of curvature on panel thickness as l/t ratio decreases from 93 to 337 (for 8 ply to 2 ply laminates respectively). This is in contrast to Tsai and Hahn [3], who state that the strain-displacement relations cannot be taken to be linear due to the magnitude of out-of-plane displacements of RT shapes being many times the laminate thickness.
The investigation of the strain / curvature relationship is investigated further in the following section.

4.2 Base Behaviour; Strain/Curvature Relationship

Epoxy resins experience a reduction in volume as a result of curing during heating and isothermal dwells (Section 1.4). However, when bonded to adjacent plies and formed under vacuum pressure, plies may be constrained and their shrinkage behaviour modified.

In addition to curing volume changes, asymmetric composite structures have plies with different CTE values sandwiched together. As a result, when temperature excursions occur, plies expand and contract differently, which can lead to the coupling of forces and residual stresses causing warpage / curvature of laminates.
In balanced, symmetric laminates the variations in these properties from one ply are countered by the balancing ply so that distortion is minimised.

In general, the presence of the fibres in the 0° plies means that the shrinkage on curing and CTE values for this orientation are much smaller than those for the 90° plies. During curing the 90° plies will try to shrink more than the 0° plies, whilst, during cooling after curing, the greater CTE of the 90° plies will cause greater contraction than that experienced by the 0° plies. This means that the centre of curvature is towards the 90° ply side of the laminate. As all radius of curvature values were determined with the laminate centre as its highest point the orientation would have the 90° plies towards the bottom of the laminate and the 0° plies uppermost, Figure 4.4. The physical model below illustrates the generation of curvature assuming that it arises from a fixed strain in the 90° ply/plies, contracting and pulling the (largely) fixed length 0° plies into a circular arc (Figure 4.4).

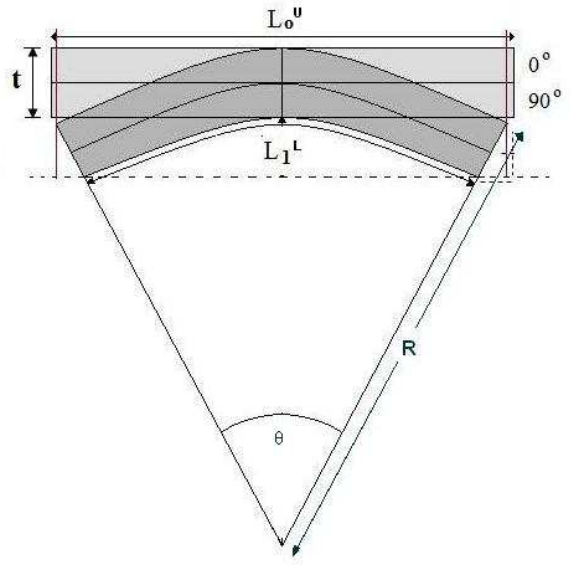

Figure.4.4; Schematic diagram of curvature generation in a 0/90 CFC laminate; where: L_0^U is the initial length of the upper 0º ply, L_1^L is the internal curvature after cure and cooling of lower 90º ply, L_0^L, and t = laminate thickness.

In the unconstrained condition the 0° and 90° plies would adopt different lengths and the resulting laminate curvature depends how these are modified by the constraint applied during curing and cooling. To elucidate the behaviour in the system studied, four extremes have been considered theoretically, whilst assumptions are made regarding the starting state.

4.2.1. Heating stage

The pre-preg plies can be measured prior to heating, although thermal expansion would be expected to alter the length during this stage. During heating the matrix resin is lightly cross-linked and, as temperature rises, enters a low viscosity phase.

In the analysis considered here, it is assumed that these variations can be neglected, especially considering the scatter in results shown in Figure 4.3. The plies are therefore considered to be aligned correctly and of equal length at the start of the curing stage, Figure 4.5. The data presented in Figure 4.3 are for longitudinal curvature and, in analysing this, the following lengths are defined, Figure 4.5.

The initial lengths of the upper (0°), lower (90°) and neutral axis (interface) are defined as L_0^U, L_0^L *and* L_0^N respectively. After curing and cooling these lines will have lengths L_1^U, L_1^L *and* L_1^N respectively, Figure 4.4.

4.2.2. No interface slippage during the cure

Assuming that the 90 º ply is constrained by the adjacent 0 º ply and no separation of the interface between the differently oriented plies (slippage) occurs during isothermal dwell, plies are continuous at mid plane, as shown by Figure 4.4. In this analysis the 0° and 90° plies are assumed to be locked together at the interface from the start of the cure cycle. If the plies were unconstrained then their contractions would be determined by (i) shrinkage during the cure and (ii) post-cure cooling. In the unconstrained condition these values will be:

$$L_1^U = L_0^U\left(1-\varepsilon_{Cure}^0\right)\left(1-\alpha_{CTE}^0\,\Delta T\right)$$
$$L_1^L = L_0^L\left(1-\varepsilon_{Cure}^{90}\right)\left(1-\alpha_{CTE}^{90}\,\Delta T\right) \qquad \text{Equations 4.1}$$

where: ε_{Cure}^0 *and* ε_{Cure}^{90} are the strains during the isothermal cure cycle and α_{CTE}^0 *and* α_{CTE}^{90} are the linear (assumed) coefficients of thermal expansion for the 0° and 90° plies respectively. ΔT is the temperature difference between the isothermal curing

temperature and room temperature (when radius of curvature measurements were made).

The 0° plies should resist curvature deformation more than the 90° plies due to the greater modulus of the fibres and hence the former plies are expected to be closest to their unconstrained behaviour with the latter adapting their dimensions to accommodate the stiffer plies. Thus, the two cases considered here are for the lower surface to be at the unconstrained length of the 90° ply and the unconstrained length of the 0° plies to be at (a) the uppermost surface or (b) at the interface.

(a) Application of Equations 4.1 with L_1^U being at the upper surface to the geometry in Figure 4.4 gives:

$$L_1^U = R\theta$$

$$L_1^L = (R-t)\theta$$

$$\theta = \frac{L_1^U}{R} = \frac{L_1^L}{(R-t)}$$

$$\frac{L_0^U\left(1-\varepsilon_{Cure}^0\right)\left(1-\alpha_{CTE}^0\,\Delta T\right)}{R} = \frac{L_0^L\left(1-\varepsilon_{Cure}^{90}\right)\left(1-\alpha_{CTE}^{90}\,\Delta T\right)}{(R-t)} \qquad \text{Equations 4.2}$$

$$(R-t)\left(1-\varepsilon_{Cure}^0\right)\left(1-\alpha_{CTE}^0\,\Delta T\right) = R\left(1-\varepsilon_{Cure}^{90}\right)\left(1-\alpha_{CTE}^{90}\,\Delta T\right)$$

$$R = \frac{\left(1-\varepsilon_{Cure}^0\right)\left(1-\alpha_{CTE}^0\,\Delta T\right)}{\left(1-\varepsilon_{Cure}^0\right)\left(1-\alpha_{CTE}^0\,\Delta T\right) - \left(1-\varepsilon_{Cure}^{90}\right)\left(1-\alpha_{CTE}^{90}\,\Delta T\right)}\,t$$

(b) If L_1^U is the length value at the interface then the situation is:

$$L_1^U = \left(R-\frac{t}{2}\right)\theta$$

$$L_1^L = (R-t)\theta$$

$$\theta = \frac{L_1^U}{\left(R-\frac{t}{2}\right)} = \frac{L_1^L}{(R-t)}$$

$$\frac{L_0^U\left(1-\varepsilon_{Cure}^0\right)\left(1-\alpha_{CTE}^0\,\Delta T\right)}{\left(R-\frac{t}{2}\right)} = \frac{L_0^L\left(1-\varepsilon_{Cure}^{90}\right)\left(1-\alpha_{CTE}^{90}\,\Delta T\right)}{(R-t)} \qquad \text{Equations 4.3}$$

$$(R-t)\left(1-\varepsilon_{Cure}^0\right)\left(1-\alpha_{CTE}^0\,\Delta T\right) = \left(R-\frac{t}{2}\right)\left(1-\varepsilon_{Cure}^{90}\right)\left(1-\alpha_{CTE}^{90}\,\Delta T\right)$$

$$R = \frac{\left(1-\varepsilon_{Cure}^0\right)\left(1-\alpha_{CTE}^0\,\Delta T\right) - \frac{1}{2}\left(1-\varepsilon_{Cure}^{90}\right)\left(1-\alpha_{CTE}^{90}\,\Delta T\right)}{\left(1-\varepsilon_{Cure}^0\right)\left(1-\alpha_{CTE}^0\,\Delta T\right) - \left(1-\varepsilon_{Cure}^{90}\right)\left(1-\alpha_{CTE}^{90}\,\Delta T\right)}\,t$$

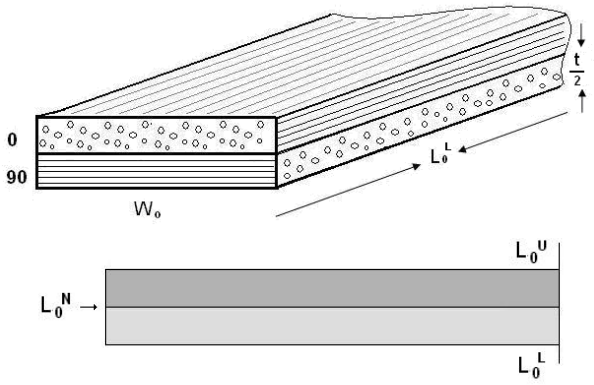

Figure.4.5; Assumed initial lengths of the upper (0°), lower (90°) and neutral axis (interface) at start of cure cycle for no slippage during curing, L_0^U, L_0^L *and* L_0^N respectively.

4.2.3. Complete slippage at the interface during the cure

As noted above, during part of the isothermal cure step the matrix resin is in a low viscosity state and so the plies can be assumed to move relative to one another during this stage as curing shrinkage occurs. This is equivalent to the plies not being locked together until after the curing shrinkage has occurred. The assumed condition at the start of the cure is then as shown in Figure 4.6, where contact between the plies is only over a length of $L_{SC}^L = L_{SC}^N$ the lower ply and interface lengths at the start of cooling (SC). Curvature generation is just due to differential thermal contraction on cooling.

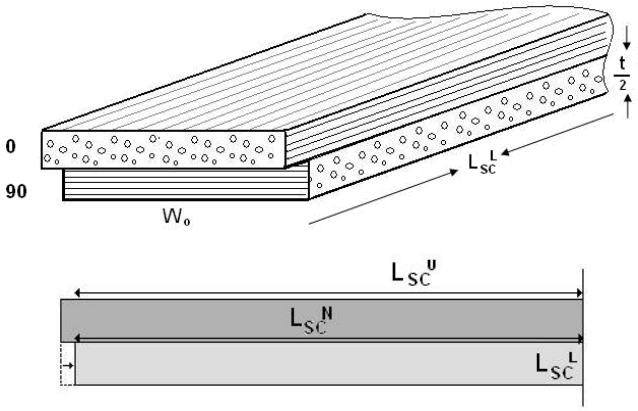

Figure.4.6; Assumed laminate geometry of the upper (0°), lower (90°) and neutral axis (interface) at start of cooling cycle for complete slippage during curing, $L_{SC}{}^U$, $L_{SC}{}^L$ *and* $L_{SC}{}^N$ respectively.

As for the situation where no slippage occurred during curing, the lower surface is assumed to be that of the unconstrained 90° plies after cooling, whilst the unconstrained 0° plies corresponds to (a) the interface of (b) the upper surface.

(a) The easier situation to model is that where the contact area between the two orientation plies shrinks from L_{SC}^{L} to L_{1}^{U}. For this situation, then:

$$L_{SC}^{L} = L_{SC}^{N} = L_{0}^{L}\left(1-\varepsilon_{Cure}^{90}\right)$$
$$L_{1}^{L} = L_{SC}^{L}\left(1-\alpha_{CTE}^{90}\Delta T\right)$$
$$L_{1}^{N} = L_{SC}^{N}\left(1-\alpha_{CTE}^{0}\Delta T\right)$$
$$L_{1}^{L} = (R-t)\theta$$
$$L_{1}^{N} = \left(R-\frac{t}{2}\right)\theta$$
$$\theta = \frac{L_{1}^{N}}{\left(R-\frac{t}{2}\right)} = \frac{L_{1}^{L}}{(R-t)}$$
$$(R-t)\left(1-\alpha_{CTE}^{0}\Delta T\right) = \left(R-\frac{t}{2}\right)\left(1-\alpha_{CTE}^{90}\Delta T\right)$$
$$R\left(\left(1-\alpha_{CTE}^{0}\Delta T\right)-\left(1-\alpha_{CTE}^{90}\Delta T\right)\right) = t\left(\left(1-\alpha_{CTE}^{0}\Delta T\right)-\frac{1}{2}\left(1-\alpha_{CTE}^{90}\Delta T\right)\right)$$
$$R = \frac{\left(\left(1-\alpha_{CTE}^{0}\Delta T\right)-\frac{1}{2}\left(1-\alpha_{CTE}^{90}\Delta T\right)\right)}{\left(\left(1-\alpha_{CTE}^{0}\Delta T\right)-\left(1-\alpha_{CTE}^{90}\Delta T\right)\right)}t$$

Equations 4.4

(b) The situation where L_{1}^{U} corresponds to the uppermost surface is more complicated as the contraction could be spread over a greater length than just that corresponding to the ‘locked-in’ interfacial contact area. However, assuming that the 0° ply is rigid enough for this to be ignored then the geometry in this case is:

$$L_{SC}^{L} = L_{SC}^{U} = L_0^{L}\left(1-\varepsilon_{Cure}^{90}\right)$$
$$L_1^{L} = L_{SC}^{L}\left(1-\alpha_{CTE}^{90}\,\Delta T\right)$$
$$L_1^{U} = L_{SC}^{U}\left(1-\alpha_{CTE}^{0}\,\Delta T\right)$$
$$L_1^{L} = (R-t)\theta$$
$$L_1^{N} = R\theta$$ Equations 4.5
$$\theta = \frac{L_1^{N}}{R} = \frac{L_1^{L}}{(R-t)}$$
$$(R-t)\left(1-\alpha_{CTE}^{0}\,\Delta T\right) = R\left(1-\alpha_{CTE}^{90}\,\Delta T\right)$$
$$R\left(\left(1-\alpha_{CTE}^{0}\,\Delta T\right)-\left(1-\alpha_{CTE}^{90}\,\Delta T\right)\right) = t\left(1-\alpha_{CTE}^{0}\,\Delta T\right)$$
$$R = \frac{\left(1-\alpha_{CTE}^{0}\,\Delta T\right)}{\left(\left(1-\alpha_{CTE}^{0}\,\Delta T\right)-\left(1-\alpha_{CTE}^{90}\,\Delta T\right)\right)}\,t$$

All situations predict a linear relationship between radius of curvature and laminate thickness for constant CTE values. This correlates with the linear relationship observed in Figure 4.3.

The relationships above are for the longitudinal curvature. In the transverse orientation, the width (w_o) of the 90º plies is assumed not to change on cooling because of the orientation of the fibres within the ply constraining shrinkage in that axis.

There will be some small change in thickness as the post cure volume of 90 º ply (after dwell but before cooling) will be given by:

$$Post\ cure\ volume = L_{SC}^{L}\,w_0\,t_{SC} = L_0^{L}\,w_0\,t\left(1-\varepsilon_{Cure}^{90}\right)^2$$

where $L_{SC}^{L} = L_0^{L}\left(1-\varepsilon_{Cure}^{90}\right)$ and $t_{SC} = t\left(1-\varepsilon_{Cure}^{90}\right)$ Equations 4.6

On cooling the final volume will be further reduced as:

$L_{SC}^{L} \rightarrow L_1^{L} = L_{SC}^{L}\left(1-\alpha_{CTE}^{90}\,\Delta T\right)$, $t_{SC} \rightarrow t_1 = t_{SC}\left(1-\alpha_{CTE}^{90}\right)$ and $w_0 \rightarrow w_1 = w_0\left(1-\alpha_{CTE}^{0}\right)$.

Equations 4.7

These alter the final volume, but the effects of thickness variation on radius of curvature are within experimental scatter and so these changes were not factored into Equations 4.2 – 4.5.

Model assumptions:

The following factors are not accounted for within the models above. The significance of these missing variables will become more apparent in later application of models.

- Strain gradients (Section 4.5.1.3)
- Variations in starting condition due to aging of pre preg (Section 4.4)
- Manufacturing variables (Section 4.4)

4.3 Model validation

The material data that are required for validation of the various models against the experimental data in Figure 4.3 are the curing shrinkage strains and the CTE values for both 0° and 90° plies. Attempts were made to measure the shrinkage values for single plies, but the errors associated with these were too high for the values to be reliable. Therefore, literature values were taken for the curing shrinkage. For epoxy resin the shrinkage on curing is reported as 3 – 4 %, Section 1.4 [18,39-41].

For the 90° plies with a v_f value of around 0.55 then the strain on curing was taken as 0.02 (2 %). The curing strain in the 0° plies would be much less and a nominal value of 0.002 was used.

CTE values were determined from unidirectional 4 ply laminates P & Q using biaxial strain gauges to give both longitudinal and transverse CTE values from room temperature (20 °C) to 120 °C of MTM28-1/T800H pre-preg material.

The experimentally determined CTE values are summarised in table 4.2.

Table 4.2. Coefficient of thermal expansion for 90º and 0º 4 ply UD carbon fibre composites P&Q (Pre-preg. Roll 3).

		Ave. CTE x10^{-6} K^{-1}	
	Measurement axis (relative to fibre)	**Laminate 1**	**Laminate 2**
0º Laminate	**Perpendicular**	35.4	23
	Parallel	2.2	0.4
90 º Laminate	**Perpendicular**	30.5	29.2
	Parallel	1.8	0.7

Curing was carried out at 125 °C, whilst radius of curvature values were measured at 20 °C giving a ΔT value of 105 K. Using this, and the values above in Equations 4.2 – 4.5 gives the expected radius of curvature dependence on laminate thickness as shown in Table 4.3.

Table 4.3 Model predictions of radius of curvature (R) dependence on laminate thickness (t) for the four sets of assumptions (where $\alpha 0$ and = 0.7 and $\alpha 90$ = 29.2 $^{x10\text{-}6\ ºC\text{-}1}$ t=0.85) along with experimental relationships from Figure 4.3.

Conditions	***R*/*t***
No slippage during curing – unconstrained 0° ply length at upper surface (Equations 4.2)	40
No slippage during curing – unconstrained 0° ply length at interface (Equations 4.3)	20
Complete slippage during curing – unconstrained 0° ply length at interface (Equations 4.4)	141
Complete slippage during curing – unconstrained 0° ply length at upper surface (Equations 4.5)	281

Experimental values for upper line (Figure 4.3)	536
Experimental values for lower line (Figure 4.3)	367

Comparison of the predicted and experimental values indicates that the radius of curvature values determined experimentally are too large to be consistent with locking in of the plies at the start of the cure and so would indicate that the curvature in the systems studied here is dominated by CTE mismatch on cooling.

4.4 Experimental Deviations from model assumptions and model limitations

The agreemment between the lower trend line in Figure 4.3. and Equations 4.5 is very good, although the upper trend line in Figure 4.3 has a larger slope than any of the predictions. This may arise from the use of older pre-preg that does not cross-link to the same extent leading to a reduced difference in CTE and so larger radius of curvature values. This would have also reduced the shinkage during the cure and so this possibility needs to be investigated.

4.4.1 CTE with cure

Initial model curvature predictions were calculated using CTE values of 29.2 x10^{-6} K^{-1} from values attained from fully cured UD 4 ply laminates. This is appropriate for composites that had been exposed to a temperature of 110 °C or greater (for the pre-pregs in this study), Figure 4.8. Lower temperatures do not achieve full cross-linking, Section 4.4.5, and so result in lower CTE values for the 90° plies. The CTE values for the 0° plies are much less dependent on the matrix CTE value and so the effect of incomplete curing on these would be less. Overall, reduction in curing would result in reduced CTE mismatch and so larger radius of curvature values for a given laminate thickness.

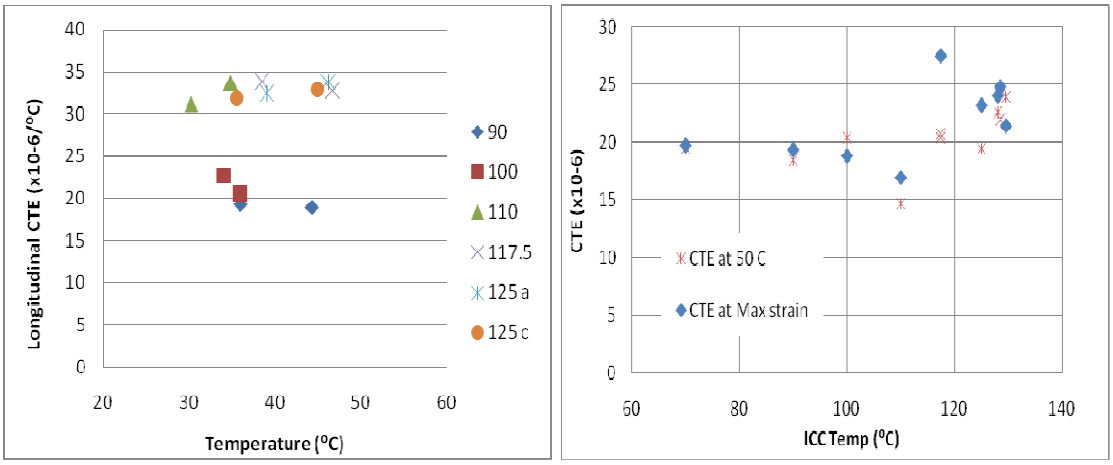

Figure 4.8, Calculated coefficient of thermal expansion for (a) interrupted cure cycle (ICC) single plies (b) 90º ply of ICC laminates.

Figure 4.8 a shows the measured CTE values for the transverse axis of ICC UD plies (90 to 125 ºC). For unidirectional laminates, expansion values are not constrained by 0º adjacent plies, in contrast to those CTEs measured on unbalanced laminates. However, the use of surface measurements (strain gauges) reveals similar values for CTE in the 90° plies, Figure 4.8 b.

4.4.2 Laminate interply bonding

Initial validation of the modelling approach shows good agreement provided that the degree of cure is known. For use in a predictive sense this would need estimating (see Section 4.4.5). The two groupings of data indicated by lines of best fit in Figure 4.3 show significant scatter (300 mm for 4 ply, B laminates) and deviation from the precise model assumptions (for the upper line). As well as the factors above this may be due to

features such as manufacturing variables that are not accounted for in the assumptions. It may also be the case that the assumptions are not representative of the actual mechanism in operation.

One aspect that would reduce the accuracy of the models would be if the interfacial bond between plies was not complete and not infinitely thin as assumed by CLT or if the plies were free to slide, (Equations 4.4 – 4.5). This would cause stress transfer to be impeded, allowing the CTE mismatch to be taken up in separation of the plies not in curvature so that the radius of curvature values would be greater than those predicted.

Although delamination / voids located in plies subject to tension would have a much larger affect on mechanical properties compared to those located in the middle plane (neutral axis), delaminations on the neutral axis in 4 ply laminate B2 (Figure 4.9) suggest a tensile strain through laminate thickness, in contrast to the assumed uniform distribution of stress through thickness of CLT (Detailed Section 4.5.1.3).

In Figure 4.3, large radius of curvature values are shown for some of the B and C batches of laminates. Sectioning of these laminates revealed a number of voids and examples of interply delamination, Figure 4.9, in these batches.

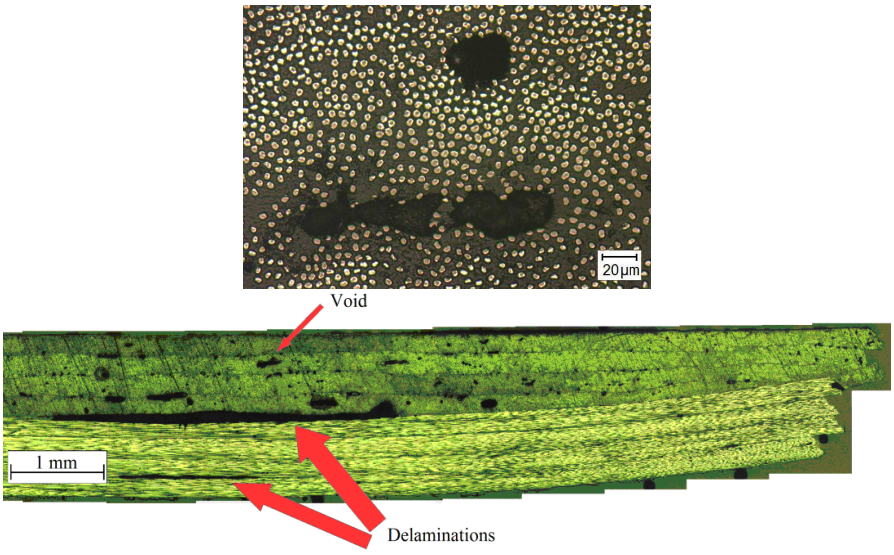

Figure 4.9; Voiding in laminate B2 and delamination between plies in laminate C1, constructed from aged pre preg batch 1.

The laminates that gave the greater numbers of these defects and largest deviation from predicted radius of curvature values were those from the thickest (8 ply) laminates and the oldest batch of pre-preg used in this study, i.e. 8 ply CI-4 and 4 ply B1-4 laminates.

Laminates fabricated from pre-preg roll 1 gave the most defects and the largest radius of curvature values, with the exception of B5, whilst those from rolls 2 and 3 lie on the lower trend line and agree with the predictions of Equation 4.5; these had few defects when sectioned, Table 4.4.

Table 4.4. Average radius of curvature achieved with pre-preg batch used.

Laminate	**Pre-Preg**	**Ave. radius of curvature (mm)**
B1-4*	Roll # 1	661
B5	Roll # 1	450
B9-11	Roll # 3	400
C1-4*	Roll # 1	1008
C5-7	Roll # 2	687

*delamination/voiding found in all laminate sections.

The curvatures predicted using basic linear theories do not have inputs to account for the starting state of the material, which are likely to impact the stress / strain transfer between plies and CTE values. Consequently the fit between calculated and experimental radius of curvature values can vary significantly, Figure 4.10.

Whilst average radius of curvature values for laminates manufactured from new pre-preg (rolls 2-3) are close to those values predicted by the linear model, (overestimating by 88 R/t, $t \approx 0.84$). Laminates manufactured from older pre-preg (Roll 1) cause radius of curvature predictions to be out by as much as 296 R/t (at $t \approx 0.84$).

More in depth analysis of both aged and new pre-pregs. and their impact on resulting curvatures are conducted using DSC and visual analysis in the following sections.

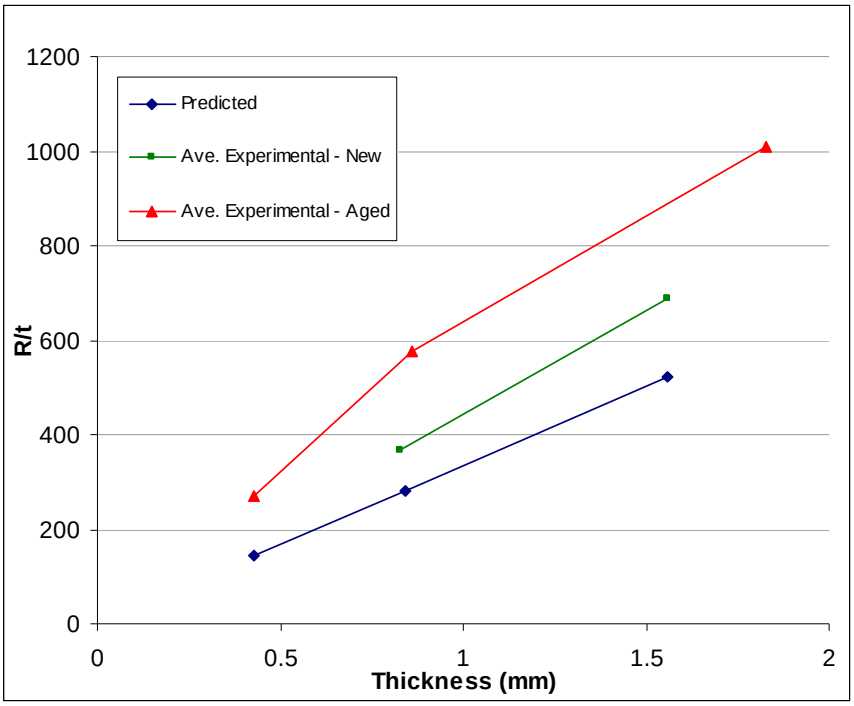

Figure. 4.10, Actual and predicted curvatures for aged (roll 1) and non-aged (rolls 2-3) pre-preg. Model inputs α^{0}_{CTE}=0.7 and α^{90}_{CTE}=29.2 (Equations 4.5).

4.4.3 Curvature with Laminate Length/Width, Aspect Ratio.

4 ply laminates were constructed with differing lengths and widths (i.e. different aspect ratios, AR) to study the effect of width variation on longitudinal radius of curvature; based on the assumptions in Equation 4.5, this should have no effect on radius of curvature for the same thickness of laminate.

Lengths ranged from 72.5 mm to 185 mm, giving a range of ARs from 1:1 to 1:3.65 (185 x 50 mm). Over the course of the study, three different pre-pregs were used, ranging from relatively new to significantly aged materials, Table 4.5 and Figure 4.11, meaning curvature values achieved had to be separated to differentiate between any effects of varying base material/laminate starting condition (as noted above) including CTE and geometric effects.

Table 4.5. Details of pre-preg rolls used in this study

Roll number	**Pre-preg Material Description**	**Features [68]**	**Date of prepreg. manufacture**	**Date of laminate manufacture**
1	VTM 264 / T800	Variable temperature, vacuum processable epoxy system. Typical cure between 65°C/149°F and 120°C/248°F.	2005 / 2006	March 2008 - March 2009
2	MTM 28-1 / T800H	Medium temperature, toughened epoxy system. Typical cure between 85°C/185°F and 160°C/320°F. Recommended cure 120°C/248°F for 1 hour.	31/03/2007 (12 month shelf life; 03/2008)	May 2009 - June 2009
3	MTM 28-1 / T800H		11/03/ 2009	July 2009 - June 2010

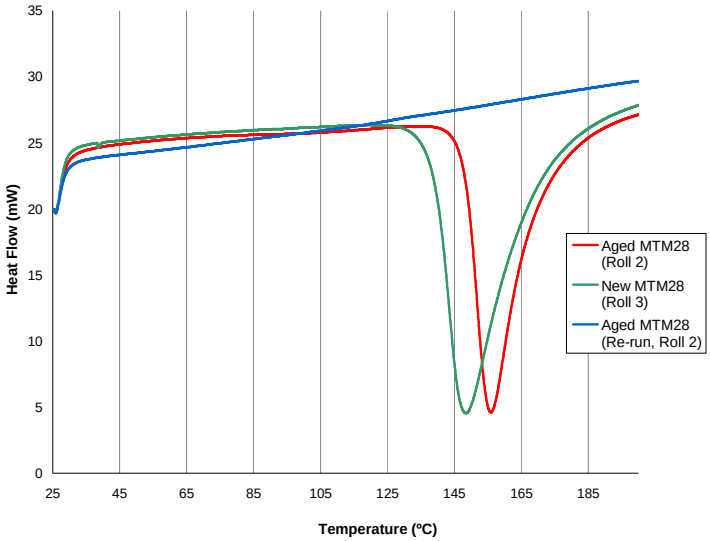

(a)

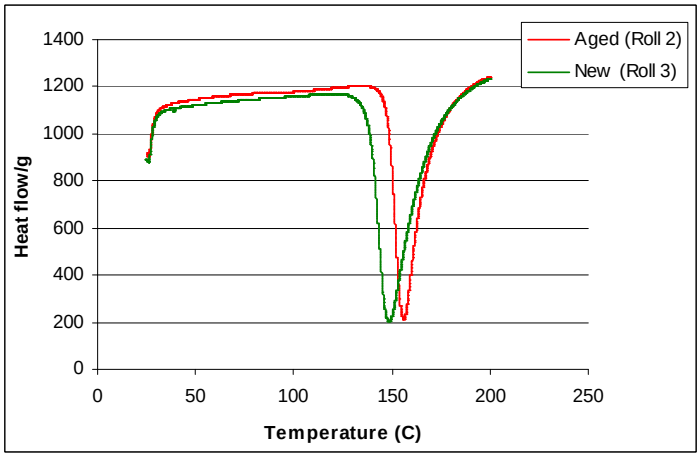

(b)

Figure 4.11: (a) Comparison of aged and new pre-preg. using DSC and (b) heat flow per unit mass for rolls 2 (aged MTM28) and 3 (New MTM28).

The area under the curve gives the amount of exothermic energy given out during the curing reaction. Therefore, when comparing old and new pre-preg. (rolls 2 and 3) data, Figure 4.11 a and b, it is evident that more heat is given out by the new pre-preg. (roll 3) and thus a higher level of cross-linking has occurred. Despite the smaller area under the heat flow / temperature curve a re-run (as for the 15 minute part-cured sample above) gave no endo- or exo-therms indicating that the epoxy had cured to its full extent during the first DSC run even for the aged MTM 28-1 (roll 2).

In addition to reduced energy output, the temperature seen for cross-linking initiation in the aged pre-preg. (roll 2). is higher than that for the new pre-preg. (roll 3). This would be consistent with a greater extent of cross-linking and reduced chain mobility in the aged pre-preg. so that greater thermal activation is needed to achieve chain mobility and continued reaction. This would correspond to a reduced CTE mismatch after laminate curing and cooling for roll 2 than for roll 3 and so larger radius of curvature values.

The DSC runs use a faster heating rate than that in vacuum bagging so that the absolute temperatures will be higher in the DSC than for the same extent of reaction in panel manufacture, although the trends will be the same. The DSC traces do indicate that a higher cure temperature should be used for the aged pre-preg. than for the new pre-preg. (rolls 2 and 3 respectively).

The radius of curvature values achieved for varied ARs and pre-pregs are shown in Figure 4.12.

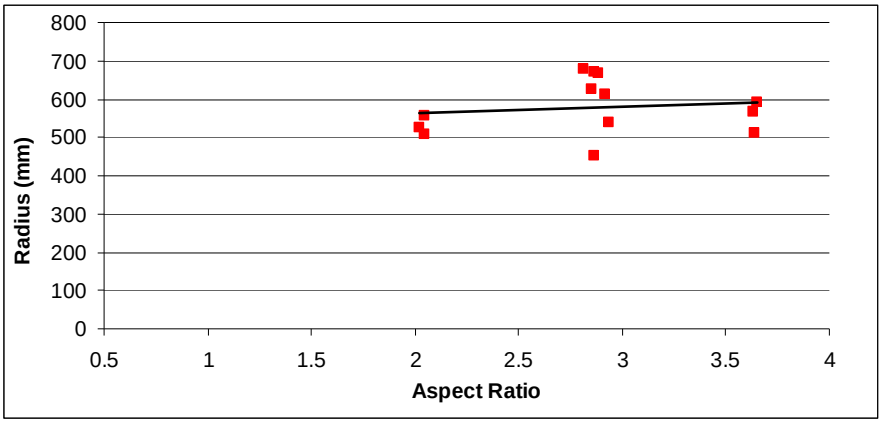

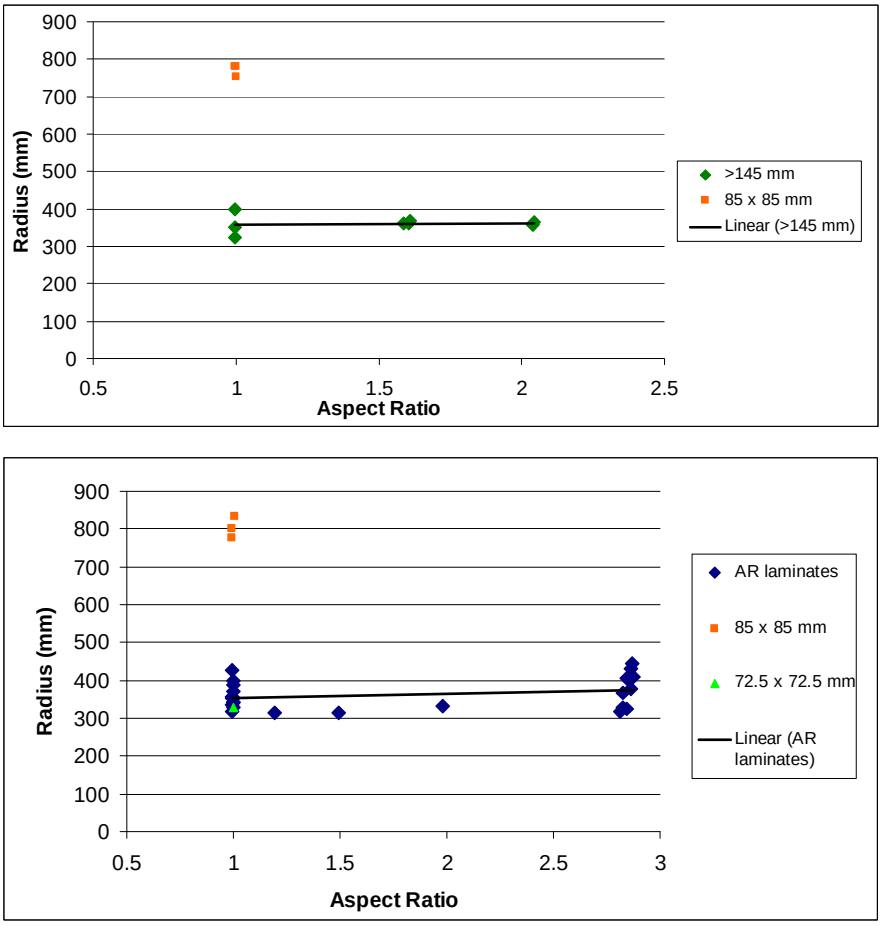

Figure.4.12, Experimentally determined radius of curvature values achieved for 4 ply laminates manufactured from (a) Roll #1 (b) Roll #2 (c) Roll # 3 pre-preg, with nominally identical thickness, but varied aspect ratios (length/width).

In general, the data trends observed in Figures 4.12, a, b and c suggest that aspect ratio has no effect on longitudinal radius of curvature achieved (within experimental scatter 315 - 444 mm). This is consistent with the assumptions in Equations 4.5, in which strain is fixed in 90 degree ply and is independent of length and width. The radius of curvature values for Roll 1, Figure 4.12 (a), are much greater than those for the two MTM 28-1 matrix rolls, Figure 4. 12 (b) and (c), consistent with the age of the pre-preg and the matrix resin, Table 4.5. The difference in age between rolls 2 and 3 does not result in a difference in radius of curvature values outside the experimental scatter range despite their difference during DSC trials, Figure 4.11.

However, within Figure 4.12 b and c, smaller 85 x 85 mm laminates I and J deviate from average radius values (350 mm), exceeding 700 mm radius, comparable with values achieved using aged pre-preg. roll 1, 676 mm for B1, Figure 4.12 (a).

Whilst the increased radius of curvature values could be due to reduced laminate length and width, smaller 72.5 x 72.5 mm square laminates Figure 4.12 (c) are consistent with the other aspect ratios This indicates that I and J laminates are likely to be anomalous with their lack of curvature due to other factors.

On visual examination of laminates I and J, reduced curvature is likely to be as a result of poor ply and fibre alignment meaning the 0/90 configuration is not achieved, Figure 4.13. Misalignment in such a small sample would inevitably contribute to warpage in directions other than longitudinal and transverse, generating a more twisted laminate, causing reduction in strain and therefore a reduced curvature. The increased level of misalignment is evident when compared to the corner conditions of other 4 ply laminates.

The curve profiles of I and J in the following section also support this irregularity of curvature generation.

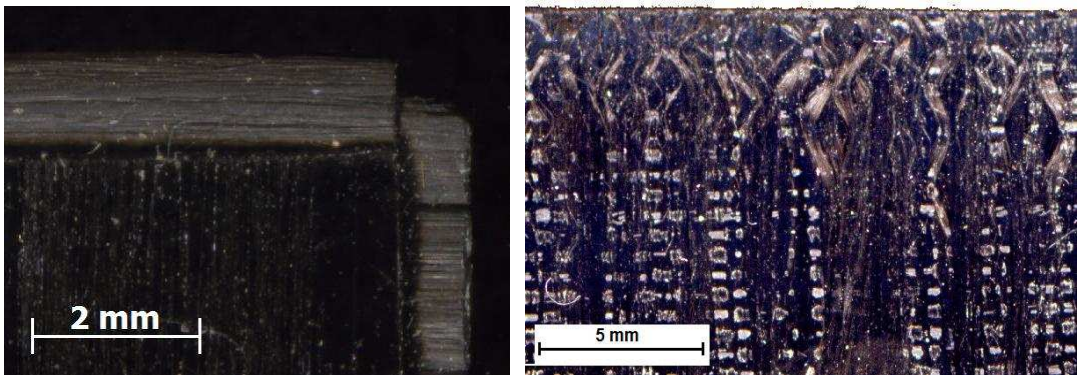

Figure 4.13; Macro images of a) laminate I, showing poor ply alignment at the laminate corner and b) fibre splay at M2 laminate edge.

This independence of laminate curvature from aspect ratio is more evident (within scatter) in the 145 mm length laminates, in which width is the only variable considered, Figure 4.14.

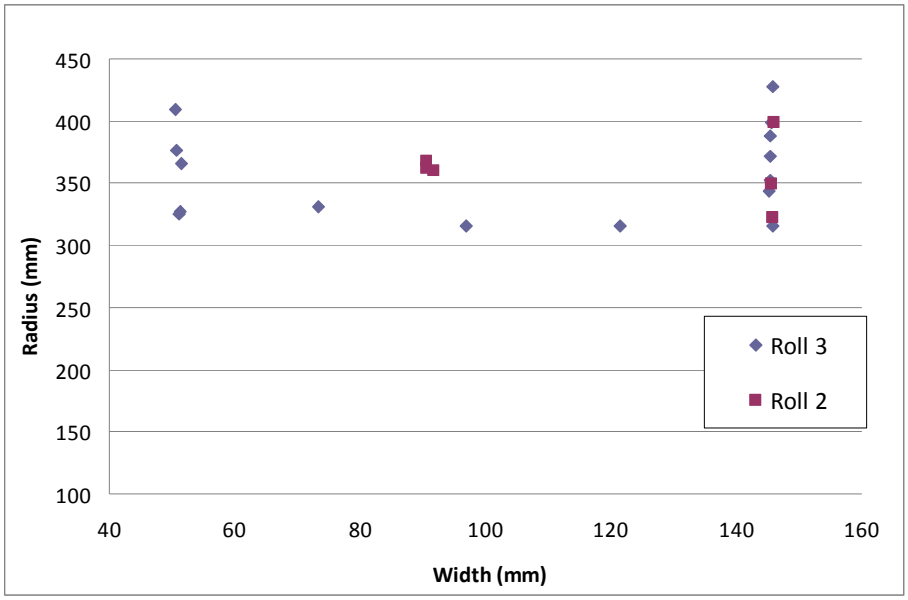

Figure 4.14; Radius of curvature values achieved for 4 ply 145 mm length laminates fabricated from rolls 2 and 3 with widths ranging from 50 - 145 mm. (Roll # 1 laminates are excluded due to aging of pre-preg material).

4.4. 4 Curve Profiles

Detailed laminate curve profiles were determined by measuring 7 points on the laminate profile length, at set intervals from the laminate centre via laser scanning, (Experimental. Section 3.2.3(b)). Curve profiles are presented in Figure 4.15 (a) and (b).

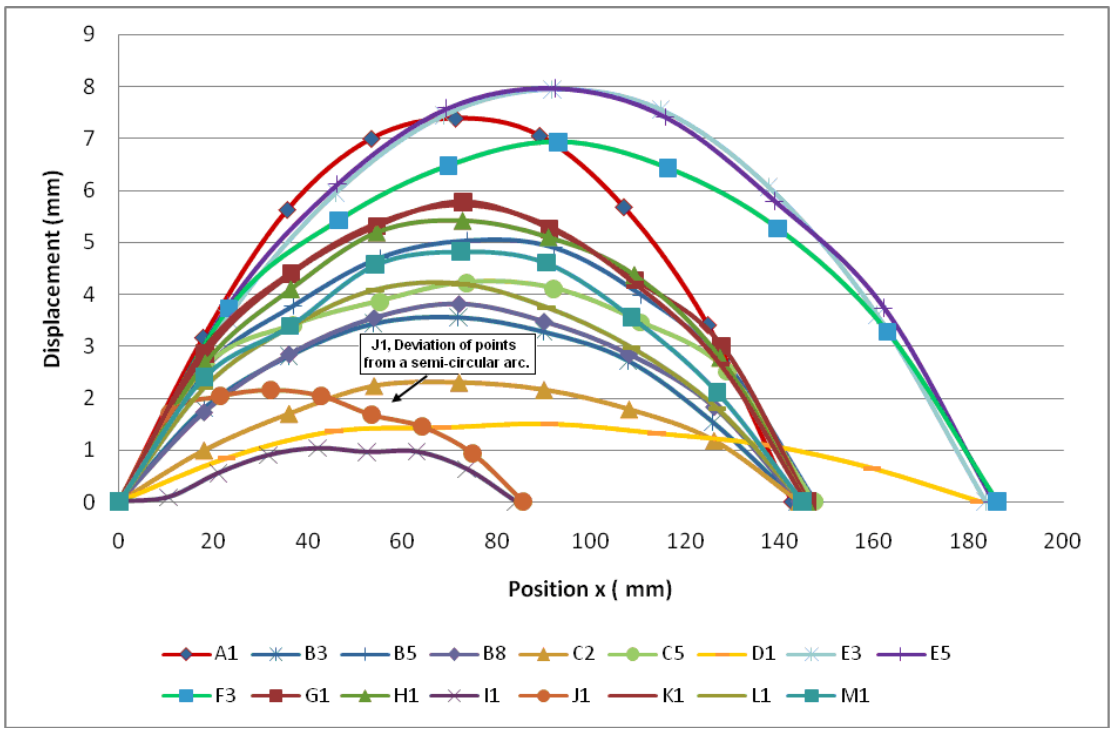

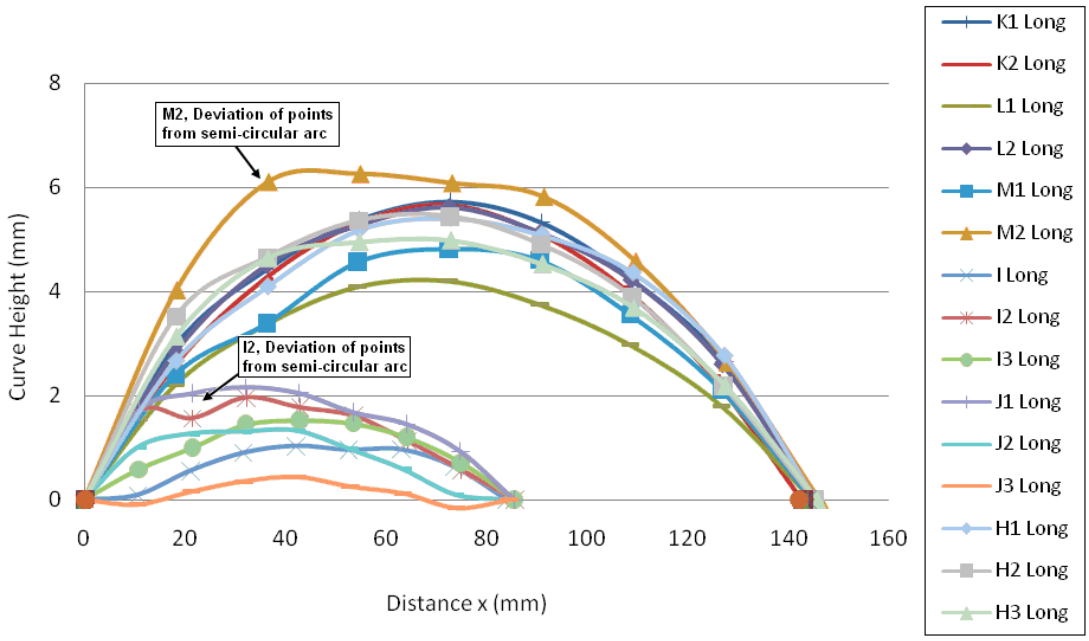

Figure 4.15. (a) Selected curvature profiles for each panel lay-up determined via laser scanning (accuracy ± 0.22 mm) and (b) curve profiles for square laminates of AR 1:1.

Examination of the laser curvature profiles in Figure 4.15 shows asymmetry of curvature (from difference in height measurements either side of the central point) and a substantial deviation of points from the symmetric smooth semi-circular arc for laminates J1, I2 and M2.

Given the magnitude of the point deviations, asymmetry is likely to be as a result of the misalignment of plies/fibres on assembly causing 'twisting' of the laminate [11] and edge effects due to the splaying of fibres on cutting (as detailed in the previous section, Figure. 4.13), rather than local differences in volume change during curing due to variations in fibre volume fraction; as the effect of would be minor.

Deviations of multiple points from a symmetric arc (such as those seen for I and J above) would not be predicted by Equations 4.5, Section 4.2 even though curvature mechanisms are suggested to be affected by fibre alignment, (reduced radius of curvature values and generation of a twisted laminate as for angle ply laminates). However, as major irregularity in curve profiles was only seen for laminates I and J, these were excluded from further consideration and model validation.

For the other laminates, radius of curvature values determined via laser profiling, differ by as little as 1.64 to >80 mm from those calculated from a central point only using

manual measurements, reinforcing the accuracy of manual methods (before reduction of curvature with stress relaxation has taken effect).

4.4.5. Development of Curvature with Cure

As detailed in the literature review (Section 1.1); curvature in asymmetric laminates has been ascribed to differences in thermal expansion coefficient (CTE), (Section 1.4.3) between differing fibre orientations and a volume change due to chemical shrinkage/crosslinking of the resin matrix, typically 3-6%.

Studying the cure kinetics of the fibre/resin system, variations in CTE and curvature development with degree of conversion should allow the relative importance of these two effects on generating curvature to be determined.

4.4.5.1 Establishing cure kinetics

The cure kinetics of MTM28-1 T800H carbon fibre pre-preg were determined by way of differential scanning calorimetry (DSC).

4.4.5.2. Dynamic DSC

Dynamic DSC was conducted at a rate of 10 ºC / min and 40 ºC / min to 180 ºC from room temperature on samples taken from pre-preg roll #3, Figure 4.16.

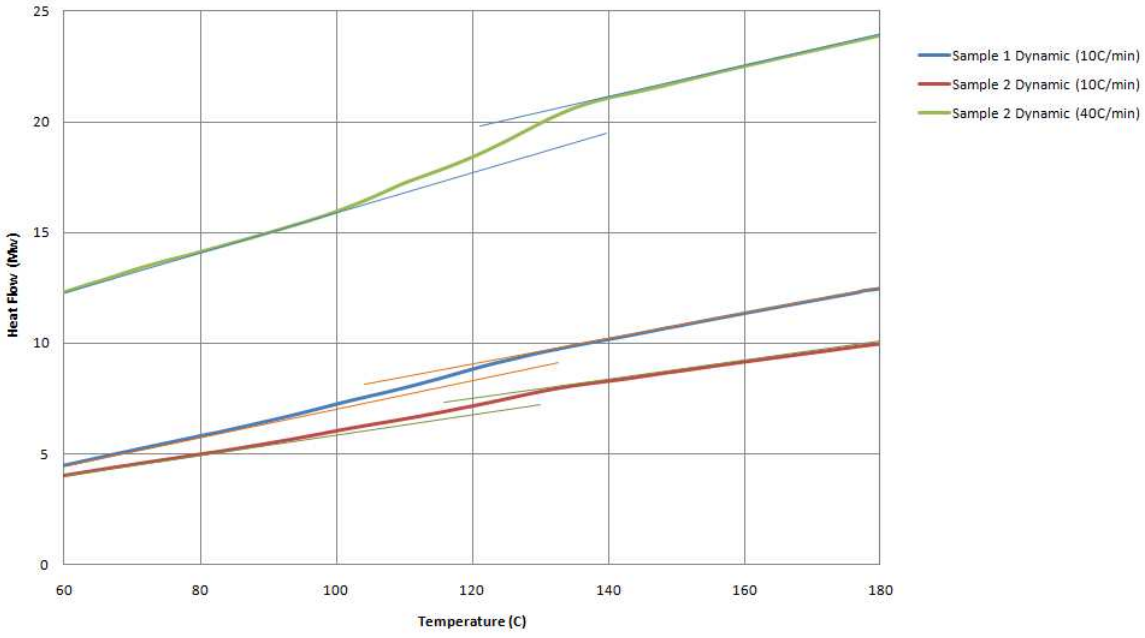

Figure 4.16; Dynamic DSC trace at 10 ºC/min and 40º C/min.

All dynamic traces show a broad glass transition (T_g), the onset of which at 100 ºC is in agreement with ACG data provided for the MTM28-1/T800H pre-preg [68], Table 4.5.
Differences in heat flow between nominally identical samples heated at 10 ºC/min is likely to be due to the small sample size (5 mm diameter disk with mass 21-25 mg), containing multiple areas of low volume fraction regions, and therefore greater resin content (four low v_f areas were identified in the ~6 mm long section in Figure 4.2) which would be expected to increase sample heat flow, highlighting the influence of varied volume fraction of fibres on resin behaviour at this scale.

4.4.5.3 Isothermal DSC

Isothermal DSC was conducted at 125 °C after a rapid (80 ºC / min.) from room temperature on pre-preg samples from Roll #3. This heating rate was selected to achieve the cleanest data possible, as previous dynamic tests revealed energies to be too small for accurate analysis, Figure 4.16, given the noise in the DSC signal.
As the heating rate from room temperature is much faster than used in laminate fabrication, some of the effects seen during isothermal dwell in this section may occur during heating of standard laminates from RT (0.5 ºC/min), but should be comparable for part-cure laminates, which undergo isothermal dwell treatments at 125 ºC.
After initial ramp up, (1.56 mins) the test was allowed to run for over an hour at 125 ºC in order to replicate the 60 minute hold used in the curing cycle, carried out during production of all laminates (as cure is a function isothermal dwell time).
The relative degree of cure, α,at time *t* can be calculated according to the cure curve from fractions of the entire exothermic energy (where total energy area, E_{tot} is assumed as 100% cure), as follows:

$$\textit{Percentage Cure}, \alpha = E_t / E_{tot}$$

Equation 4.8

where, E_t is the energy at time *t*; E_{tot} is the total energy for full cure, assumed at t = 60 minutes.

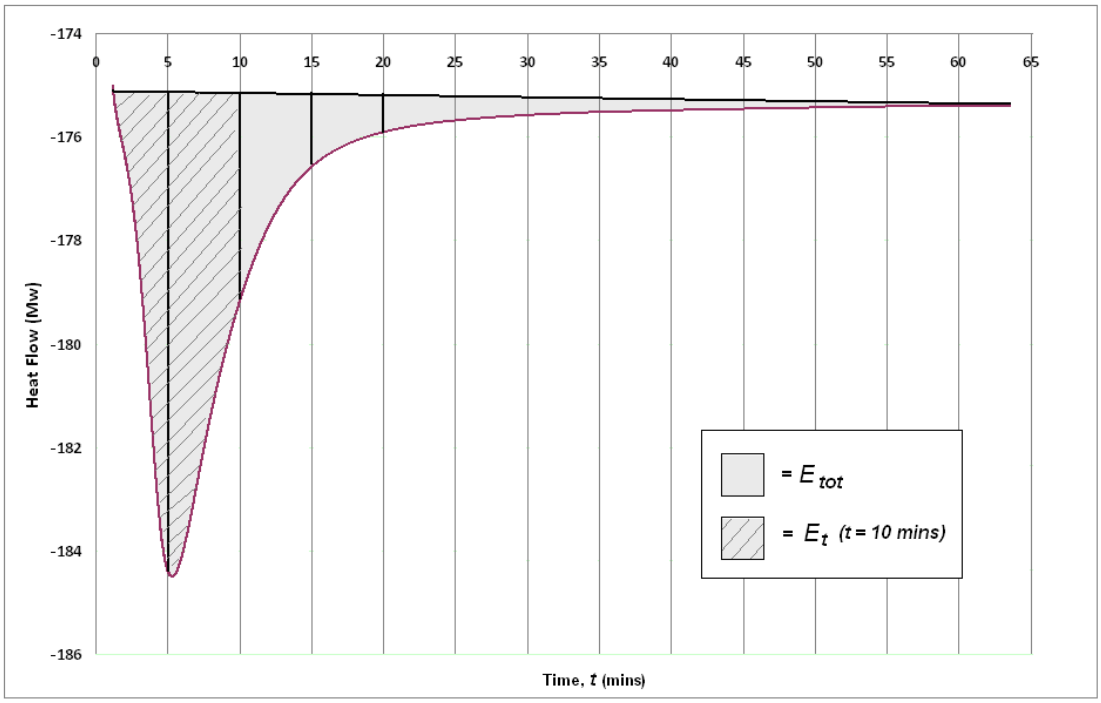

Figure 4.17; Schematic diagram indicating how DSC energy values were used to determine the degree of cure using 10 minutes isothermal hold as an example.

The calculated degree of cure as a function of isothermal dwell time values determined from DSC traces are given in Figure 4.18, and Table 4.6.

Table. 4.6, Calculated percentage cure as a function of dwell time at 125 ºC

Time, t (mins)	**Area , E_t between DSC curve and baseline, up to t**	**% Cure**
5	14.78	22
10	48.15	71
15	59.19	87
20	63.05	93
> 60	68.14	100

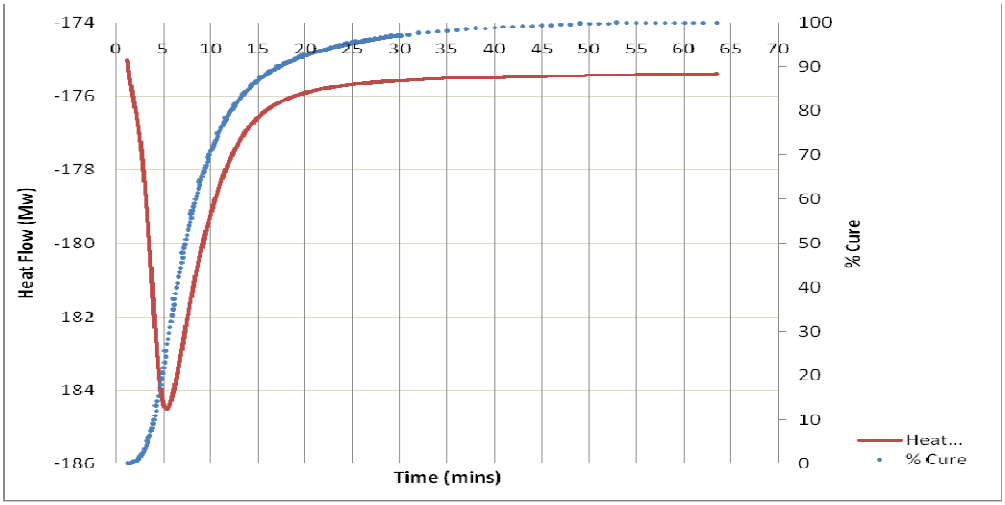

Figure 4.18 ; Isothermal DSC trace with calculated degree of cure.

The variations in exothermic energy and degree of cure values with isothermal dwell time shown in Figure 4.18 suggest that cross-linking occurs early when held at 125 ºC. The variation in percentage cure indicates the samples are already 50% cured after 7 minutes. This suggests that any 'part-curing' experiments are most effective between 5 and 25 minutes (20-95 % cure).

An Avrami analysis was used to determine the relationship between degree of cure and cure time in the isothermal experiment, Figure 4.19.

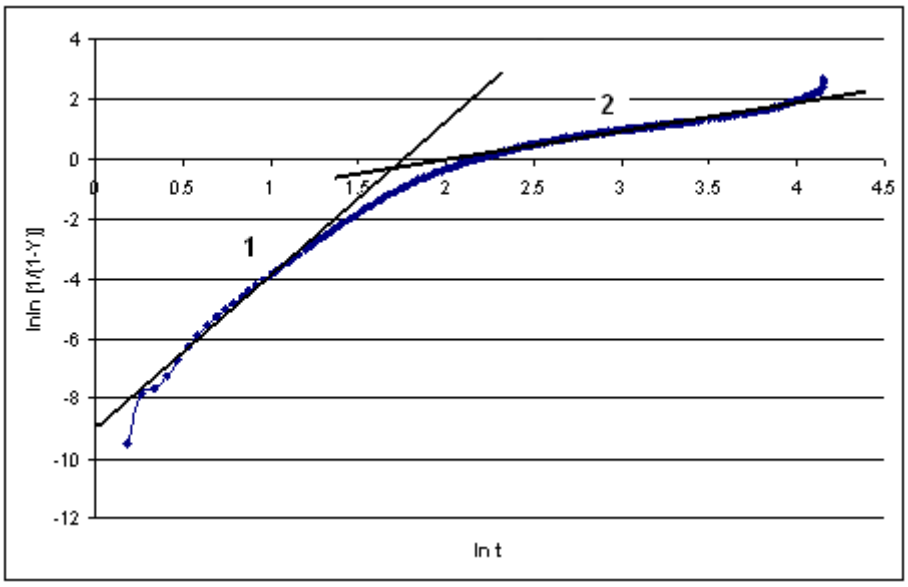

Figure 4.19; Avrami plot, showing transformation lnln(% cure) against ln(time).

An initial Avrami line appears to hold for early stages (Trace 1), then deviates at 13 mins, ~79 % cure (Trace 2), signifying a change in resin time dependent behaviour as a result of change in mechanism of nucleation/growth. This implies that that the full 60

minute dwell time used in standard laminate manufacture may not be required in order to reach full cure, given the extended ramp time from RT to 125 ºC dwell (~49 minutes at temperatures exceeding resin T_g of 100 ºC).

The slowing of cross-linking kinetics (>79 % cure) is likely to be due to the reduction of reactive free sites due to the creation of physical chain entanglements as the three-dimensional cross-linked network is formed, reducing chain flexibility

Also, if the initiation of the cross-linking reaction occurs around the carbon fibres themselves, as cross-linking progresses the epoxy matrix would be free of that influence.

4.4.6. Pre-Cure

DSC traces have indicated that the resin matrix begins to cross-linking/shrinkage at temperatures exceeding T_g, (100 ºC). Therefore, if plies are exposed to temperatures of ~125 ºC (in-line with isothermal dwell temperature used during standard processing) immediately from room temperature for varied exposure times, some initial chemical shrinkage should occur (referred to here as pre-cure). Pre-curing prior to stacking together to form a 145 x 50 mm laminate and subjected to a full curing cycle should modify the degree of shrinkage experienced during the cure, but should result in the same CTE mismatch. Therefore, any decrease in curvature seen for increased pre-cure exposure should indicate the dependence of curvature generation on magnitude of shrinkage.

Initial pre-cure studies were conducted for 2, 3, 4 and 10 minutes at 80 and 125 ºC (laminates N,O,R,S,T,U) to give between 5 and 70 % predicted cure, using polymer sheets to stop plies adhering to the Al forming plates, Table 4.7, Trial 1.

The experimental methodology was refined for final pre-cure (laminates V, W, X, Y and Z) using backing paper in preference to polymer sheet to prevent the carbon fibre pre-preg from adhering to the aluminium. This reduced the amount of ply damage/fibre splaying on pre-curing.

The time taken for plies to reach the target part-cure temperature of 125 ºC varied due to initial ambient temperature of the oven and rate of heat absorption (4 – 12 minutes for panels W, X, Y and Z).

Table 4.7. Experimental matrix of pre-cure times and temperatures and final part cure. Initial pre-cure time and pre-cure temperature with expected degree of conversion resulting from DSC.

		(1) Pre-cure					**(2) Final Cure**	
Trial No.	**Laminate**	**Time (mins)**	**Temp. (ºC)**	**Time to pre-cure temp (mins)**	**Degree of conversion after isothermal dwell (%)**	**Total Exposure time to temps >100 ºC (mins)**	**Oven Target Temp. (ºC)**	**Temp. removed from oven (ºC)**
1	**N**	10	80	-	*Unknown at 80ºC. Full cure after 13 hours [68]*	*N/A*	-	-
1	**O**	10	80	-	*Unknown at 80ºC Full cure after 13 hours [68]*	*N/A*	-	-
1	**R**	10	125	-	70	-	-	-
1	**S**	4	125	-	13	9.95	-	-
1	**T**	2	125	-	5	8.34	-	-
1	**U**	3	125	-	3	9.8	-	-
2	**V**	3.48	125	33 (Ramped from RT)	-	15.98	125	-
2	**W**	2.25	125	8		10.33	125	40
2	**X**	5	125	12	13	16.05	125	40
2	**Y** (1-3)	10	125	10	70	19.8	125	23
	Y (4-6)	10	125	10	70	17.48	125	35
2	**Z (**1-3)	8	125	7	55	15.75	125	25
	Z (4-6)	8	125	4		11.21	125	42

Pre-curing at 80 °C is not expected to lead to any major shrinkage and so the curvature developed during the standard final cure as the laminates are fabricated should be the same as those noted above. Figure 4.20 shows that the radius of curvature values for panels O and N were in the same scatter band as for non-pre-cured 4 ply laminates.

The radius of curvature values achieved for plies subjected to 125 ºC pre-cure and assembled into 4 ply laminates are given in Figure 4.21.

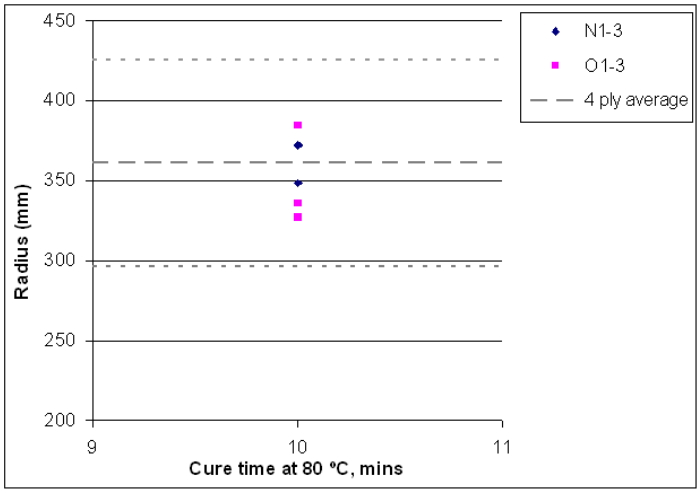

Figure 4.20; Radius of curvature for laminates N and O, cured at 80 ºC for 10 minutes, with 4 ply average curvatures.

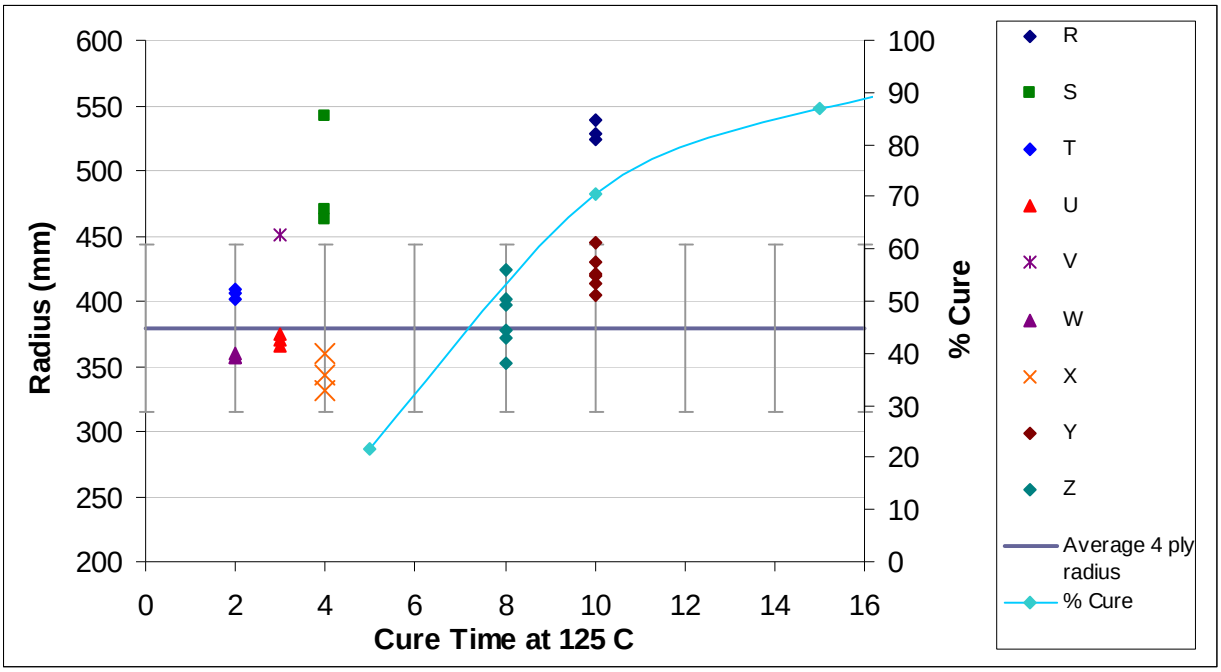

Figure 4.21; Calculated radius of curvature values for all pre-cured laminates exposed to 125 ºC (Trials 1 laminates R, S, T, U and Trial 2, laminates V, W, X, Y) versus predicted % cure from DSC.

The majority of the laminates shown in Figure 4.21 give radius of curvature values that fall within the scatter band for the standard panels without pre-cure. This behaviour is consistent with the assumptions of Equation 4.5.

However, laminates R, S and V give radius of curvature values that are outside the standard laminate scatter bands, implying stress transfer has been affected in the

laminates. This lack of curvature can be attributed to differences in the cure history and processing of these laminates. For example, V laminates had an extended 33 minute ramp up time to 125 ºC due to experimental error, causing increased curing/cross-linking before manually stacking the pre-preg plies to form a laminate. This would be expected to reduce resin flow on final cure, resulting in little, or, no adhesion between plies, indicating bonding limitations with increased cure time, as shown by sectioning, Figure 4.22.

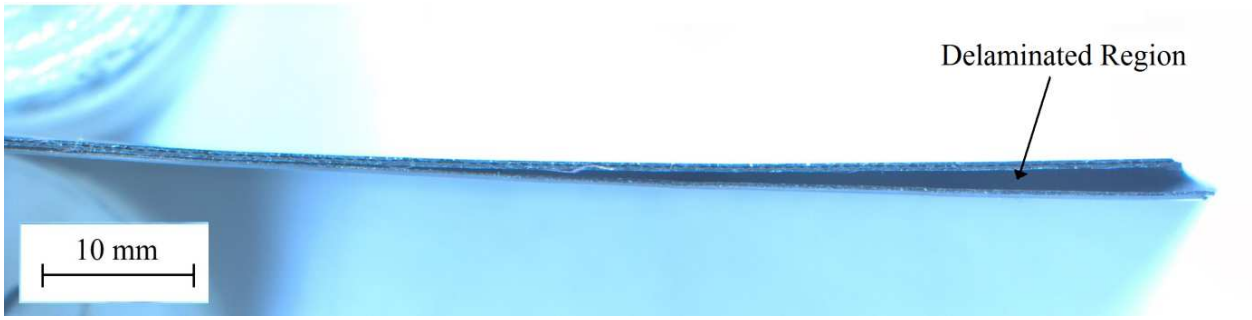

Figure 4.22; Macro-imaging of section of panel V1. Notice the delaminated region as a significant lack of bonding at midplane (2/3 ply interface).

R laminates exhibited a ‘non tacky’ surface before laminate assembly implying that significant cross-linking/shrinkage had occurred during the 10 minute pre-cure, with up to 70% curing being expected from DSC data. Due to the reduced adhesion upon laminate assembly for pre-cured plies, additional epoxy layers were added between all plies (~158 µm) to ensure plies were sufficiently bonded, Figure 4.23.

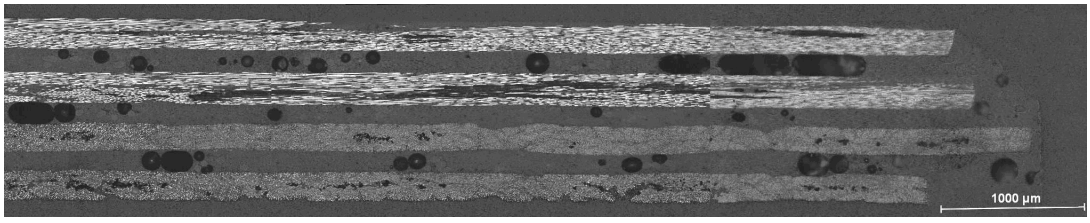

Figure 4.23 ; Laminate R1, 10 min pre-cure, 70% cure. Pre-cured plies bonded using epoxy resin layers (~158 µm).

Despite the increased thickness of R laminates (from 4 ply average of 0.85 mm to 1.33 mm) and the high void content of the epoxy layers; radius of curvature values reached an average of 530 mm, close to the radius of curvature predicted for a 1.33 mm 0/90

configuration using Equations 4.5 and the 541 mm radius achieved in laminate ‘S1’ with a 0.87 mm thickness.

The generation of curvature in R laminates suggests that curvature is affected by the quality of the interfacial bond and dominated by differences in thermal expansivity values between ply orientations, as the 30% remaining cure on final curing would be unlikely to cause such curvature on isothermal dwell.

Using the line of best fit, Figure 4.2 and Equations 4.5, the 0.87 mm thickness of laminate S1 would be expected to give a radius of curvature of ~430 mm, or at least match the 460 mm radius of curvature of S2-3.

This significant deviation from S2 and 3 is suggestive of poor stress transfer/bonding in laminate S1, verified by visual analysis, Figure 4.24.

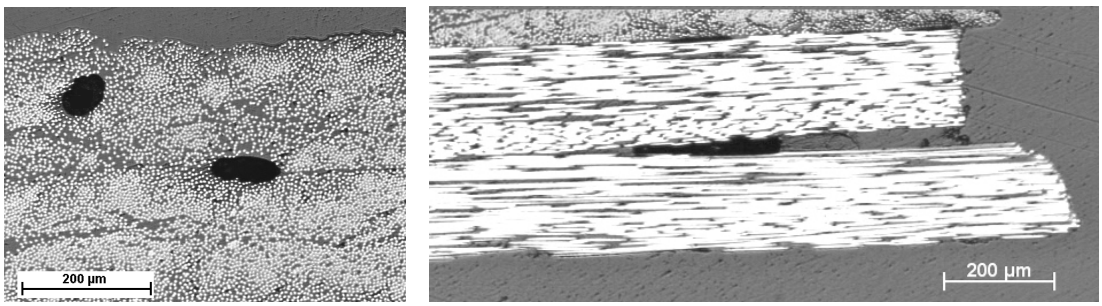

Figure 4.24; Micro images of laminate S1, showing voiding, poor resin flow (clear ply separation) and delamination.

Because of the influence of thickness on laminate curvature (Figure 4.3), it is important to differentiate between part-curing on stress transfer/bond strength and thickness effects. Figure 4.25 shows significant scatter seen for laminates of similar nominal thicknesses. However, the largest radius of curvature values are for panels S and V, that, as noted above, are atypical in their behaviour. Discounting these would then result in similar scatter to that shown for non-pre-cured material from the same pre-preg. rolls. Thus, the influence of curing shrinkage (and hence pre-cure time) on curvature formation is negligible, provided the laminates are fully cured subsequently. This is consistent with the assumptions behind Equations 4.5. For the remaining panels (R and T – Z) the slope (albeit based on two points) is ~400, which would be close to the predictions of Equations 4.5.

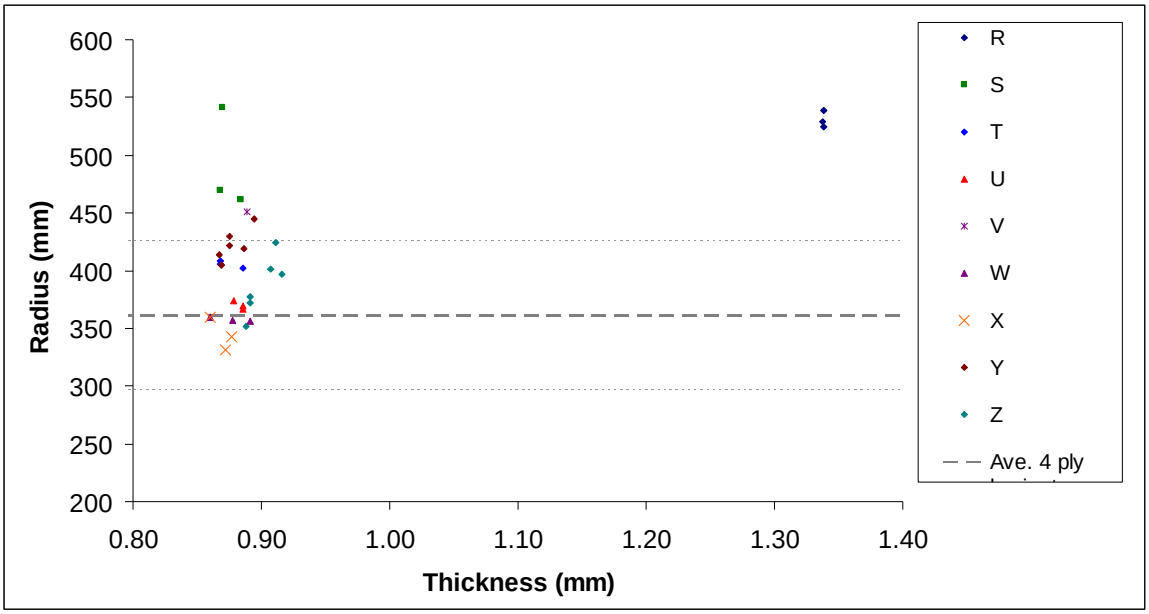

Figure 4.25. Relationship between radius of curvature and thickness for pre-cured laminates.

The results to date indicate that CTE mismatch is dominating curvature generation and this should be related to the total degree of cure achieved prior to cooling from the curing temperature. As DSC traces indicate a T_g value of 100 ºC, and a greater amount of time spent above Tg on heating to 125 ºC shows a weak trend towards greater radius of curvature values, Figure 4.26.

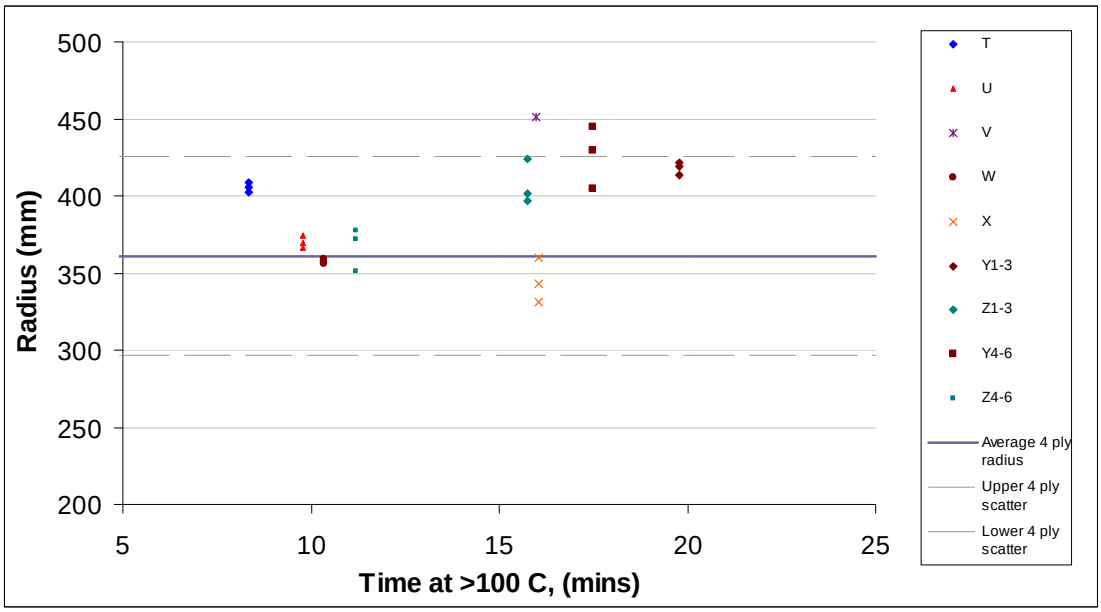

Figure 4.26; Radius of curvature values achieved, versus exposure time to temperatures >100 ºC on heating.

The weak relationship shown in Figure 4.26 is due mainly to the higher radius of curvature values shown for Y and Z panels that are towards the top end of the normal scatter band seen for this thickness of laminate. These panels were exposed to temperatures above T_g for 15 minutes or more. This corresponds to the change in curing / cross-linking mechanism observed from Avrami analysis of DSC results, Figure 4.19. Thus, there may also be a reduction in resin flow between plies pre-cured for longer times, reducing the interply flow and so bondline strength. This would relax one of the assumptions used in Equations 4.5 and so give greater radius of curvature values than predicted. Evidence supporting this proposed variation in resin flow with cure time is observable through macro-imaging of the laminate surface, Figure 4.27. The 'glossy', resin-rich surface of short pre-cure laminates W, X, Z (2 - 8 minute pre-cure) Figure 4.27 (a), suggests that resin flow is similar to that of a standard laminate, mimicking the smooth glassy finish of the base plate on final curing. In contrast, the longer pre-cure time in laminate 'Y' (10 minute) Figure 4.27 (b), has hindered the flow of resin, suggesting the matrix is almost fully cured as a result of the 10 minute pre-cure (corresponding to 70% cure from DSC data).

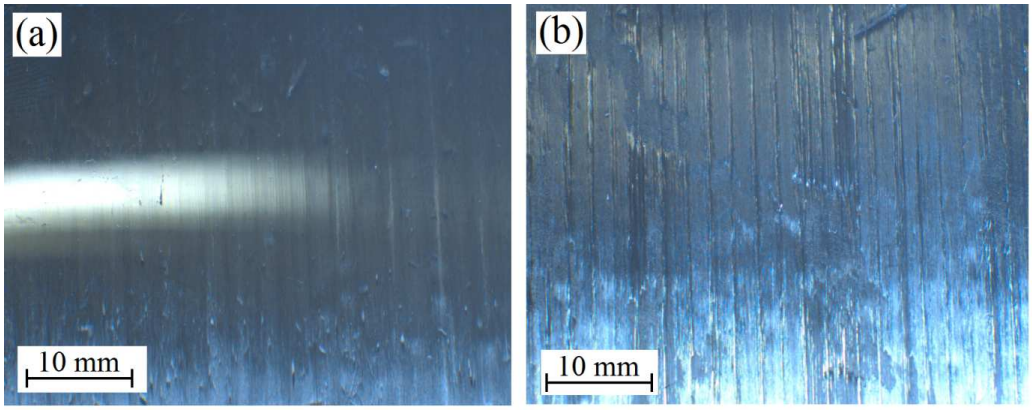

Figure 4.27; (a) 'Glossy' resin-rich surface of specimens W, X and Z (10-16 minutes at >100 ºC), and (b) dull, undulating surface finish of specimen Y (17-19 minutes >100 ºC).

In addition to macro-scopic differences in surface finish above, micro-scopic analysis reveals differences in microstructure between laminates X3 and Y3 (16 and 19 minutes at >100 ºC respectively).

Whilst X3 has only 4 minor voids across the sample length, Figure 4.28 (a), Y3 has a series of voids, Figure 4.28 (b) and a clear separation between plies at 0/90 interface, Figure 4.28 (c).

This is consistent with a reduction in resin flow due to 19 minute exposure at >100 ºC limiting the bonding of plies.

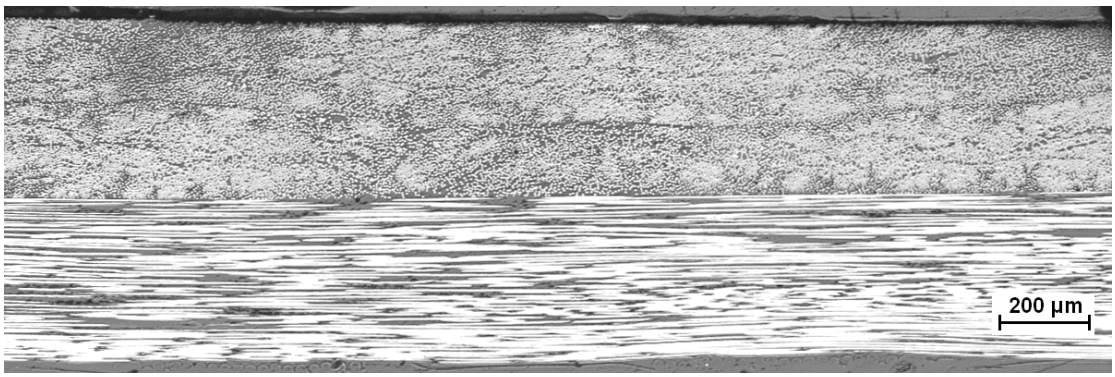

(a)

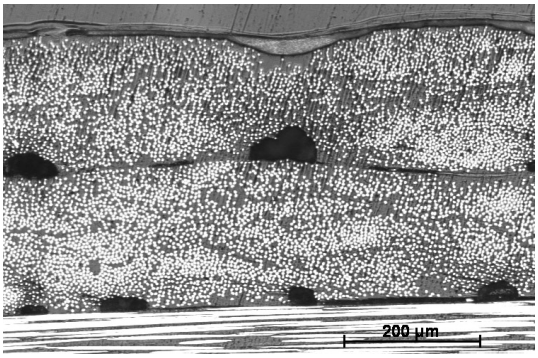

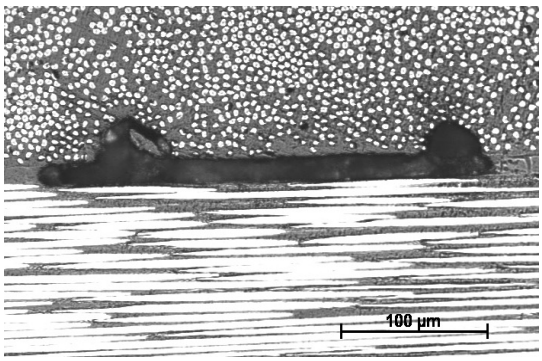

(b) (c)

Figure 4.28; (a) Void free section of laminate X3 (16.05 minutes at >100 ºC) (b) Severe voiding, (central void measuring 100 x 49 µm) and (c) 311 x 14.6 µm delamination of laminate Y3 (19.48 minutes at >100 ºC) at ply interface.

The lack of vacuum pressure on pre-curing of plies may also contribute to the extent of voiding, as stacked plies are not forced together under pressure. This leaves areas unfilled by resin that would require greater flow of the (now more viscous) resin during the laminate curing. This would be expected to reduce the quality of interfacial adhesion between plies. For laminates with good resin flow, this would not be expected to have such an impact as resin would flow into these areas bonding the plies together.

Fourier Transform Infra Red (FTIR) spectra of pre-cured laminates, as well as fully cured plies, were investigated, but did not reveal any significant differences in material composition/structure with pre-cure. However, given the noise of the signals, results were inconclusive and would require greater experimentation to quantify the degree of cure independently of the DSC analysis.

Data suggest that reduced and more scattered curvature seen for extended pre-curing of plies is likely to be as a result of poor resin flow during final processing and poor bonding of plies/interfacial due to pre-cure exposure to temperatures exceeding T_g rather than reduced strain on laminate assembly as a result of initial cross-linking/strain reduction. This is supported by laminate R, in which the laminate still curved even though laminate is >70% cured before assembly and full curing. In this laminate the provision of extra epoxy resin accomplished full bonding between the plies. The epoxy resin adhesive layer would have shrunk on curing, but that would have been isotropic in the plane of the plies allowing stress transfer across the interface, but not contributing strongly to curvature. The difference in modulus values between the 0° and 90° plies would result in differential stresses from the in-plane strain but this would give greater curvature than the CTE mismatch, which accounts for the radius of curvature values based on Equations 4.5.

4.4.7. Interrupted Cure Cycles (ICC)

The development of curvature in 4 ply asymmetric laminates during the standard curing cycle was studied by interrupting the standard curing cycle at designated times. Curvature data should be directly comparable to standard 4 ply laminates in section 4.2.1, as interply bonding in these laminates should be similar (unlike laminates fabricated from the pre-cured plies).

By quenching the laminates directly on removal from the oven in a thin layer of water (external to the airtight vacuum bag), any additional cross-linking was prevented.

Any strains generated during matrix cross-linking are ‘locked into’ the system given modulus is high enough to the resist complete relaxation of stresses upon cooling [43].

Curvatures achieved at designated cure cycle intervals during the standard curing cycle are shown in Figure 4.29.

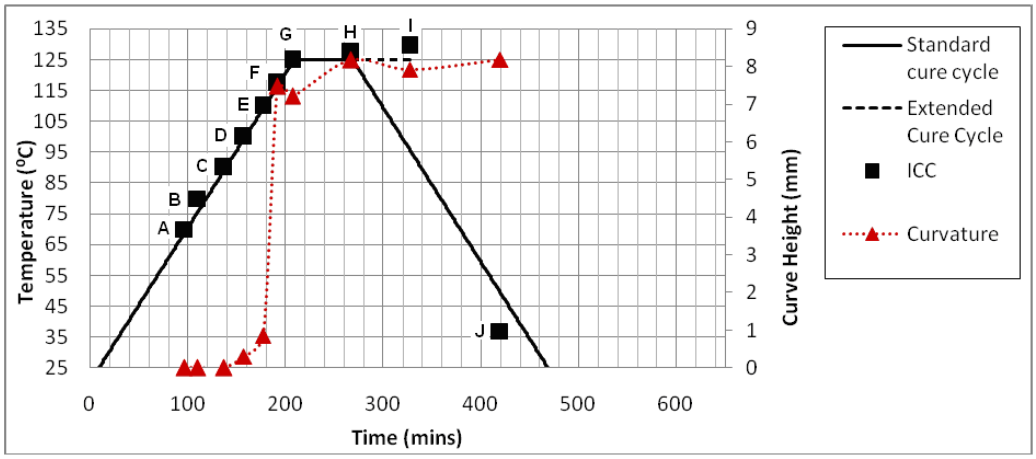

(a)

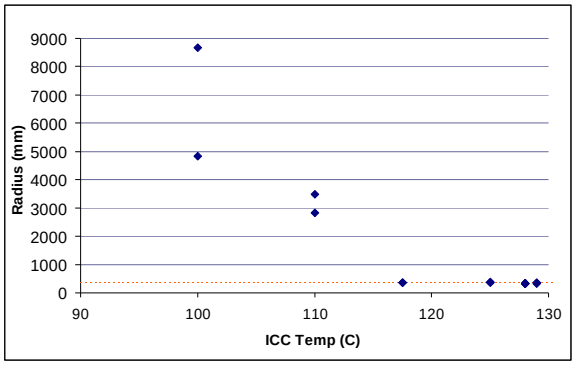

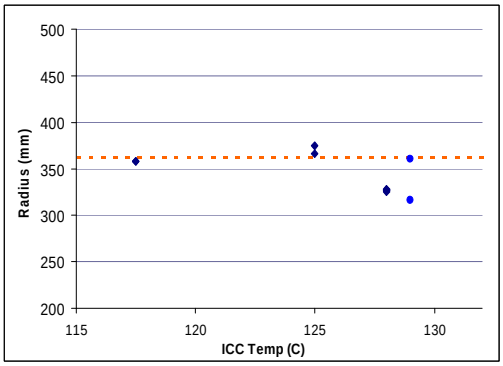

(b) (c)

Figure 4.29; Radius of curvature generation with ICC (a) minutes (b) temperature for all curved laminates (c) temperatures >115 ºC. Average 4 ply radius of curvature (361 mm) is indicated by the dashed orange line.

Referring to Figure. 4.29, no curvature arises until laminates are heated over 100 ºC (157 minutes into curing cycle; sample D). This is consistent with a T_g value of 100 ºC (confirmed via dynamic DSC). The absence of curing cross-linking would leave the matrix resin in a rubber-like state with low CTE values and a small CTE mismatch, leading to large radius of curvature values.

Curvature development follows the steep curing kinetics seen in DSC trace, Figure 4.29 (a). The final radius of curvature value increases steadily with further cure within scatter, (E - G) as the matrix converts from tacky resin into a hard resin generating curvature through CTE differences. It then reaches a plateau after vitrification at 267 mins, ~125 ºC (H - J), ~330 mm radius, suggesting full curing and cross-linking at 125 °C are complete and that no further increases in CTE mismatch occur.

This saturation of CTE differences is confirmed by a lack of curvature increase upon extending the isothermal dwell for an additional hour from the standard manufacturing cycle, point I, Figure 4.29 (c).

The ICC experiment reveals a strong relationship between curvature generation in standard laminates at 100 ºC due to cross-linking of the resin matrix (increasing the CTE mismatch); the critical temperature in pre-cure laminate experiment; and dynamic DSC.

4.4.8. Modulus Development with Cure, ICC

Figure 4.30 (a) shows the laminate modulus development over the curing cycle, and resulting curvature. Modulus follows the same trend as degree of cure and radius of curvature as matrix cross-linking is the basis for all three. The modulus of the composite is dominated by the fibres provided that load transfer occurs, which requires sufficient matrix cross-linking.

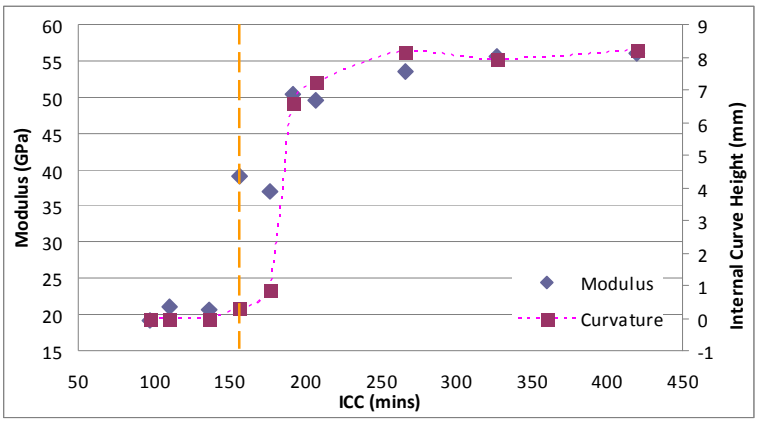

(a)

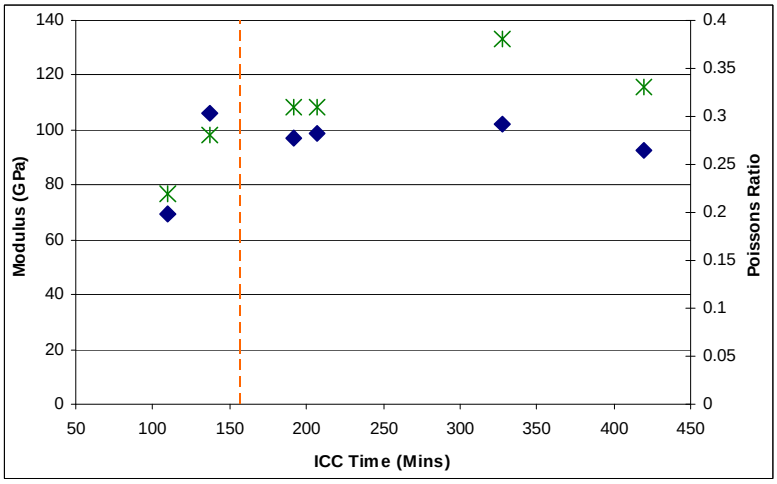

(b)

Figure 4.30 (a) Modulus and curvature for selected ICC laminates, (b) longitudinal Modulus for ICC single ply tensile specimens with Poissons ratio.
Dashed orange line indicates 100 ºC, 157 minutes.

4.4.9. End Constraints

The general behaviour of composite plies during a fabrication cycle is summarised in Figure 4.31. The generally good agreement between the predictions of Equations 4.5 and experimentally measured radius of curvature values supports the hypothesis that curvature is dominated by CTE mismatch during the cooling stage.

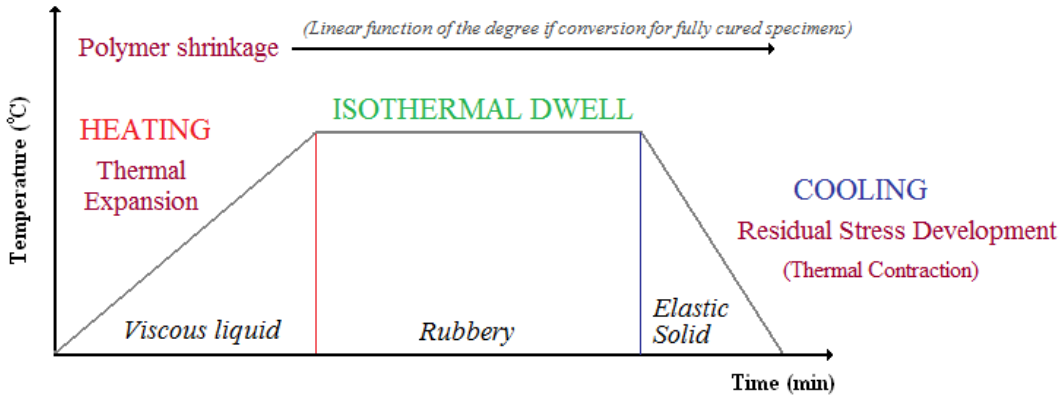

Figure 4.31. Schematic diagram of material changes during fabrication of carbon fibre / epoxy composites (adapted from [41,43]).

If shrinkage during curing played a major role then the plies would need to be locked in at the start of the isothermal dwell, in which case, the alignment between ply ends should be good. The latter feature would be especially clear for pre-preg. stacks that were trimmed prior to bagging (co-cured laminate). Sectioned ends of cured and cooled laminates, Figure 4.32, show considerable amounts of slippage between the plies. This would be consistent with movement during the low viscosity phase of the matrix resin, i.e. the early stages of the cure and would not be consistent with the plies being locked in during the whole of the isothermal dwell.

This movement is accentuated when fully cured plies were laminated with un-cured pre-preg.(co-cure), when extensive flow of the uncured pre-preg. took place on curing, Figure 4.33, leading to variations in fibre fraction. These sections clearly indicate that the plies are not locked in during the cure.

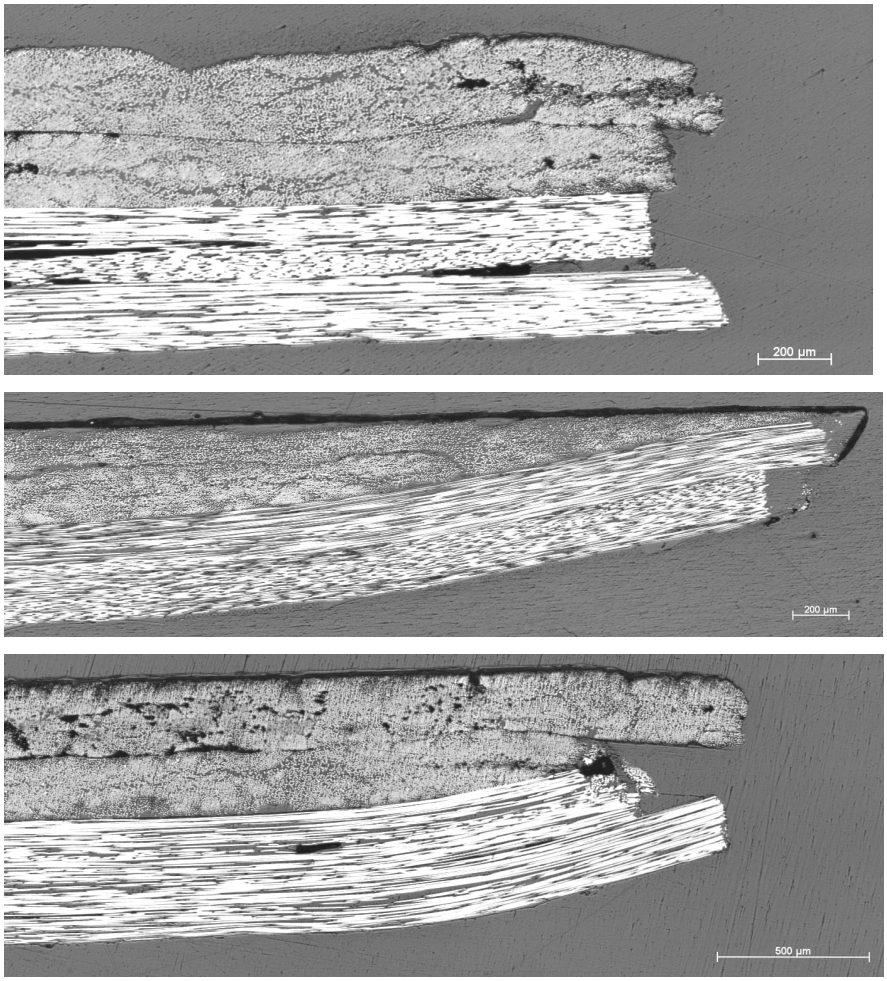

Figure 4.32; End conditions of laminate (a) S1, (b) X3 and (c) Y3

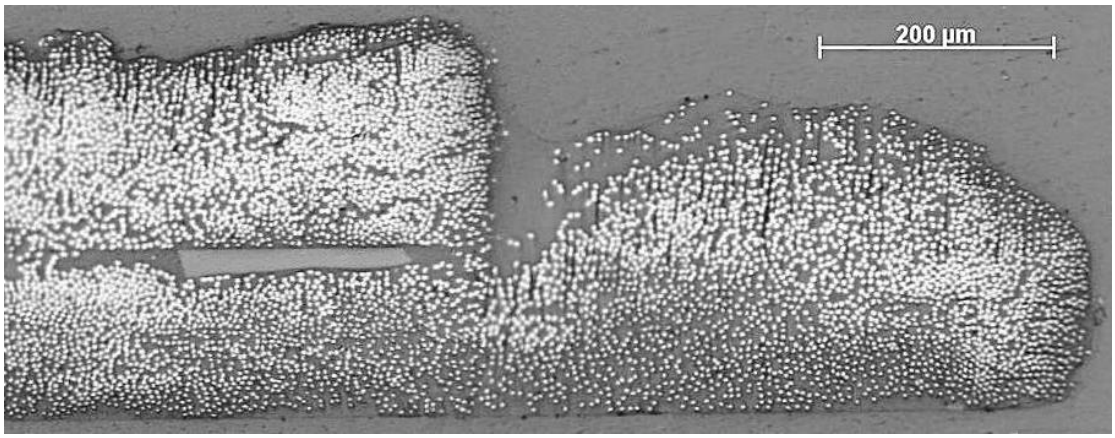

Figure 4.33; End constraint of co-cured laminate, where fully cured plies (top) were laminated with un-cured pre-preg (bottom), showing extensive flow of the uncured pre-preg. on curing .

4.4.10. External Factors; Deviations from Baseline Curvature

The mechanism for initial curvature for asymmetric laminates in the system studied has been established and accounted for using Equations 4.5. The use of asymmetric

composites would be affected by aspects such as temperature, whilst loading may result in stress relaxation over time, altering the shape of the component.

Time and environment are key factors in the long term behaviour of composite parts. Whilst fibres do not show a strong dependence upon temperature, the epoxy matrix is very sensitive to temperature variations causing brittle and elastic behaviour at low temperatures or ductile and viscoelastic behaviour at high temperatures. Consequently, the mechanical properties of a composite vary significantly within its operating environment and will change with the aging process.

4.4.10.1. Decay of curvature; stress relaxation / creep

The curvature of unbalanced laminates is maintained as a result of residual stresses 'locked into' the resin matrix on cooling, in its high modulus state. The magnitude of these residual stresses depends on the curing process, history of environmental exposure as well as the constituent properties.

Traditionally, stress-strain behaviour is modelled using Maxwell, Voigt or combined systems, such as four element models. Estimates of residual stresses can be made by measuring resultant curvature [48].

In order to determine the time-dependence of these stresses (and therefore the stability of unbalanced laminates over time), the change in central curve height (h) as a result of additional stresses (Laminates 2-4: 10 - 49 N) and relaxation of residual stresses (Laminate 1: Unloaded) were monitored for >6760 hours / 282 days. The decrease in laminate curve height is shown in Figure 4.34.

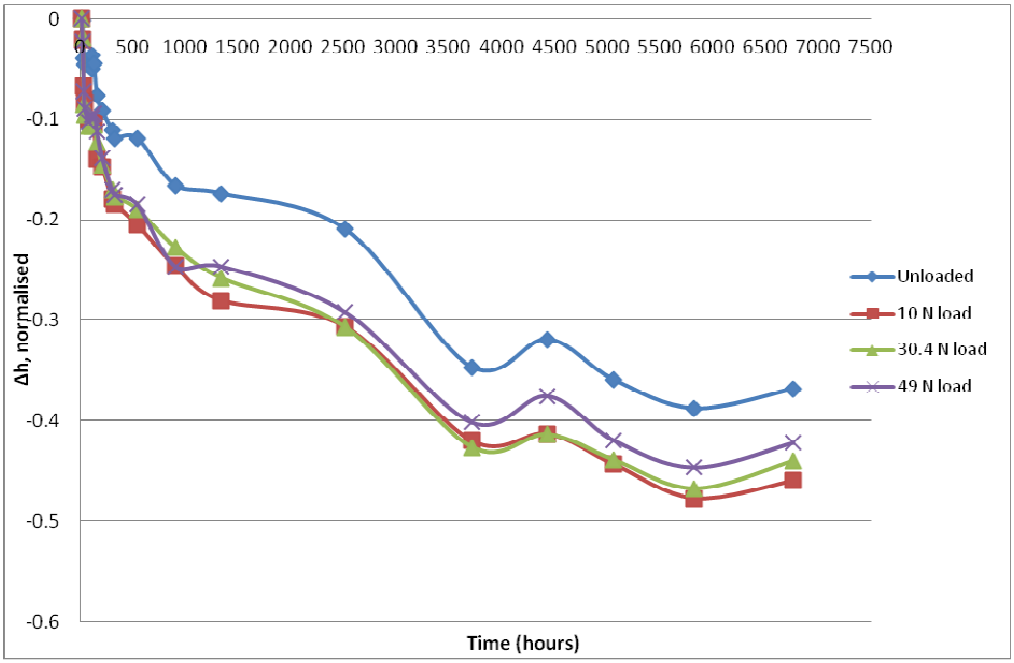

Figure 4.34; Normalised change in height of all laminates after 6760 hours/282 days, ±0.02 mm.

The data shown in Figure 4.34 were gathered over 9 months, during which period ambient temperature fluctuations occurred, which resulted in the periodic variations in Figure 4.34. These fluctuations are superimposed on a general exponential decay of the height with time.

For the unloaded laminate, the change in curve height over time is due to the relaxation of residual stresses within the matrix. After 6000 hours, this appears to have reached an asymptote (within scatter) at the value of -0.387 ε, suggesting that the maximum change in curve height has occurred (-3.39 mm). This said, it is possible that eventually all residual stresses would relax from the matrix and the laminate would return to its flat pre-cure state.

With the addition of load, the relaxation rate increases, which may include an element of creep. The relaxation rate of all loaded laminates appears to be accelerated initially, when compared to rate of the unloaded laminate.

Even though varied loads are applied, relaxation curves for all loaded laminates appear the same within scatter. This is due to the applied loads (10 - 49 N) exceeding the average 4.7 N load required to flatten them completely, making strain experienced on loading laminates nominally identical.

4.4.10.2 Analysing stress relaxation / creep

For the unloaded laminate, the change in curve height over time is due to the relaxation of residual stresses within the matrix.

As stress relaxation/creep is governed by Avrami type parameters (constants k and n relating to constant applied load and time) an Avrami analysis can be applied:

$$\exp(-kt^n) = \frac{R(t) - FRi}{Ro - FRi}$$

where *Ro* = initial radius of curvature, *FRi* = final radius of curvature as a function of load and *R(t)* is radius of curvature at time *t*.

By extending the exponential curvatures, the final radius (*FRi*) at which an asymptote is reached can be determined for a given load, Table 4.8.

Table 4.8. Final and initial radius of curvature values, with total change in radius (*FRi*, *Ro* and ΔR respectively, all in mm).

	Applied load (N)	***Ro***	***FRi***	Δ ***R***
	None	305	530	225
Nominally identical laminate strain	10	363.1	700	316
	30	334.5	657	322.5
	49	363.6	670	306.4

A linear relationship between radius of curvature and time can then be derived from the natural log *(ln)* of the exponential curve using:

$$ln\,[exp(-kt^n)] = \ln\left(\frac{R(t) - FR_i}{Ro - FR_i}\right)$$

$$-k\,t^n = \ln\left(\frac{R(t) - FRi}{Ro - FRi}\right)$$

At $t = 0$ then $R = Ro$, but at $t = \infty$, $R = FRi$. As it is not possible to take a natural log of a negative number then the equation needs to be of the form:

$$R(t) = Ro + (FRi - Ro)\left(1 - \exp\left(-k\,t^{n}\right)\right)$$

$$\frac{R(t) - Ro}{FRi - Ro} = 1 - \exp\left(-k\,t^{n}\right)$$

$$\exp(-k\,t^{n}) = 1 - \frac{R(t) - Ro}{FRi - Ro} = \frac{FRi - Ro - R(t) + Ro}{FRi - Ro}$$

$$\exp\left(-k\,t^{n}\right) = \frac{FRi - R(t)}{FRi - Ro}$$

$$-k\,t^{n} = \ln\left(\frac{FRi - R(t)}{FRi - Ro}\right)$$

The left hand side will be negative after the first ln operation, which prevents a second ln operation and so:

$$k\,t^{n} = -\ln\left(\frac{FRi - R(t)}{FRi - Ro}\right)$$

but

$$-\ln\left(\frac{a}{b}\right) = \ln\left(\frac{b}{a}\right)$$

so that

$$k\,t^{n} = \ln\left(\frac{FRi - Ro}{FRi - R(t)}\right)$$

$$\ln(k) + n\ln(t) = \ln\ln\left(\frac{FRi - Ro}{FRi - R(t)}\right)$$

where k and FRi are functions of loading condition and n is independent of load.

Figure 4.35 plots the ln(t) against the double ln for each of the four loading conditions.

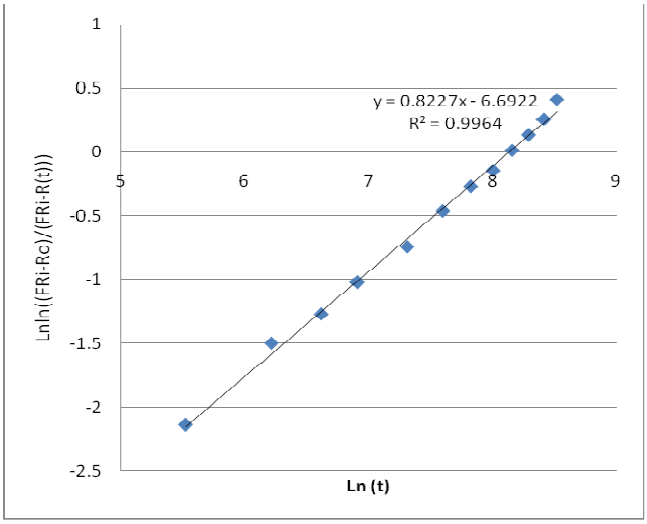
y = 0.8227x - 6.6922
R² = 0.9964
Lnln((FRi-Rc)/(FRi-R(t)))
Ln (t)

(a)

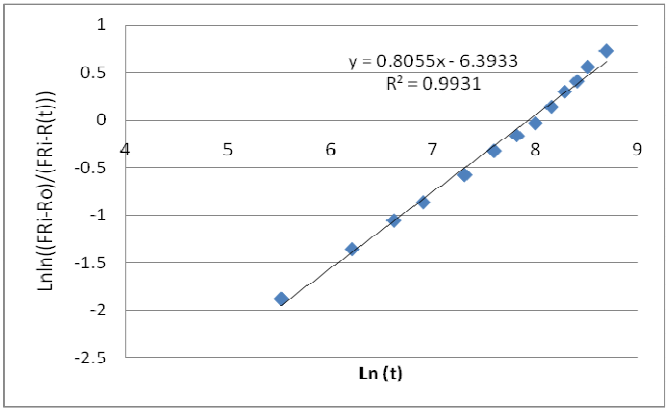
y = 0.8055x - 6.3933
R² = 0.9931
Lnln((FRi-Ro)/(FRi-R(t)))
Ln (t)

(b)

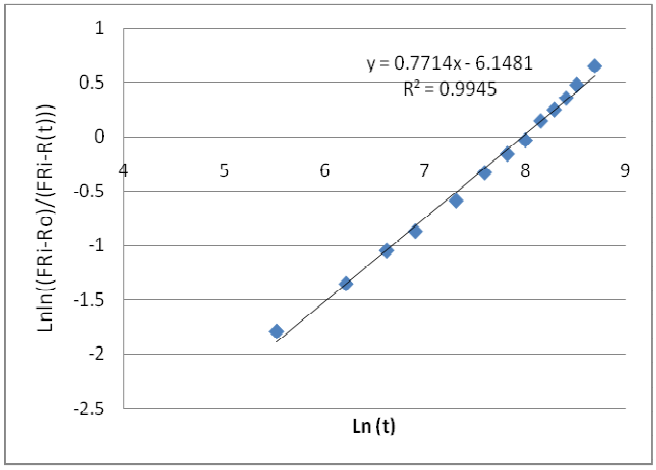
y = 0.7714x - 6.1481
R² = 0.9945
Lnln((FRi-Ro)/(FRi-R(t)))
Ln (t)

(c)

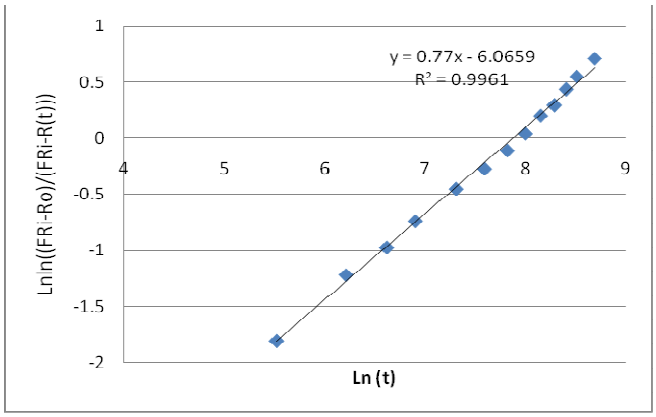

(d)

Figure 4.35; Ln time/radius plots for all loading conditions, (a) unloaded; (b) 10 N; (c) 30.4 N; and (d) 49 N.

Analysis of the Avrami-type plots in Figure 4.35 reveals the slopes (*n*) and the intercept (ln(*k*)) values. These values are presented in Table 4.9.

Table 4.9. Summary of Avrami parameters from variation of radius with time.

Load (N)	Ln(*k*)	*k* (units to be determined)	*n*
0	-6.692	0.00124	0.8
10	-6.393	0.00167	0.8
30.4	-6.148	0.00214	0.8
49	-6.066	0.00232	0.8

The values of n determined are identical (within experimental error) indicating that the same mechanism is acting over the times, temperatures and loads studied.

The increase in *k* value despite identical applied strain and the saturation of *n* values above 30 N for loaded laminates relaxing for >4000 hours is consistent with an energy increase due to compression of laminates as a result of loading.

From these relationships, for a given load and hence *k* and *n*, the variation in radius of curvature can be estimated from:

$$R(t) = Ro + (FRi - Ro)\left(1 - \exp\left(-k\,t^{n}\right)\right)$$

This will require knowledge of *FRi* to be fully predictive, but the rate of relaxation can be predicted.

4.4.10.3 Variation of curvature with temperature

The epoxy matrix of carbon fibre composites is very sensitive to temperature variations due to thermal activation of molecular motion/re-arrangement rates. However, the influence of temperature is not only limited to matrix material. In the fibre direction, a composite can also experience a change in properties with temperature.

To demonstrate variations in laminate behaviour with temperature, laminate strains were monitored during heating and cooling, from RT to 130 ºC to RT.

Figure 4.36 shows an example of the change in strain on heating and cooling of a 4 ply laminate, Y2.

On heating, the laminate increased in longitudinal strain, (Matrix) (Region I), then entered a near neutral strain state at ~90 °C (Region II) where the laminate lost all curvature and flattened out as the 90° ply expands to its maximum, (restricted by adjacent 0° plies as they will not compress under expansion of 90º plies; required to cause reverse curvature) and strain mismatch is equalised, determined as its stress free temperature (T_{SF}). At temperature there may be some creep of the 90° ply material at the interface so that it expands and matches the 0° ply – this would be equivalent to slippage during the curing process, although further curing may not be taking place. The laminates were also not re-heated immediately after fabrication and so some stress relaxation would have taken place; this would explain why the stress-free temperature is not the original curing temperature.

On cooling, the CTE mismatch would act immediately to cause laminate curvature, i.e. curvature re-formation is not delayed until the stress-free temperature on heating was achieved on cooling. This would then lead to a greater difference in contraction between the differently oriented plies and so a greater curve height (Δh) on cooling back to room temperature.

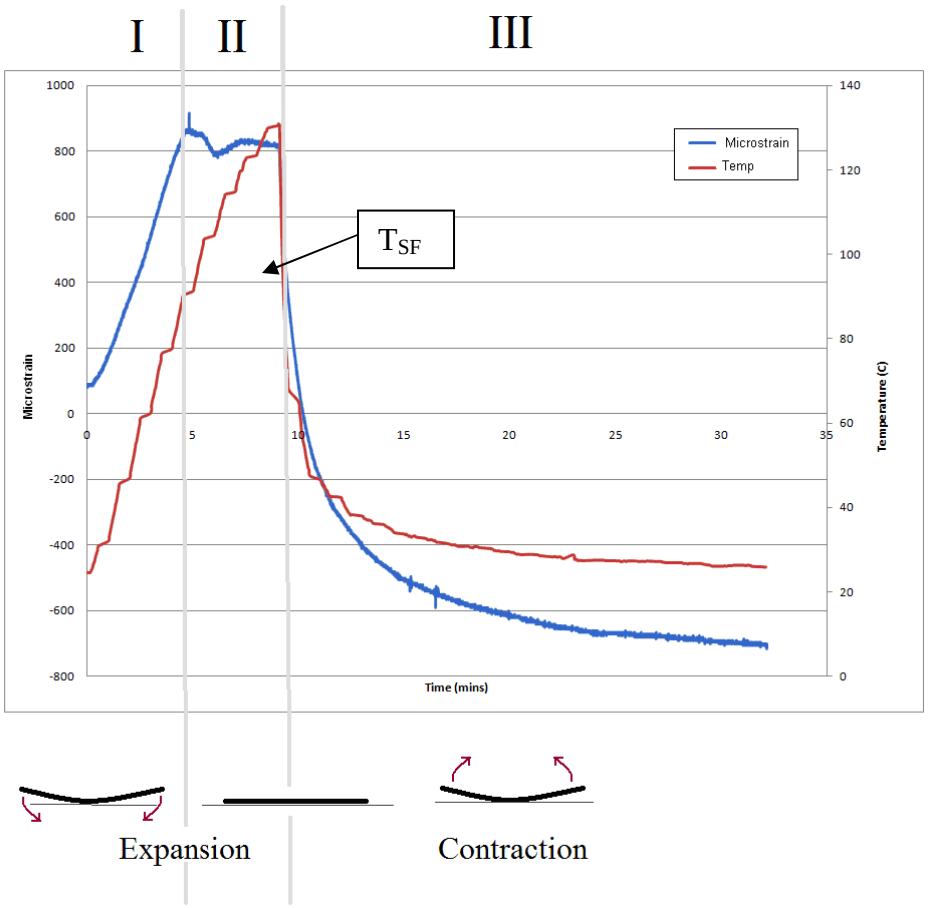

Figure 4.36; Measured laminate strain on heating and cooling of laminate Y2, (10 min part-cure+ full cure) and respective warpage variation.

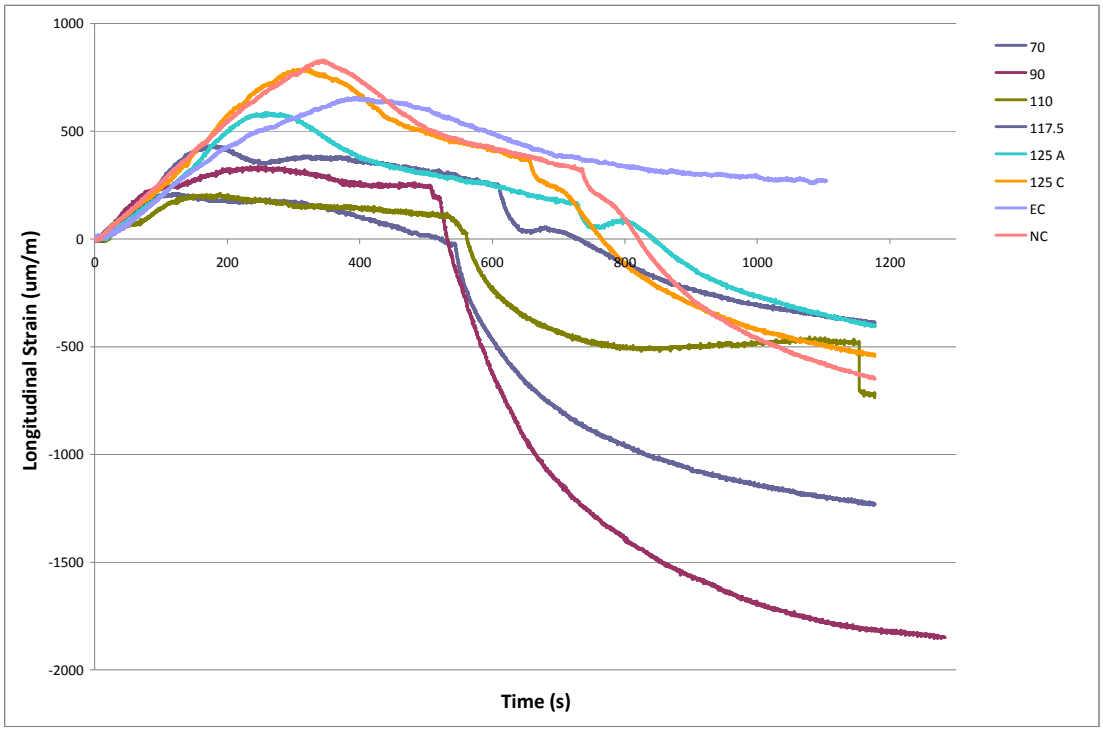

Figure 4.37; ICC laminate longitudinal/matrix strain, on re-heating to 130 ºC

The behaviour for re-heating of fully cured laminates in Figure 4.36 is also shown for ICC laminates, Figures 4.37 and 4.38, Table 4.10, but the effect is exaggerated for laminates cured to 90-110 ºC initially. This would be consistent with increased curing and cross-linking occurring during the re-heating of these laminates that would not occur for those initially cured at higher temperatures.

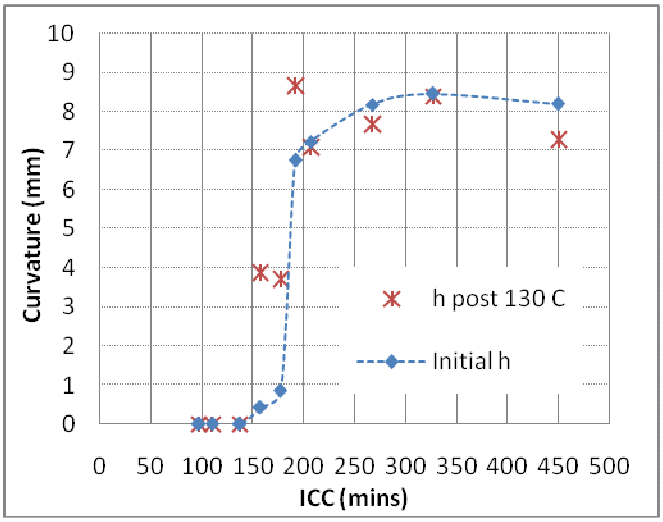

Figure 4.38; Initial and final internal laminate curve height as a result of re-heating to 130 ºC.

Table 4.10. Change in curve height (Δh) (mm) following heating of ICC laminates

ICC Temp (ºC)	**ICC Time (mins)**	**Curve height Init**	**Curve Height Final**	**Δh**
70	97	0	0	**0**
90	137	0	0	**0**
110	177	0	4.56	**4.56**
117.5	192	3.69	6.24	**2.55**
125	207	5.63	7.94	**2.32**

The variation in curve height with temperature for cooling below room temperature is linear, Figure 4.39; a trend that extends up to the stress-free temperature. As the effect of CTE mismatch is assumed to be linearly dependent on the temperature change, this further supports the dominant role of CTE mismatch on curvature and so curve height.

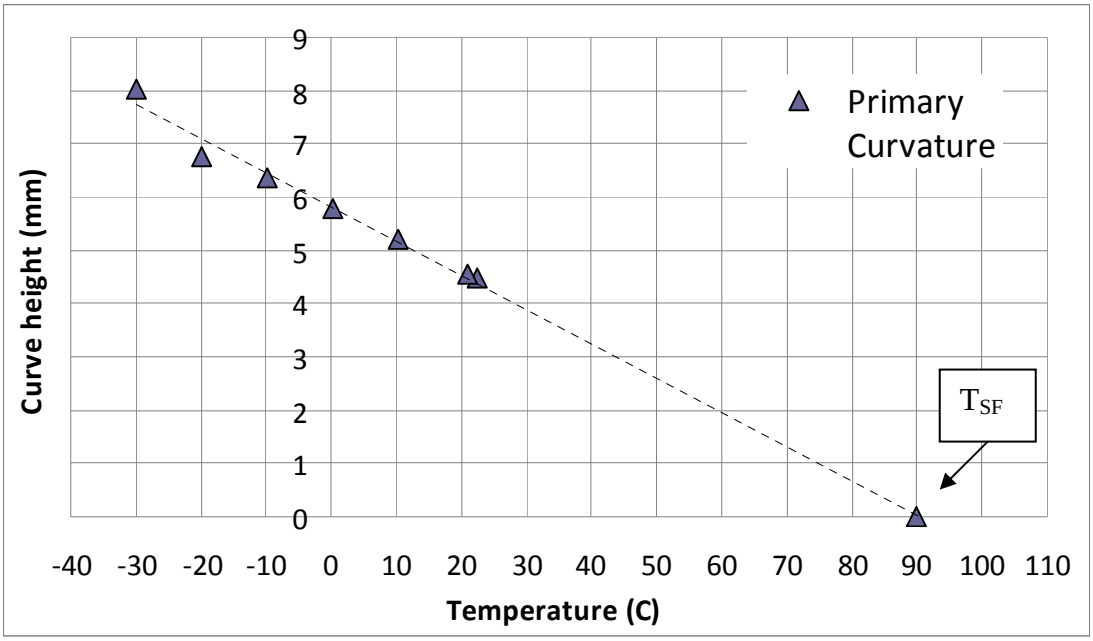

Figure 4.39; Curve height with temperature for AR1 4 ply laminate, curve height equals zero at pre determined stress free temperature (T_{SF}), 90 ºC.

4.5 Limitations of linear theory

The simple models presented in Section 4.2, Equations 4.2-4.5 use linear coefficients of thermal expansion and a constant strain gradient through thickness to determine curvature-thickness relations. These assumptions stem from the basic principles of the bending of beams, bimetallic strip theory (Figure 1.18).

Models assuming that curvature generation is dominated by differential thermal contraction between 0 and 90° plies on cooling and omitting shrinkage (Equations 4.4 – 4.5) are closest to those curvatures determined experimentally. These, however, still overestimate the degree of curvature.

Boundary conditions for best fit model, Equations 4.5

1) Plies are not locked in during the cure and can move relative to one another during the shrinkage stage.

2) Complete slippage of plies at the interface during the curing hold.

3) Curvature is just due to differential thermal contraction on cooling after the cured plies are locked together.

As applied, the models (Equations 4.2 – 4.5) assume that CTE and strain inputs to be independent of ply orientation and position assuming homogeneity and isotropy (properties be the same in tension and compression) and no temperature dependence over the cooling temperature range. The material is assumed to be fully cured at the start of cooling and is allowed to cool and contract in an unconstrained condition, i.e. mould surface and vacuum bag effects are ignored. The curvature generated is assumed to fit a circular arc, but may also fit an ellipse.

The assumptions of the simple models and their effects on curvature will be detailed in the following sections.

4.5.1 Model Assumptions

4.5.1.1 Constraints

Model boundary conditions assume upper and lower laminate surfaces are unconstrained and that the plies at those locations undergo 'free thermal contraction'. The only effect of neighbouring plies would be that to give a constant strain gradient through thickness. In practice, however, individual plies may influence the expansion or contraction of the adjacent plies preventing the outer plies from undergoing 'free thermal contraction'. The effect of vacuum pressure constraint and stress relaxation will be detailed later in this section.

4.5.1.2 CTE

The linearity of thermal expansion coefficients of composites has been shown to be affected by a number of factors including the thermal and elastic properties of the constituents, extent of cross-linking and thermal history of the resin matrix, ply cure constraints upon stacking to form a laminate and on processing, orientations and distribution of the fibres within the matrices, strain transfer and quality of interply bonding.

Model input values for α^{0}_{CTE} and α^{90}_{CTE} ($\alpha 1$ and $\alpha 2$) were determined by measuring CTE values as $\Delta\varepsilon / \Delta T$ at select intervals over the entire temperature range, from room temperature to ~90 °C then taking an average. As CTE with temperature is only a smooth function if the material is not undergoing a phase transition, any deviation from linear trend will not be accounted for in the model by using average values, assuming

uniform CTE. The calculated CTEs for each temperature step are presented in Table 4.11

Table 4.11 Calculated α^{0}_{CTE} and α^{90}_{CTE} (α1 and α2) for each temperature step from RT - ~90°C

Laminate	CTE (x10-6 / ºC)	29ºC	39ºC	48ºC	58ºC	68ºC	77ºC	87ºC	97ºC	Ave. CTE (x10^{-6} / ºC)
CFC 0º Laminate 1	α2 Matrix	34.2	37.2	37.3	35.2	35.2	36.7	32.2		**35.4**
CFC 0º Laminate 2	α2 Matrix	23.0	22.7	22.8	22.2	22.7	23.9	23.7	22.7	**23.0**
CFC 0º Laminate 1	α1 Fibre	0.4	1.7	3.4	2.2	2.2	0.6	2.7	4.7	**2.2**
CFC 0º Laminate 2	α1 Fibre	0.4	0.7	0.6	1.2	0.7	-0.5	-0.3	0.7	**0.4**

Laminate	CTE (x10^{-6} / ºC)	29ºC	37ºC	46ºC	55ºC	64ºC	74ºC	83ºC	92ºC	Ave. CTE (x10^{-6} / ºC)
CFC 90º Laminate 1	α2 Matrix	25.7	37.3	33.4	33.4	28.4	30.7	29.5	25.6	**30.5**
CFC 90º Laminate 2	α2 Matrix	22.7	36.7	31.7	32.3	26.1	29.2	32.8	22.3	**29.2**
CFC 90º Laminate 1	α1 Fibre	5.7	0.4	2.8	1.1	0.0	1.2	0.6	2.3	**1.8**
CFC 90º Laminate 2	α1 Fibre	4.7	-1.4	1.1	0.0	-0.5	0.2	0.6	0.6	**0.7**

Figure 4.40 shows experimental strain behaviour (change in dimension/orignal dimension) for the UD 4 ply laminates (P & Q). These are similar for most laminates at temperatures ≤40 °C, (excluding 0° Laminate 2) following an approximately linear trend until higher temperatures (>55 °C) where the strain and calculated CTE values show a greater deviation from linearity and between laminates. This could result from the molecular structure of the polymeric resin, such as from the relaxation accompanying the softening of the resin associated with an approach to the glass transition temperature.

The range in average linear experimental α2 CTE values 22.2 - 37.3 $^{x10\text{-}6\ /\ ºC}$ would result in a 41 % variation on predicted curvature (R/t 367.63 - 215.96 respectively) with α1 constant at 0.7 $^{x10\text{-}6\ /\ ºC}$, Equations 4.5, maintaining the significance of model input data accuracy for model validation. Given this variation the non-linearity effects would be small.

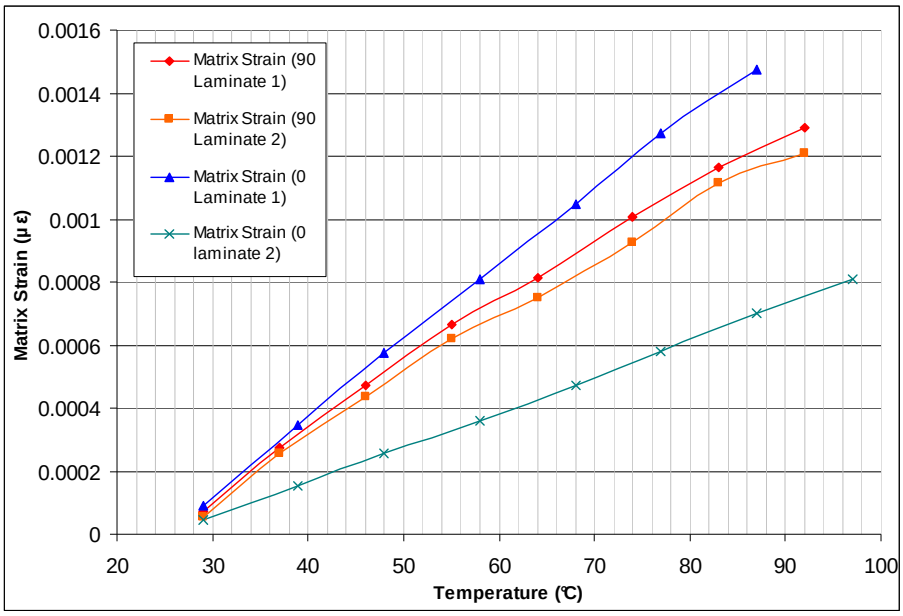

Figure 4.40. Strain perpendicular to fibre axis versus temperature for UD 4 ply laminates

As in-plane thermal expansion behaviour α1 is dominantly dependent on the reinforced carbon fibre, its temperature dependence would be expected to be more linear in agreement with model assumptions. This said, the strain parallel to the fibre vs temperature does show a slight non-linearity, Figure 4.41, resulting in a range in calculated α1 CTE values from -1.4 to 5.7 $^{x10\text{-}6\ /\ ^{o}C}$, giving a 23 % variation on predicted curvature (R/t 258.36 - 336.17 respectively) when α2 is assumed constant at 29.2 $^{x10\text{-}6\ /\ ^{o}C}$, Equations 4.5.

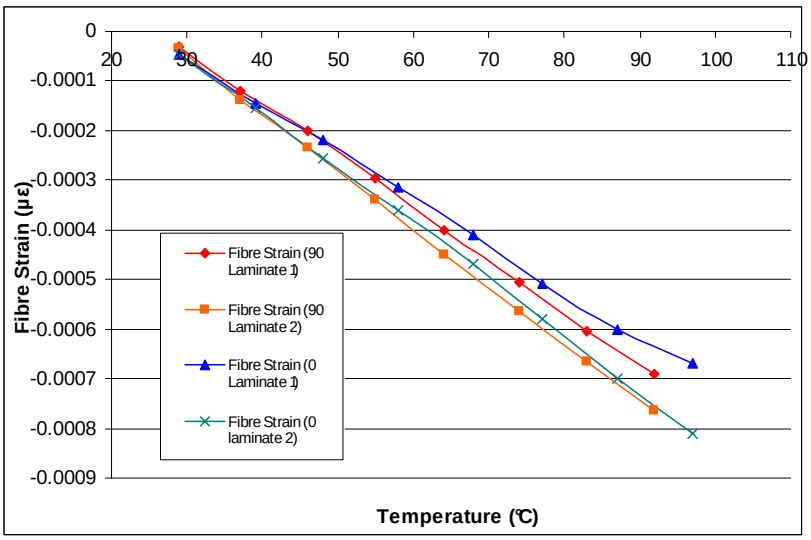

Figure 4.41. Strain parallel to fibre axis versus temperature for UD 4 ply laminates

This non-linearity with response to temperature means that assuming uniform CTE input value and assuming a fixed strain in the 90º plies does not account for individual ply behaviour, and can only function as an approximation of curvature generation. Factors such as differences in expansion behaviour due to varied fibre orientation, alignment of plies, degree of cure and/or strain gauge placement (supported by the significant difference between nominally identical 0° Laminates 1 and 2 strain behaviour, Figure 4.40) will tend to reduce the curvature generated compared with th simple model.

To improve the accuracy of model predicted curvatures, non-linear thermal behaviour may need to be considered and used to expand the basic simple model, applying the CTE in temperature steps to follow the development of curvature during and at the end of the cure cycle as CTE values vary.

4.5.1.3 Strain Gradients – Slippage at Ply Interfaces

In addition to non-linearities seen experimentally in input CTE values, it is also important to consider the effect of strain gradients on the generation of residual stresses between the surface and inner of laminate structure. The assumption of a linear through-thickness strain gradient would give squared off ply ends; experimentally the plies ends tended to be stepped, Section 4.4.9. This would be consistent with slippage at the ply interfaces during cooling, which would reduce stress transfer between plies and reduce the curvature achieved experimentally when compared to that predicted in Equations 4.5. The simple model assumes that laminate strain is continuous and linear, Figure 4.42 b. However, the stress / strain relationships in carbon fibre composites are non-linear and are dependent on geometric conditions such as thickness ratio, material relations (modulus) and loading parameters (composite modulus varies in compression than tension during bending). This non-linear stress / strain behaviour in multidirectional laminates is caused because modulus values vary from ply to ply giving discontinuities in stress distribution through-thickness (Figure 4.42 c). These discontinuities in stress through-thickness would be amplified for the case of complete interply slippage during curing (Equations 4.4 – 4.5), (Section 4.4.9)

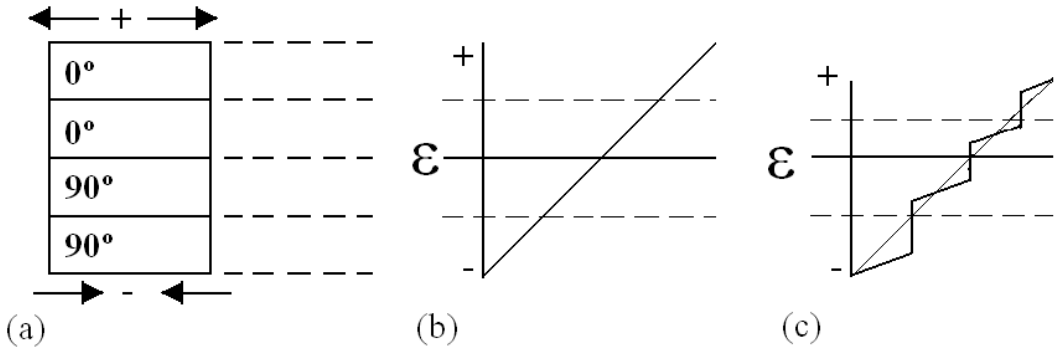

Figure. 4.42, Schematic of strain distribution in 0/90 laminate a) tensile and compressive strains of asymmetric laminate, through-thickness b) continuous and linear strain c) discontinuities in stress as a function of slippage between plies.

Experimentally, the significant effect of laminate length to thickness ratio on curvature and the magnitude of the out of plane displacements of RT shapes support that strain is not constant through thickness and stress distributions are not symmetric about the mid plane.

A decrease in curvature with an increase in numbers of plies suggested by *Jun and Hong 1992* [11] is likely if stress transfer is non linear, in comparison to the linear curvature/thickness relationship predicted in basic models, Figure 4.43.

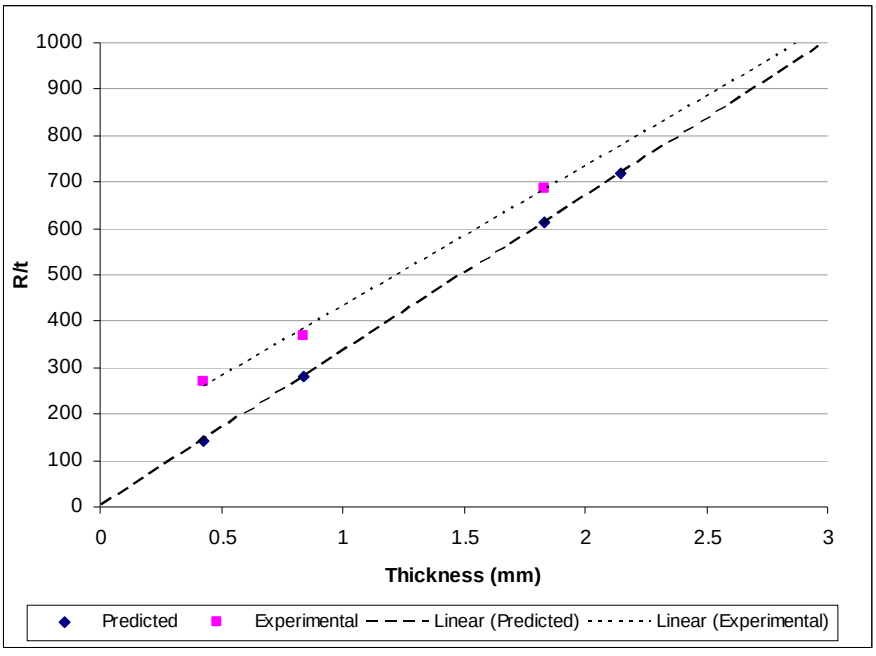

Figure. 4.43 Predicted and experimental curvatures with thickness, α0CTE=0.7 and α90CTE=29.2 (Equations 4.5)

Further model developments should include non-linear strain-displacement behaviour of asymmetric laminates, modelling the entire thickness to include the spatial variation of strains, shear strains, strain fields and displacement functions as *Jun and Hong* [11] to account for the presence of thermal residual in-plane shear strain (deviation from perfect cylinder), material inhomogeneity (non-uniform fibre distribution between layers, defects) and laminate stiffnesses considered.

4.5.1.4 Stress relaxation.

In addition to the interply constraints detailed previously, the time / load dependence of the epoxy matrix must also be considered. The application of pressure / load upon the composite laminate through the vaccum bagging process (88000-91000 Pa) is suggested to constrain the laminate on cooling causing a relaxation of stresses in the epoxy matrix which would reduce experimental curvatures. The stress relaxation effect is greater under higher loads and temperatures (Section 4.4.10), such as those during cure

The omission of stress relaxation effects in the simple model may also contribute to the overprediction of curvature values. A change in curve height (Δh) (2.32 mm) following the re-heating of 'fully cured' ICC laminates to above Tg is representative of the cure height that would be achieved without vacuum constraint under standard atmospheric pressure (101325 Pa). As vacuum-bagged, the radius of curvature for the ICC 4 ply laminate was 315 mm. Re-heating and cooling resulted in a radius of curvature of 250 mm, in line with predicted curvatures of 281 mm (Equations 4.5).

4.6 Applications

4.6.1. Bistability

Aspect ratio (length:width) has been shown, Section 4.4.3, to have little effect on longitudinal panel curvature, although it may strongly influence the bistability of the panels.

Laminates with an aspect ratio of 1:1 (squares), are expected to achieve curvature in both longitudinal and transverse directions due to (mostly) differences in CTE values between plies. Thus if strains are equal throughout, and CTE values comparable, the entire panel should reduce uniformly producing equal curvatures in transverse and

longitudinal directions, generating a ‘saddle’ shape deformation, widely predicted in CLT [7,11,13-15].

Laminates with differing aspect ratios (1 - 2) were manufactured to assess curvatures generated in both longitudinal and transverse directions; primary and secondary curvatures, Figure 4.44.

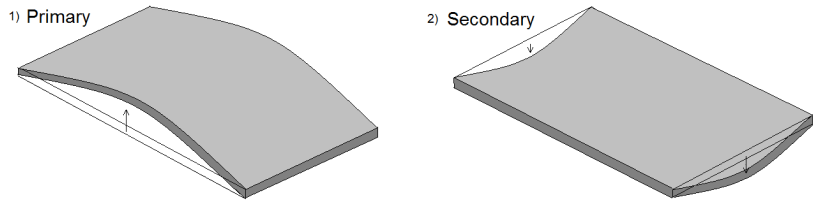

Figure 4.44; Primary and secondary curvatures: Cylinders 1 and 2. Where primary curvature of square laminates was determined by the greater strain in the 90° ply.

Laminates with AR values from 1 - 1.5 all exhibit bistability, with stable curvatures in both longitudinal and transverse directions.

AR = 1 laminate 145 x 145 mm shows similar radius of curvature values in both axes and requires a force of 7 N to snap through from the primary to secondary curvature state.

In comparison, with a decrease in laminate width (AR = 1.5) the radius of curvature for secondary curvature significantly decreased and the force required to change between states is significantly reduced (4 N), Figure 4.45.

For laminates with AR = 2, no radius of curvature for secondary curvature could be measured as the laminate was not stable in the secondary curvature morphology and immediately snapped back to the primary curvature on unloading.

Data show a correlation between secondary curvature curve height and bistability of laminates. Therefore, any decrease in curve height as a function of aging (stress relieve / creep) will alter the behaviour of carbon fibre laminates and may lead to a loss in bistability altogether.

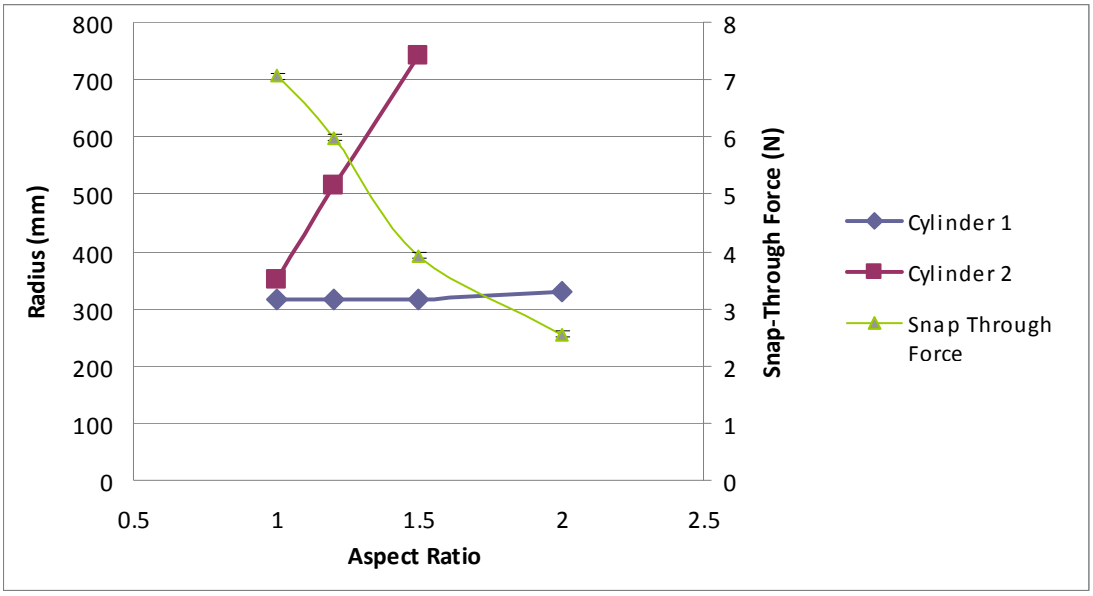

Figure 4.45; Radius of curvature values for primary and secondary curvatures of various AR laminates along with snap through force required to initiate secondary stable shape.

4.6.2. Predicting bistability

Plotting laminate length against width, with its ability (or lack of ability) to change between cylinders 1 and 2 provides a tool to predict the bistability of 4 ply laminates by keeping l:w outside of red/orange areas, Figure 4.46.

The red region in Figure 4.46 showed no bistability, whilst the orange area represents panels that showed initial bistable behaviour, which was lost as stress relief / creep resulted in loss of secondary curvature curve height with time. The boundary between the orange and green regions will be time-dependent and will move to the right until the loss of curvature with time has saturated, Figure 4.34.

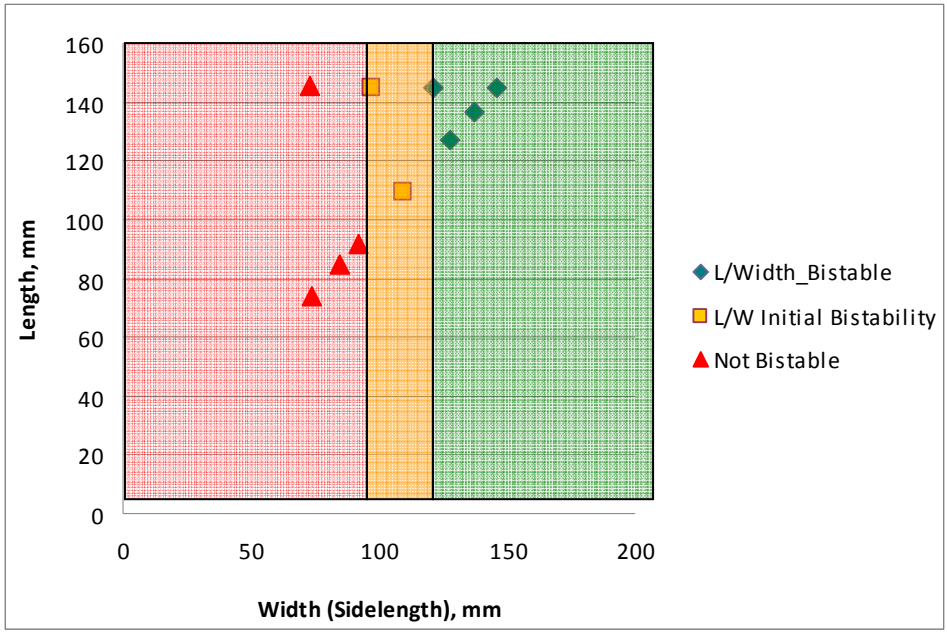

Figure 4.46; Diagram summarising the bistable nature of different aspect geometry asymmetric laminates.

4.6.3. Snap through with temperature

Bistable asymmetric laminates with AR = 1 experienced a large increase in primary curve height (+ 3.5 mm at -30 °C) and snap through force (+ 7 N at -30 °C), on exposure to decreased temperatures, Figure 4.47. This increased snap through force is likely to be as a result of increased differential thermal strain due to CTE mismatch as temperature decreases, Figures 4.39 and 4.48.

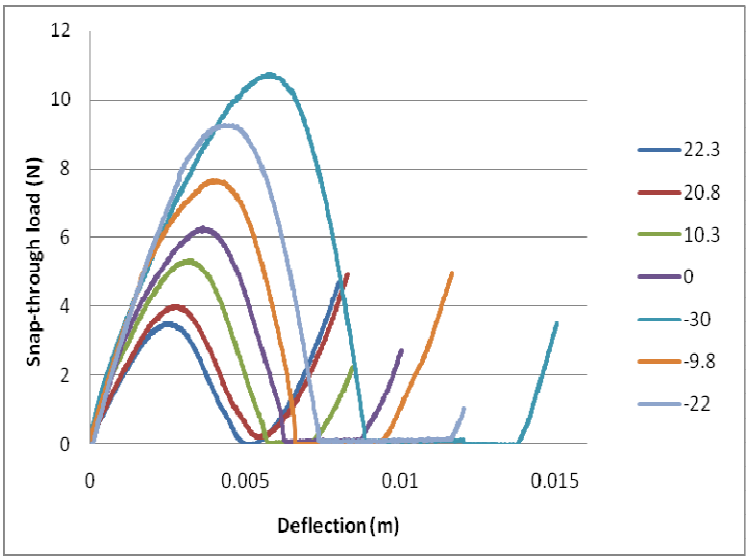

Figure 4.47; Load/deflection traces for laminate with AR = 1 with temperature (in °C in legend).

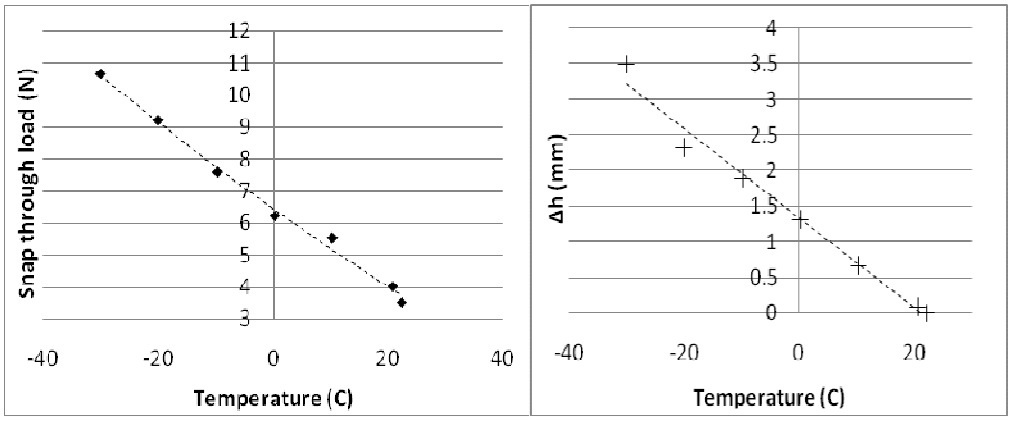

(a) (b)

Figure 4.48; Temperature dependence of (a) snap through force and (b) change in curve height (Δh) for laminate with AR = 1.

Although the two radius of curvature values for square laminates should be equal, that for secondary curvature is often less than that for primary curvature, Figure 4.49. This would indicate that some aspect of manufacturing, e.g. the presence of a breather fabric means that the shrinkage during cooling normal to the fibres in one set of plies is less than that for the other set of plies. The cause of this manufacturing effect has not been identified nor fully quantified, but it does mean that bistability is lost at temperatures well below the primary curvature stress-free temperature, Figure 4.49. For laminates fabricated in this study, bistability is lost at temperatures slightly above room temperature.

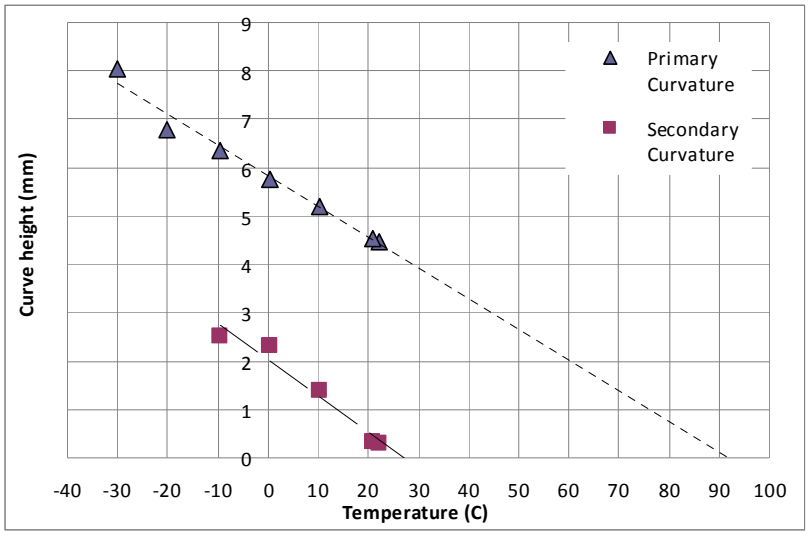

Figure 4.49; Primary and secondary curve heights of 4 ply laminate with AR = 1, where extending line of best fit indicates temperature which curvatures is predicted to equal zero.

4.6.4. Snap through with stress relaxation

As noted above, stress relaxation should cause curve height to reduce over time. Given the strong relationship between secondary curvature and bistability, reduction of curvature with time will result in only one cylinder generated, and will therefore no longer exhibit bistability. Figure 4.50, shows the reduction in both primary and secondary curve heights for AR 1-2 laminate after 20 days at room temperature, when the bistability would be expected to decrease.

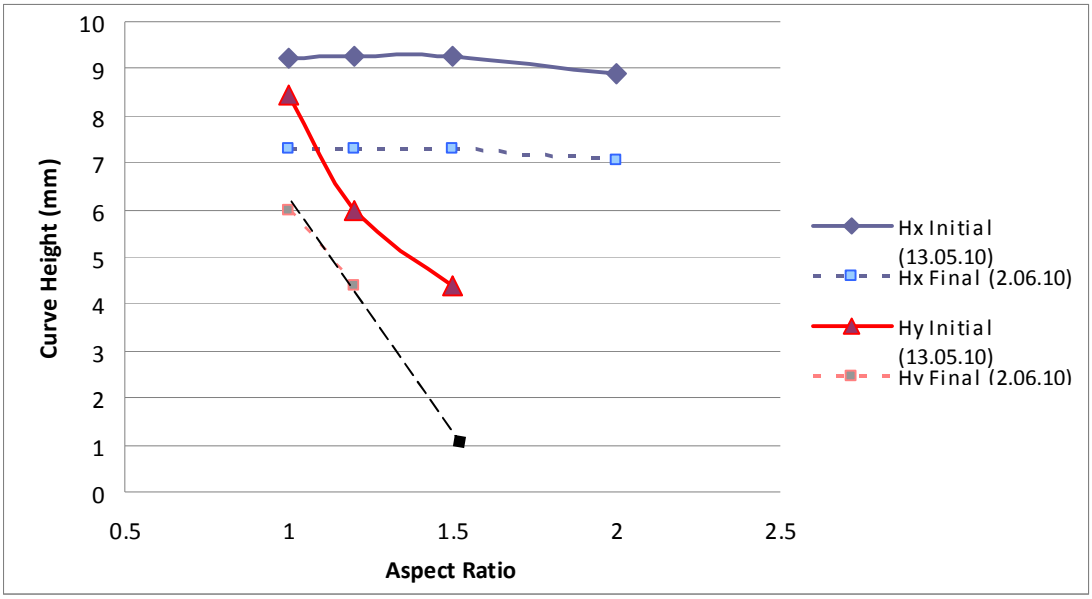

Figure 4.50; Reduction in primary (Hx) and secondary (Hy) curvature curve heights for different AR value panels over a period of 20 days after laminate manufacture.

5. Conclusions and Further Work

5.1. Conclusions

The aim of this project was to identify the factors controlling curvature generation in asymmetric carbon fibre laminates in order to quantitatively describe their behaviour.
A range of carbon fibre composite laminates were manufactured, with varied geometries and cure conditions to establish the effect of these factors on curvature.
In addition, the bistability and stability of curvature with pre-preg. age, temperature and time was also investigated. The major findings from this study are listed below.

- The largest effect on radius of curvature is that of thickness, showing a linear dependence, which is consistent with the geometrical effect and a constant strain.
- The longitudinal radius of curvature is not affected by aspect ratio (given laminate manufacturing variables, stacking sequence and pre-preg. age are comparable), which is in agreement with constant strain. However, aspect ratio is shown to influence the laminates bistability.
- Comparison between predicted and experimental values indicates that curvature in the epoxy systems studied is dominated by the CTE mismatch on cooling.
- Accuracy of the developed models is highly dependent on the quality of the interfacial bond between plies, with model curvature suggesting plies are not ‘locked in’ during the isothermal curing dwell, allowing for the slippage of plies, the extent of which is validated by image analysis.
- The dependence of curvature formation on cure shrinkage is negligible for the MTM28-1 epoxy system.
- Reduced degree of cure is shown to result in reduced CTE mismatch, giving larger radius of curvature values for a given laminate thickness.
- The development of curvature with temperature on cooling below room temperature is linear, the strain due to CTE mismatch is also a linear function of temperature in this range.
- Largest deviations from model predictions were seen for laminates with extensive voiding (resulting in varied forces within the matrix) and for aged matrix material.

- The stability of asymmetric laminates is a function of time and temperature. Over a period of weeks to months, laminates showed reduction of curvature due to stress relaxation/creep, whilst some lost the ability to ‘snap-through’, either permanently or until lower temperature increased stiffness / residual stresses.
- Unbalanced laminates that developed unequal strains on curing for the opposite sides resulted in panels showing bi-stability, i.e. panels, which showed both primary and secondary stable shapes. Bi-stable panels will ‘snap-through’ if the strain in the secondary state is sufficiently large to overcome the restorative force from the primary state. This study found that bi-stability was shown for square and rectangular panels, provided that the length was sufficiently large compared with the thickness.

5.2. Future Work

A mechanism has been established for curvature generation in a small range of carbon fibre composite systems. Extension of this work should be made to generalise this to a wider range of fibre reinforced systems, e.g. different matrices including thermoplastic materials and glass fibres. The behaviour has been accounted for by consideration of curing and CTE mismatch stresses, but this is not at a stage where it is predictive. Hence, the curing / CTE / modulus behaviour needs to be quantified and linked to Equations 4.5 in this study so that lay-ups and thermal treatments can be designed for given curvature / bistability criteria. These designs would then need to be fabricated and assessed in order to validate and verify the modelling / design approach.

The decay of curvature and bistability has been characterised, but, again, this needs to be quantified and a resin system state established that will provide either a greater final curvature or a curvature that resists stress relief / creep more effectively. The behaviour of these modified systems would need to be quantified.

The original thrust of this project was related to shape changing sports equipment and so, once bistable shapes have been designed with sufficient longevity, actuating devices (shape memeory alloys and piezoelectrics) can be incorporated to give control of the bistability beyond just a load trigger.

References

[1] Powell P. Engineering with fibre-polymer laminates. Chapman and Hall; (1994). Hull D, Clyne TW. An introduction to composite materials 1st and 2nd Ed. Cambridge; (1981,1996)]

[2] Ashby MF. Materials selection in mechanical design. 2nd Ed. (1999) Butterworth-Heinemann

[3] Tsai SW, Hahn HT. Introduction to composite materials. Westport, CT: Technomic Publishing CO; (1980).

[4] Balta JA, Bosia F, Michaudi V, Dunkel G, Botsis J, Manson JA. Smart composites with embedded shape memory alloy actuators and fibre Bragg grating sensors: activation and control. Smart Mater. Struct. 14 (2005) 457–465.

[5] Gude M, Hufenbach W. Design of novel morphing structures based on bistable composites with piezoceramic actuators. Mech Compos Mater (2006);42(4):339–46.

[6] Powell P. Engineering with fibre-polymer laminates. Chapman and Hall; (1994).

[7] Hull D, Clyne TW. An introduction to composite materials 2nd Ed. Cambridge; (1996).

[8] Tawfik S, Tan X, Ozbay S, Armanios E. Anticlastic Stability Modeling for Cross-ply Composites. J Composite Materials (2007); 41; 1325.

[9] Yoon KJ, Kim JS. Effect of Thermal Deformation and Chemical Shrinkage on the Process Induced Distortion of Carbon/Epoxy Curved Laminates. J Composite Materials 2001; 35; 253

[10] Peeters LB, Powell PC, Warnet L.Thermally-Induced Shapes of Unsymmetric Laminates. J Composite Materials (1996); 30; 603.

[11] Jun WJ, Hong CS. Cured Shape of Unsymmetric Laminates with Arbitrary Lay-Up Angles. J Reinforced Plastics and Composites (1992); 11; 1352.

[12] Hamamoto, A. and Hyer, M.W. Non-linear Temperature-curvature Relationships for Unsymmetric Graphite-epoxy Laminates, International Journal of Solids and Structures, (1987) 23: 919–935.

[13] Hyer, M.W. Some observations on the cured shape of think unsymmetric laminates. J. of comp. Materials (1981), 15:175-194.

[14] Hyer, M.W. Calculation of the room temperature shapes of unsymmetric laminates. J. of comp. Materials (1981), 15:296-310.

[15] Hyer MW. The Room-Temperature Shapes of Four-Layer Unsymmetric Cross-Ply Laminates. Journal of Composite Materials (1982); 16; 318.

[16] Guo ZS. Strain and Temperature Monitoring of Asymmetric Composite Laminate using FBG Hybrid Sensors.Structural Health Monitoring (2007); 6; 191

[17] Schlecht, K. Schulte. Advanced Calculation of the Room-Temperature Shapes of Unsymmetric Laminates. Journal of Composite Materials (1999); 33; 1472

[18] Wisnom MR, Gigliotti M, Ersoy N, Campbell M, Potter KD. Mechanisms generating residual stresses and distortion during manufacture of polymer–matrix composite structures. Composites: Part A 37 (2006) 522–529.

[19] M. Gigliotti, M.R. Wisnom, K.D. Potter. Development of curvature during the cure of AS4/8552 [0/90] unsymmetric composite plates. Composites Science and Technology 63 (2003) 187–197.

[20] H. Thomas Hahn. Residual Stresses in Polymer Matrix Composite Laminates. Journal of Composite Materials 1976 10: 266

[21] G. Jeronimidis and A.T. Parkyn. Residual Stresses in Carbon Fibre-Thermoplastic Matrix Laminates. Journal of Composite Materials 1988; 22; 401

[22] S.R. White and H.T. Hahn. Process Modelling of Composite Materials: Residual Stress Development during Cure. Part I. Model Formulation. Journal of Composite Materials (1992); 26; 2402

[23] S.R. White and H.T. Hahn. Process Modelling of Composite Materials: Residual Stress Development during Cure. Part II. Experimental Validation. Journal of Composite Materials (1992); 26; 2423

[24] Matthews FL, Rawlings RD. Composite materials: Engineering and science. Woodhead publishing. (1999).

[25] Pagano NJ, Pipes RB.The Influence of Stacking Sequence on Laminate Strength. Journal of Composite Materials (1971); 5; 50

[26] Ross GR, Ochoa OO. Environmental Effects on Unsymmetric Composite Laminates. J Thermoplastic Composite Materials (1991); 4; 266.

[27] Timoshenko, S.P. and S. Woinowsky-Krieger. Theory of plates and shells. (1964) McGraw-Hill

[28] Dang, J. and Y. Tang. 1986. "Calculation of the Room-Temperature Shapes of Unsymmetric Laminates," Proc. Int. Sym. on Composite Materials and Structures, China, pp. 201-206.M.

[29] Hahn HT, DG Hwang. Residual stresses and their effect in composite laminates. Proc of NCKU/AAS Int. Symposium on Eng. Sciences and mechanics, (1981) Taiwan.

[30] Thomas P. Kicher. The Analysis of Unbalanced Cross-Plied Elliptic Plates Under Uniform pressure. Journal of Composite Materials (1969); 3; 424

[31] Dano M.L, Hyer M.W. Thermally-induced deformation behaviour of unsymmetric laminates. International journal of solids and structures 35 (1998)

[32] A Pirrera, D Avitabile and PM Weaver. Bistability of composite cylindrical shells, The University of Bristol.

[33] G. Vargas, A. Arrese, N. Carbajal and F. Mujika. Analysis of In-plane and Out-of-plane Thermo-mechanical Stresses in Un-symmetric Cross-ply Curved Laminated Strips. Journal of Composite Materials 2009; 43; 3157

[34] Radford, D.W, Balancing Mechanisms of Distortion to Yield Distortion-free/Shape Stable Composites. Journal of Reinforced Plastics and Composites (2010) 29: 1875

[35] R. M. Verette. Temperature/Humidity Effects on the Strength of Graphite/Epoxy Laminates. J. Airpcraft, 90. Vol. 14, No. 1

[36] Chi-Hung Shen and George S. Springer. Effects of Moisture and Temperature on the Tensile Strength of Composite Materials. Journal of Composite Materials 1977; 11; 2

[37] Fu-Kuo Chang, Iqbal Shahid and Roger A. Engdahl. Predicting Moduli and Strengths Reduction of Unidirectional Graphite/Epoxy Composites Due to Hygrothermal Effects. Journal of Reinforced Plastics and Composites 1989; 8; 106

[38] Theocaris PS, Marketos E. Shrinkage stress concentrations in plane two phase systems. (1970) Laboratory for Testing Materials, Athens National Technical University (Greece).

[39] Hoa SV, Ouellette P, Ngo TD. Determination of Shrinkage and Modulus Development of Thermosetting Resins. Journal of Composite Materials (2009); 43; 783.

[40] Li C, Potter K, Wisnom MR, Stringer G. In-situ measurement of chemical shrinkage of MY750 epoxy resin by a novel gravimetric method. Composites Science and Technology 64 (2004) 55–64.

[41] Zarrelli M, Skordos AA, Partridge IK. Investigation of cure induced shrinkage in unreinforced epoxy resin. Plastics, Rubber and Composites Processing and Applications 31(2002). 377-384.

[42] Travis A. Bogetti and John W. Gillespie, Jr. Process-Induced Stress and Deformation in Thick-Section Thermoset Composite Laminates. Journal of Composite Materials (1992); 26; 626

[43] Spellman, G.P, Cure Shrinkage Effects in Epoxy and Polycyanate Matrix Composites. MS Thesis (1995) Lawrence Livermore national laboratory.

[44] Capehart TW, Kia HG, Abujoudeh T. Cure Simulation of Thermoset Composite Panels. J Composite Materials (2007); 41; 1339

[45] Barnes J.A, Simms I.J, Farrow G.J, Jackson D, Wostenholm G, Yates B. Thermal expansion behaviour of thermoplastic composite materials. J Composite Materials (1990) 3; 66.

[46] Eric Leroy, Je´roˆme Dupuy, Abderrahim Maazouz, Ge´rard Seytre. Evolution of the coefficient of thermal expansion of a thermosetting polymer during cure reaction. Polymer 46 (2005) 9919–9927.

[47] Crasto A.S, Kim R.Y. On the determination of residual stresses in fibre-reinforces thermoset composites. J reinforced plastics and composites (1993); 12;545.

[48] Kevin D. Cowley & Peter W. R. Beaumont. The measurement and prediction of residual stresses in carbon-fibre/polymer composites. Composite Science and Technology 57 (1997) 1445-1455.

[49] Mills NJ. Plastics; microstructure and engineering applications 2nd Ed. Edward Arnold publishing (1993).

[50] Fomitchov PA, Kim YK, Kromine AK, Krishnaswamy S. Laser Ultrasonic Array System for Real-Time Cure Monitoring of Polymer-Matrix composites. Journal of Composite Materials (2002); 36; 1889.

[51] M. Buonsanti M, Cacciola M, Calcagno S, Megali G, Morabito F.C, Pellicanò D, Versaci M. Evaluation of Defects in Multi-Layer Carbon Fibre Epoxy for Aeronautics Applications. University “Mediterranea” of Reggio Calabria - Faculty of Engineering. Italy

[52] Wang X, Zhang Z, Xie F, Li M, Dai D, Wang F. Correlated Rules between Complex Structure of Composite Components and Manufacturing Defects in

Autoclave Molding Technology. J Reinforced Plastics and Composites (2008) Vol. 00, No. 00/2008.

[53] Cantwell WJ, Morton J. The significance of damage and defects and their detection in composite materials: A review. J Strain analysis (1992) Vol 27, No 1.

[54] Saravanos DA, Hopkins DA. Effects of delaminations on the damped dynamic characteristics if composite laminates: Analysis and experiments. J Sound and Vibration (1996) 192 (5), 977-993.

[55] Shen M.H.H, Grady J.E. Free vibrations of delaminated beams. Am, Inst. Of aeronautics and astronautics (1992), Vol 30,5. 1361-1370.

[56] Tang LG, Kardos JL. Review of Methods for Improving the Interfacial Adhesion Between Carbon Fiber and Polymer Matrix. POLYMER COMPOSITES (1997), Vol. 18, No. 1.

[57] Needles HL, Kenneth WA, Okamoto R. Adhesion at the Interface in Cured Graphite Fiber Epoxy-Amine resin composites. J Reinforced Plastics and Composites (1987); 6; 357

[58] Joseph B, Hanratty FW, Kardos JL. Model Based Control of Voids and Product Thickness during Autoclave Curing of Carbon/Epoxy Composite Laminates. J Compos Mater (1995); 29; 1000.

[59] Oberlin A, Carbon, 22, 521 (1984).

[60] Huntley M. Comparison of static and dynamic carbon fibre golf club shaft properties and their dependence on structure. PhD thesis. (2006) The university of Birmingham.H.

[61] Cease, P.F. Derwent, H.T. Diehl, J. Fast, D. Finley. Measurement of mechanical properties of three epoxy adhesives at cryogenic temperatures for CCD construction, Fermi National Accelerator Laboratory, Batavia IL 60510 (2006)

[62] H.M. Ledbetter and G. Maerz.Temperature dependence of Young's modulus and internal friction of G-10CR and G-11CR epoxy resins. (1980) Cryogenics.

[63] Shiqiang Deng, Meng Hou, Lin Ye.Temperature-dependent elastic moduli of epoxies measured by DMA and their correlations to mechanical testing data. Polymer Testing 26 (2007) 803–813

[64] G.C. Papanicolaou, S.P. Zaoutsos, E.A. Kontou. Fiber orientation dependence of continuous carbon/epoxy composites nonlinear viscoelastic behaviour. Composites Science and Technology 64 (2004) 2535–2545

[65] Chui W.K, Galea S.C, Jones R, Williams J.F. Time-dependent response of carbon fibre/epoxy composites. DSTO Aer. and Maritime research lab. Dpt. Mech Eng, Monash University (1995).

[66] O'Brien DJ. Viscoelastic Properties of an Epoxy Resin during Cure. Journal of composite materials, (2001) Vol. 35, No. 10/2001

[67] www.appliedgroup.com/abaqus-fea (2012)

[68] Advanced Composites Group (ACG), Heanor Derby, UK. http://www.advanced-composites.co.uk

[69] Frekote® WOLO HS™ (http://www.henkelna.com/product-search-1554.htm?nodeid=8797754851329) (2012)

[70] www.bertram31.com/proj/tips/vaccuum.htm (2009).